SUSTAINABLE THERMOSETTING POLYMERS: BIOBASED EPOXY RESIN SYSTEMS AND AQUEOUS NON-ISOCYANATE POLYURETHANES

A Dissertation
Submitted to the Graduate Faculty
of the
North Dakota State University
of Agriculture and Applied Science

By

Raul Abdon Setien

In Partial Fulfillment of the Requirements
for the Degree of
DOCTOR OF PHILOSOPHY

Major Department:
Coatings and Polymeric Materials

May 2022

Fargo, North Dakota

North Dakota State University
Graduate School

Title

SUSTAINABLE THERMOSETTING POLYMERS: BIOBASED EPOXY RESIN SYSTEMS AND AQUEOUS NON-ISOCYANATE POLYURETHANES

By

Raul Abdon Setien

The Supervisory Committee certifies that this ***disquisition*** complies with North Dakota State University's regulations and meets the accepted standards for the degree of

DOCTOR OF PHILOSOPHY

SUPERVISORY COMMITTEE:

Dr. Dean Webster
Chair

Dr. Andriy Voronov

Dr. Ghasideh Pourhashem

Dr. Ewumbua Monono

May 16th 2022
Date

Dr. Dean Webster
Department Chair

ABSTRACT

In recent years, there has been a desire to seek alternatives to petrochemically derived materials. These alternatives can be derived from renewable sources such as vegetable oils However, methods for achieving sustainability are not limited to only resourcing materials from bio-based sources but can also be achieved by utilizing safer synthesis techniques, reducing cure times, and eliminating volatile organic content in thermoset coating formulations. This dissertation sets out to achieve a goal the sustainability across different fields. Epoxidized sucrose soyate is a versatile bio-based materials that is typically synthesized utilizing hydrogen peroxide and acetic acid. A proposed safer alternative utilizes Oxone to generate dimethyldioxirane intermediates at room temperature to achieve the epoxidation of unsaturated sites in sucrose soyate and other vegetable oils such as soybean oil and hempseed oil. Thermosets made from epoxidized bio-based sources synthesized from dimethyldioxirane intermediates or in-situ generated peracids showed little to no difference in thermal and coatings properties. The use of epoxidized sucrose soyate with reactive diluents in cationic photopolymerization was also explored. The thermal characterizations of the thermoset coatings created utilizing this method indicate that crosslinking had not occurred to completion. In an effort to reduce the use of volatile organic content the feasibility of utilizing cyclic carbonates and primary carbamates in water borne polyurethane systems was explored. It was found that utilizing cyclic carbonates with higher ring strain, such as 6-membered cyclic carbonates, provides a potential way for creating non-isocyanate crosslinking thermoset coatings from waterborne polyurethane dispersions.

ACKNOWLEDGMENTS

I express my gratitude to my advisor Dr. Dean Webster. Thank you for the opportunity to work in your group and allowing for an interest in this field to become a lifelong passion. Your guidance and feedback are greatly appreciated. To my committee members Andriy Voronov, Ghasideh Pourhashem, and Ewumbua Monono thank you for the advice you've given me through my graduate career.

I would also like to extend my thanks to Dr. Chunju Gu, Greg Strommen, and James Bahr for guiding me through instrumentation use and experimental set ups. To all my colleagues including those who have been at my side since the beginning, I sincerely thank you for making Fargo feel like a "home away from home". My graduate school experience would not have been the same without you folks.

Thank you to my family, for all your love and support. Without them these last few years of my life would have been impossible. And finally, to my wife Kristen. Thank you for all your love and support. You never cease to amaze and inspire me, and I look forward to spending the rest of our lives together.

TABLE OF CONTENTS

LIST OF TABLES

LIST OF FIGURES

LIST OF SCHEMES

CHAPTER 1. INTRODUCTION

1.1. Approaching Sustainability

Over the course of the last few decades, the concept of manufacturing products with a focus on sustainable and environmentally responsible production has garnered significant attention. In the early 1990s, the United States of America introduced the US Pollution Prevention Act to establish programs that focused on investigating alternative synthetic pathways to proactively mitigate pollution via different manufacturing processes. As time went on, the program was expanded and with the help of many other organizations belonging to groups such as academia, industry, and government agencies, the underlying principle of what is known today as "green chemistry" was established.[1]

The steps taken to develop more environmentally friendly approaches were of course a direct consequence of past environmental and hazardous disasters that lead to these changes to take place. As the development of industrial chemical production plants increased, attention to environmental impacts and human health was often overlooked and thus incidents like the Love Canal tragedy affected the lives of the general public.[2] As these events gained more exposure to the public eye, the research surrounding the topic moved and developed rapidly to meet the ever so evolving economic and legislative changes.

With the annual polymer plastic production estimated at 300 million tons in 2010, many different approaches have been investigated to achieve the goal of sustainability.[3] Some examples include advances in catalysis for sustainable synthesis,[4]incorporation of bio-based sources to replace non-renewable petroleum based materials,[5-7] redesigning synthesis and methodologies in order to reduce the use of volatile organic matter (VOC).[8, 9]

This thesis is a culmination of work that investigates the feasibility of sustainability in different areas of coatings and polymeric materials through different approaches. These projects explore the incorporation of green chemistry principles by utilizing bio-based sources, exploring alternative curing applications like radiation curing, exploring new alternative synthesis that utilize safer to handle reagents, and creating waterborne dispersions of polyurethane resins with novel and less hazardous crosslinking chemistries to replace the use of VOC solvents with water.

1.2. Thermosets

One of the most prevalent class of polymers in the industry of materials manufacturing includes thermosetting polymers also called thermosets. This class of polymers is commonly used in many industrial applications such as adhesives, sealants, coatings, and fiber composites. Thermosets consist of individual polymer chains that are connected or crosslinked by reactions of other polymeric chains (Figure 1.1). These interconnected chains form a network of covalently bonded species which contribute to a wide array of properties which include but are not limited to thermal resistance, mechanical characteristics, and chemical resistance. In contrast to their thermoplastic counter parts these crosslinks form three-dimensional networks which are considered irreversible and may be subjected to permanent deformation.

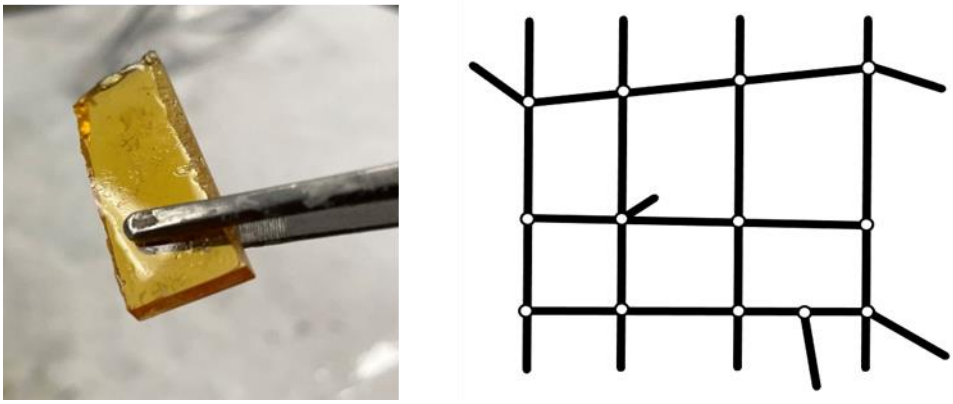

Figure 1.1: Photographic image of a thermoset (left). Basic general representation of a crosslinked thermoset network (right).

Conventionally, once a thermoset polymer has been produced it may no longer undergo the physical changes that thermoplastics undergo such as melting, reshaping and solubilize. Two common classes of resins used in thermoset applications are epoxy resins and polyurethanes.

1.3. Epoxy Resins

Epoxy resins have been a dominant force in the field of coatings and polymeric materials due to their high versatility and their high-performance applications. In thermosetting application epoxy resins have garnered some attention not just in coatings applications, but also composite reinforcement applications. Under the right circumstances, epoxy resins can be cured to provide high cross-linked structures which can potentially yield products with desirable qualities for performance coatings such as, high strength, adhesion, chemical resistance, thermal resistance, and storage modulus. These properties lead to epoxy resins being applied to a wide field of areas such as structural parts and adhesive markets.

The reasoning behind the overall properties of cured epoxy resins can be explained by their structure. The name “epoxy resin” is mainly referring to the main active functionality of the resin since the architecture of the resin itself may vary greatly. Typically, epoxy resins consist of three membered rings of which two are carbons and one is an oxygen (Figure 1.2). This heterocyclic structure is under a significant amount of ring strain which explains the relatively high reactivity of the resins to and its ability to react at mild reaction conditions.

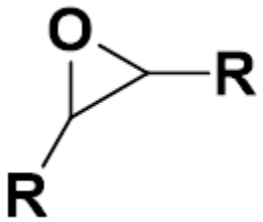

Figure 1.2: Structural representation of an epoxy functional group.

Depending on the curing conditions, these highly reactive functionalities yield highly crosslinked networks while maintaining the presence of low molecular weight species at a minimum. As a result, cured epoxy resins typical yield product that are desirable to industrial applications such as mechanical strength, thermal resistance, and chemical resistance.

As discussed before, a big interest in research pertaining to epoxy resins is their sustainability and health hazards. Currently petroleum-based epoxy resins do not have a role in a circular economy and taking a cradle-to grave view of the life cycle, one can observe that most of the resins end their lifecycle in landfill as discarded waste where degradation is slow to occur. The issue of health hazards is also one that needs to be addressed. One common example is bisphenol A (Figure 1.3). Bisphenol A is a petroleum-based precursor to synthesizing a commonly used epoxy resin known as bisphenol A diglycidyl ether.

Figure 1.3: Representation of bisphenol A and bisphenol A diglycidyl ether.

However, a study[10] conducted by the Center for Disease Control and Prevention (CDC) 95% of adults tested contained derivatives of Bisphenol A in urine samples indicating some sort exposure to Bisphenol A which may cause a variety of different health hazards.[11] As a result, industrial research is focused on replacing BPA in coatings, especially those that come into contact with food.Bio-Based Epoxy Resins

Most epoxy-based resins used industry are derived from precursors that are produced from petroleum-based sources. An option to create more sustainable epoxy resins is to derive them from more sustainable sources such as renewable feedstocks, vegetable oils, and proteins.

Vegetable oils have been extensively studied for use as alternative sources of epoxy resins. Oils produced from vegetable sources structurally consist of a triglyceride with unsaturated fatty acid chain illustrated in Figure 1.4. There are many different types of fatty acids. Some common ones re highlighted in Table 1.1.

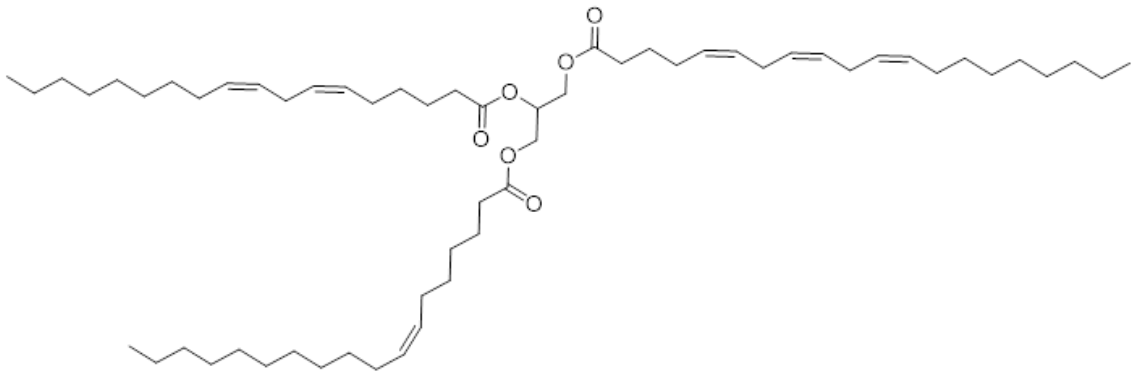

Figure 1.4: Chemical structure of a common vegetable oil triglyceride.

The composition of the fatty acids in vegetable oils can be influenced by a variety of different variables such as the type of plant the oil is derived from and the climate from which the plant was grown. The degree of unsaturation is measured by analytical methods and is commonly reported as an iodine value. Table 1.2 highlights how different plant-based oils will yield very different iodine value measurements

Table 1.1: Highlighting the degree of unsaturation in some common fatty acids.[12]

Fatty Acid	Unsaturation	Position(s) of Unsaturated Site
Oleic	C18:1	9
Linoleic	C18:2	9,12
Linolenic	C18:3	9,12,15
Palmitic	C16:0	N/A

.

These differences in fatty acid composition will yield a difference in degree of unsaturation. The unsaturated sites of the oils are they key starting points for producing epoxy resins.

Table 1.2: List of different plant-based oils and calculated iodine values.[5, 13-20]

Type of oil	Iodine Value (g/100 g)
Crude palm oil	53
Jatropha oil	105
Kenaf oil	86
Peanut oil	123
Coconut oil	9.9
Rapeseed	97-108
Corn oil	127-133
Sunflower oil	118-141
Soybean oil	124-139
Hempseed oil	154-165

The use of oxidizing agents allows for the addition of an oxygen atom in in the unsaturated site of the fatty acids. Techniques for epoxidizing vegetable oils can range and have development significantly over time. Some techniques which are known in the literature are the Prilezhaev epoxidation, ion exchange resin epoxidation, chemo-enzymatic epoxidation and metal-catalyzed epoxidation.[13-16] Currently, the most widely used method from the list is the ion exchange resin epoxidation and it was derived from the Prilezhaev epoxidation method as a response to mitigate the use of strong mineral acids and a homogenous catalyst for the sake of moving towards a more sustainable synthetic method. This characteristic is due to the use of solid ion exchange resins as catalyst that can be easily separated and recycled and allows for the use of relatively weaker acids such as acetic acid. There have been many published research works which have investigated the

epoxidation of plant based oil from different sources.[17] More recently, the use of Oxone (potassium peroxymonosulfate) has been garnering some attention as a non-chlorinated oxidizer due to the ease of handling and relatively safe reagents[18, 19].

However, most work[18, 20-23] that focuses on the epoxidation using dimethyldioxirane intermediates are on small alkene containing molecular species. The use of Oxone in vegetable oils is not as thoroughly investigated. The Oxone is used to form dimethyldioxirane intermediate in a biphasic system (Figure 1.5). These dimethyldioxirane intermediates are unstable and too reactive to isolate which causes a reaction with the unsaturated sites of the vegetable oils to yield an epoxidized product.[24] As of today, epoxidized soybean oils have found some commercial success in as plasticizers for PVC. Their relative low viscosity as means that epoxidized vegetable oils may have more success as reactive diluents in thermoset coating formulations.

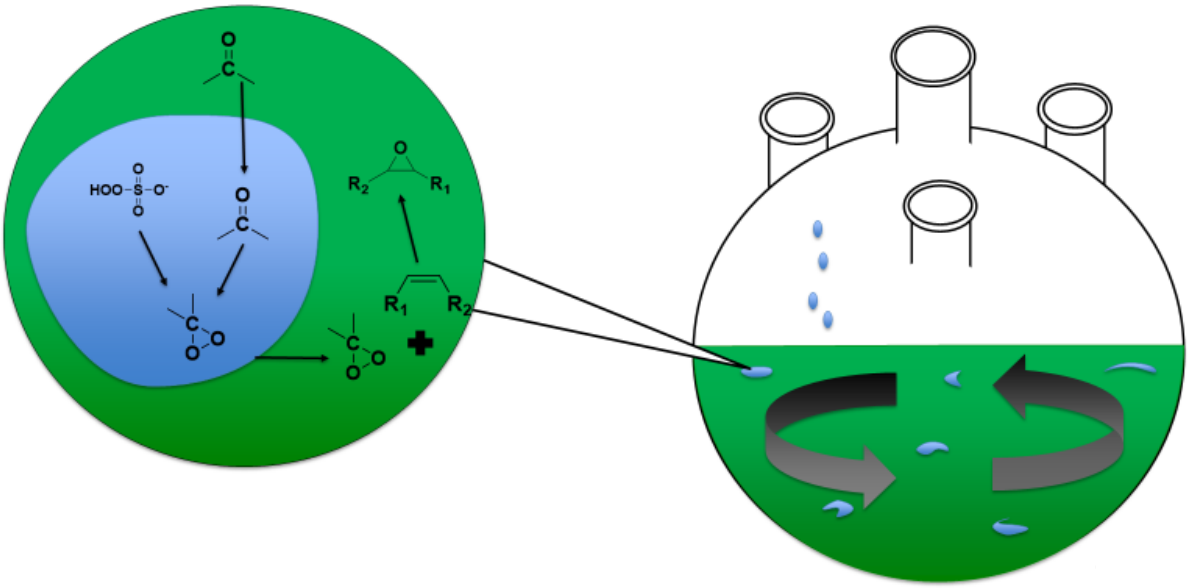

Figure 1.5: Visual representing the use of Oxone to generate dimethyl dioxirane intermediates in a biphasic system of oil and water.

1.4. UV-Curable Resins

Radiation curing consist of coating formulations that are specifically designed to undergo crosslinking reactions when subjected to high intensity radiation such a ultraviolet light. Implementation of radiation curing technology for thermoset resins is a means to crosslink resins in a more sustainable way. This technique provides several advantages when compared to conventional oven curing. Radiation curing generally has cure times that consist of a few seconds to a matter of a few minutes and are done at ambient temperature environments as opposed to large ovens. These requirements lead to formulations designed for radiation curable applications to have low energy requirements. From an industrial perspective, products can be coated faster and can be moved out quicker from production facilities to a customer's site. Formulations for radiation curing are generally designed to be low viscosity leading to formulations being designed for radiation curing to have little to no VOC since the use of solvents is not implemented. As such, radiation curing has found its way into many markets such as dental, coatings, composites, and 3D-printing.[25, 26]

While there are many methods that fall under the category of radiation curing, one particularly implements the use of Ultraviolet (UV) light to initiate polymerization using cationic species. The photodecomposition of an initiator that is sensitive to UV light will generate a strong acid that is highly reactive and initiates polymerization (Scheme 1.1).[27, 28]

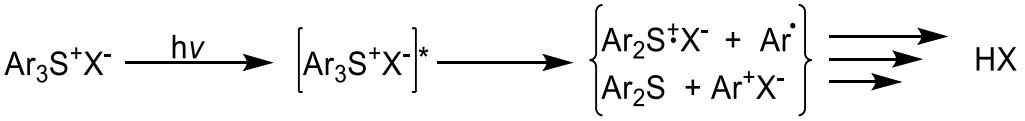

Scheme 1.1: General scheme of triarylsulfonium generating photoinitiators, where the X represents counteranions.

Significant work carried out by Crivello in the 1970's[29, 30] investigated the use of onium salts, which consist of cationic moieties and anionic moieties, to initiate cationic

photopolymerization of monomeric species. The structural architecture of the moieties has an impact on the overall properties of the photo initiator. The cationic moiety determines the light absorbing characteristics of the photoinitiator, thus, influencing the photosensitivity, quantum yield, and thermal stability of the compound. Meanwhile, the anionic moiety, also known as the counter anion, influences the strength of the acid that is generated, photo acid, which influences the curing kinetics of the reaction.

Virtually any cationically polymerizable system can be utilized which includes epoxy resins. When compared to other methods of photopolymerization, cationic photopolymerization yields products with better adhesion to substrates[31]. However, in the case of cationically induced photopolymerization of epoxy resins, low adhesion and impact resistance is typically observed. These properties can be explained by the highly crosslinked network that is created in a short amount of time. The crosslinked polymer chain network undergoes a significant amount of internal stress as it undergoes vitrification and thus shrinkage occurs at an average of 2-6% in volume which makes the coating prone to delamination[32]. There have been many different studies investigating ways to mitigate this issue such as exploring different polymer architectures in different formulations and using reactive diluents to modify the overall polymer properties all with the overall goal towards of moving towards a more sustainable production of polymeric materials.[33, 34]

1.5. Polyurethanes

Polyurethanes are polymer compounds that can be identified by their carbamate linkages in Figure 1.6.

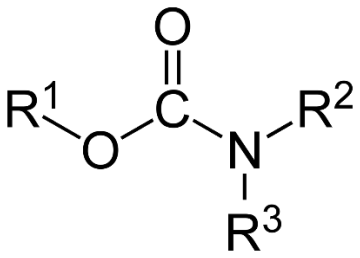

Figure 1.6: Representation of a urethane linkage chemical structure.

Thermoset applications for polyurethanes are myriad and range from two component urethanes utilized in automobile coatings to foams used in such applications as insulation or upholstery.[35, 36] The versatility of polyurethanes stems from the fact that most polyurethanes are made from "building block" chemical species that can widely vary in functionality and structure. A polyurethane may have a molecular architecture that utilizes different chemical species like isocyanates, polyols, ethers, esters, amines, and urea.[37-39] Additionally, the molecular structure of those different chemical species could vary from monomeric to polymeric as well as cyclic, aromatic, or aliphatic. That versatility is still being expanded upon today by investigating the feasibility of new chemical species to polyurethanes building blocks.

The numerous applications of polyurethanes in the coatings market extend from automotive, wood, artificial leather, and even protective industrial for marine environments. Depending on the design of the formulation, polyurethanes can achieve high performance characteristics such as durability, abrasion, strength, and flexibility. Depending on the application, different synthesis and formulation pathways exist. A polyurethane targeting automotive bodies will be formulated very differently from a polyurethane targeting wood home furniture. Common polyisocyanate curing agents that are used in two-component polyurethane coatings consist of aliphatic isocyanate trimers from isophorone diisocyanate (IPDI) and hexamethylene diisocyanate (HDI). The structures of the isocyanates are illustrated in Figure 1.7

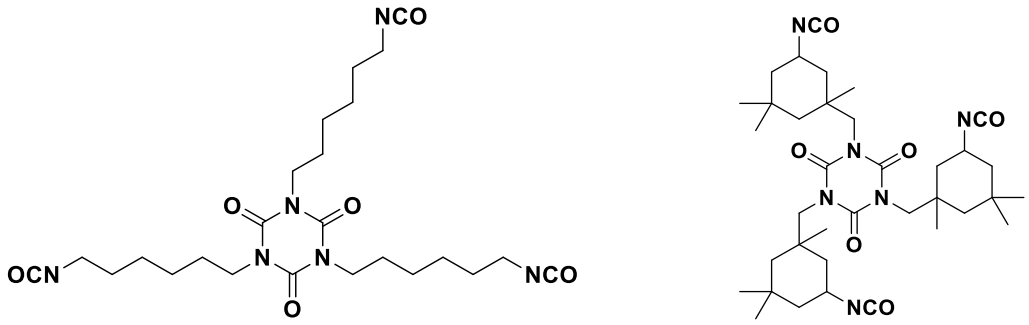

Figure 1.7: Chemical structure of HDI (left) and IPDI (right) trimers.

The functionality of the trimers consists of at least about three reactive functional groups which allow for formation of crosslinked three-dimensional networks. The aliphatic structures of the isocyanates are less prone to UV damage when compared to those that are aromatic. It is quite common for mixtures of different trimers to be employed in a formulation. HDI trimers contribute to flexibility which the IPDI trimers contribute to rigidity and hardness. It is clear that polyurethane technologies have been successful in applications regarding industrial use. However, there have been some concerns regarding the hazards associated with utilizing isocyanates in polyurethane formulations.

1.6. Non-Isocyanate Crosslinking

Isocyanate production generally utilizes reagents such as phosgene which is a gas that can cause serious harm if not handled correctly. Another issue is that some isocyanates now fall under the classification of carcinogenic, mutagenic and reprotoxic.[40-42] Hence, prolonged exposure to these compounds without proper personal protective gear is strongly discouraged. As a result, there have been some attempts in utilizing safer alternatives to minimize the use of isocyanates. This idea is the foundation behind non-isocyanate polyurethanes (NIPU).

There are several routes one can take to achieve a NIPU. [43-45] However, this body of work will focus on ring opening polymerization of cyclic carbonates. The pathway that consists of the ring opening reaction of cyclic carbonates gains its advantages on the fact that moisture sensitivity

and side products like urea and carbon dioxide are not a concern. Additionally, the versatility of this class of NIPU is further enhanced by the presence of hydroxyl groups that form when a reaction with amines is carried out. In coatings, the hydroxyl groups can alter the overall coatings properties with changes to the intermolecular forces. The hydroxyl functionality can also serve as an avenue for further polymerization through other chemistries which makes these NIPU a potential route for pre-polymer synthesis.

The reactivity of the cyclic carbonates when reacted with amines is a topic that has garnered some interest. The mechanism for the ring opening reaction of cyclic carbonates by amines as proposed is highlighted in Scheme 1.2.[46]

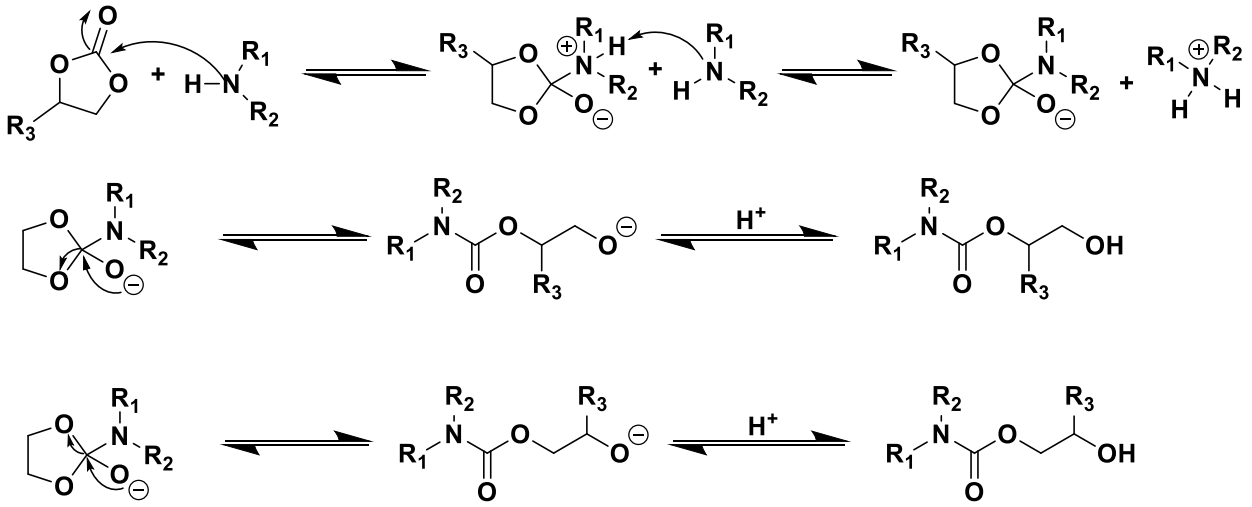

Scheme 1.2: Proposed mechanism for the reaction of 5 membered cyclic carbonates with amines.[46]

The reaction is carried out via the nucleophilic attack of the amine on the carbonyl atom creating a tetrahedral intermediate. Then, the intermediate undergoes deprotonation via a second amine and the ring opens at the carbon oxygen bond yielding the urethane species. This reaction is generally slower than the conventional isocyanate crosslinking reaction and thus different techniques to speed up the reaction have been investigated. Of these include studies[47-50] investigating the influence of cyclic carbonate structure on reactivity. It has been proposed that a

more feasible way to achieve ambient curing conditions is through the use of cyclic carbonates that contain higher number of atoms. Hence there is work studying the feasibility of 6, 7, even 8 membered cyclic carbonate rings for use in NIPU coatings. When comparing 6 membered cyclic carbonates 5 membered cyclic carbonates, it has been reported that under certain conditions the 6-membered cyclic carbonates can be 30 times more reactive than the 5 membered cyclic carbonates. The larger the cyclic structure the more reactive it is due to the ring strain of the molecule which may provide an opportunity for NIPU to be used as an alternative to isocyanate crosslinking polyurethanes in industrial applications.

A lesser-known route to achieve a NIPU considers the use of aldehyde-carbamate crosslinking chemistries to produce urethane linkages (Scheme 1.3).[51] The reaction consists of utilizing an acid catalyst which causes a reaction which allows for two carbamate functional group to react with one aldehyde group to yield two urethane linkages.[52]

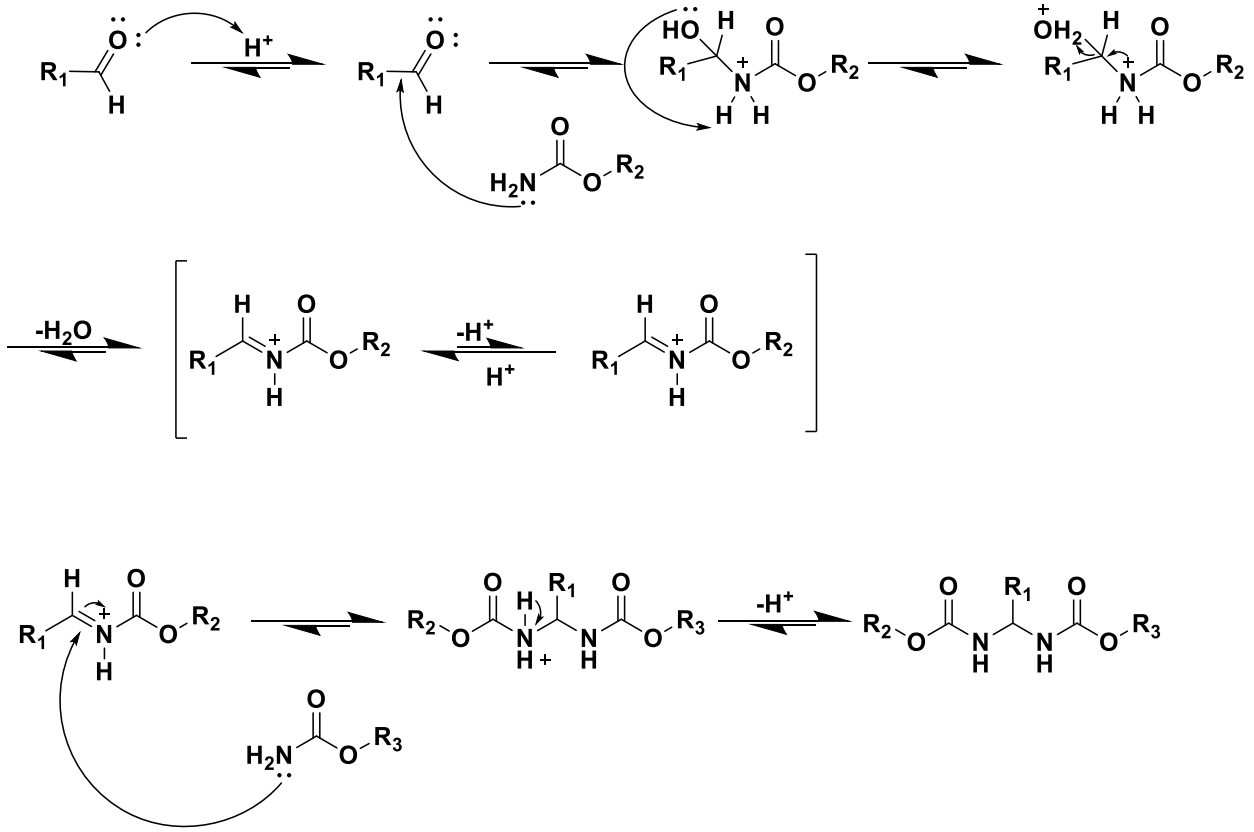

Scheme 1.3: Tentative mechanism for the crosslinking reaction of carbamates and aldehyde. Proposed in literature.[52]

Not only does this reaction fall under the NIPU category, but it merits further sustainability by potentially reducing the amount of crosslinker required to form a fully crosslinked network. Unfortunately, literature investigating the nuances and details of the reaction mechanism is severely lacking.[53, 54] Hence, the need to investigate the feasibility of the reaction in different systems is apparent.

1.7. Polyurethane Dispersions

Another means to approach sustainability with polyurethane technologies is to create dispersions that utilize water as opposed to solvents that are considered VOC. The use of solvents in general polyurethane synthesis and coatings formulations has always been a topic that is of interest due to the ever-increasing restrictions on the use of solvents. A way to achieve water borne

polyurethanes consists of the polyurethane designed to contain blocks in their polymer structure which consist of hydrophilic emulsifiers that stabilizes the polyurethane in water. These internal emulsifiers can consist of chemical compounds such as polyether-based materials that provide steric stability to a polymer species or through ionic stabilizers by which the dispersion is stabilized thought the electric double layer mechanism. The work in this dissertation focuses on the non-ionic mechanism of stabilization.

Although external emulsifiers exist, a non-ionic water borne polyurethane dispersion can be created by utilizing non-ionic internal emulsifiers in the backbone of the polyurethane structure. The dispersion of the polyurethane can be dictated by controlling three main factors includeing the reduction of the interfacial tension, high shear application, and low viscosity of the polyurethane component.[55] The interfacial tension is most commonly controlled by the composition of the polyurethane utilizing hydrophilic species of different molecular chain lengths such as polyethylene oxide or other ether moieties . As the dispersed particles come to close proximity, the hydrophilic chains in the water phase gain a restricted degree of freedom. As a result, there is an unfavorable reduction in entropy for the particles resulting in particle stability.

The non-ionic dispersions contain several advantages when compared to their ionic counterparts. Non-ionic dispersions tend to retain stability when subjected to pH changes.[56] This characteristic is advantageous when considering a crosslinking formulation that utilizes catalytic species which induce significant changes in pH. High shear mixing is typically implemented to achieve smaller particle sizes which contribute to greater stability.[57] However, high shear may place a dispersion at risk for coagulation, but resistance to coagulation via high shear mixing is another advantage of non-ionic dispersions. Incorporating a greater portion of hydrophilic components in the composition of a waterborne polyurethane dispersion will yield greater stability

due to smaller particle sizes. However, high concentrations of the hydrophilic moieties will cause the polyurethane to have less characteristics of a dispersion and more water-soluble characteristics which will increase viscosity and negatively affect coatings properties regarding moisture sensitivity.[58]

The work in this dissertation investigates several different aspects of synthetic and formulative work regarding epoxy and polyurethane resins with the overall goal to work towards sustainability. The use of Oxone to synthesize bio-based epoxy resins was investigated along with coatings characterization. These experiments were carried out to compare between ion exchange synthesized epoxy resins and dimethyl dioxirane synthesized epoxy resins. The study was followed by utilizing said synthesized bio-based epoxy resins in cationic photopolymerization with other petroleum-based diluents. Following that, waterborne borne polyurethane dispersion were synthesized for use in non-isocyanate crosslinking methods. The crosslinking chemistry consisted of cyclic carbonate-amine crosslinking and explored both 5-membered cyclic rings and 6-membered cyclic rings. Lastly, the feasibility of carbamate-aldehyde crosslinking chemistries was explored by direct comparison of solvent borne and water borne formulation applications.

1.8. References

1. Glavič, P.; Lukman, R., Review of sustainability terms and their definitions. *Journal of Cleaner Production* **2007,** *15* (18), 1875-1885.
2. Phillips, A. S.; Hung, Y.-T.; Bosela, P. A., Love canal tragedy. *Journal of Performance of Constructed Facilities* **2007,** *21* (4), 313-319.
3. Halden, R. U., Plastics and Health Risks. *Annual Review of Public Health* **2010,** *31* (1), 179-194.
4. Woodley, J. M., New frontiers in biocatalysis for sustainable synthesis. *Current Opinion in Green and Sustainable Chemistry* **2020,** *21*, 22-26.
5. Alam, M.; Akram, D.; Sharmin, E.; Zafar, F.; Ahmad, S., Vegetable oil based eco-friendly coating materials: A review article. *Arabian Journal of Chemistry* **2014,** *7* (4), 469-479.
6. Bobade, S. K.; Paluvai, N. R.; Mohanty, S.; Nayak, S. K., Bio-Based Thermosetting Resins for Future Generation: A Review. *Polymer - Plastics Technology and Engineering* **2016,** *55* (17), 1863-1896.
7. Fox, N. J.; Stachowiak, G. W., Vegetable oil-based lubricants-A review of oxidation. *Tribology International* **2007,** *40* (7), 1035-1046.
8. Zhou, X.; Li, Y.; Fang, C.; Li, S.; Cheng, Y.; Lei, W.; Meng, X., Recent Advances in Synthesis of Waterborne Polyurethane and Their Application in Water-based Ink: A Review. *Journal of Materials Science & Technology* **2015,** *31* (7), 708-722.
9. Sangermano, M.; Razza, N.; Crivello, J. V., Cationic UV-Curing: Technology and Applications. *Macromolecular Materials and Engineering* **2014,** *299* (7), 775-793.

10. Calafat, A. M.; Kuklenyik, Z.; Reidy, J. A.; Caudill, S. P.; Ekong, J.; Needham, L. L., Urinary Concentrations of Bisphenol A and 4-Nonylphenol in a Human Reference Population. *Environmental Health Perspectives* **2005,** *113* (4), 391-395.

11. Vandenberg, L. N.; Hauser, R.; Marcus, M.; Olea, N.; Welshons, W. V., Human exposure to bisphenol A (BPA). *Reproductive Toxicology* **2007,** *24* (2), 139-177.

12. Zhang, C.; Garrison, T. F.; Madbouly, S. A.; Kessler, M. R., Recent advances in vegetable oil-based polymers and their composites. *Progress in Polymer Science* **2017,** *71*, 91-143.

13. Hilker, I.; Bothe, D.; Prüss, J.; Warnecke, H.-J., Chemo-enzymatic epoxidation of unsaturated plant oils. *Chemical Engineering Science* **2001,** *56* (2), 427-432.

14. Lane, B. S.; Burgess, K., Metal-Catalyzed Epoxidations of Alkenes with Hydrogen Peroxide. *Chemical Reviews* **2003,** *103* (7), 2457-2474.

15. Freites Aguilera, A.; Rahkila, J.; Hemming, J.; Nurmi, M.; Torres, G.; Razat, T.; Tolvanen, P.; Eränen, K.; Leveneur, S.; Salmi, T., Epoxidation of Tall Oil Catalyzed by an Ion Exchange Resin under Conventional Heating and Microwave Irradiation. *Industrial & Engineering Chemistry Research* **2020,** *59* (22), 10397-10406.

16. Monono, E. M.; Bahr, J. A.; Pryor, S. W.; Webster, D. C.; Wiesenborn, D. P., Optimizing Process Parameters of Epoxidized Sucrose Soyate Synthesis for Industrial Scale Production. *Organic Process Research and Development* **2015,** *19* (11), 1683-1692.

17. Lewandowski, G.; Musik, M.; Malarczyk-Matusiak, K.; Sałaciński, Ł.; Milchert, E., Epoxidation of Vegetable Oils, Unsaturated Fatty Acids and Fatty Acid Esters: A Review. *Mini-Reviews in Organic Chemistry* **2020,** *17* (4), 412-422.

18. Charbonneau, L.; Foster, X.; Zhao, D.; Kaliaguine, S., Catalyst-Free Epoxidation of Limonene to Limonene Dioxide. *ACS Sustainable Chemistry and Engineering* **2018,** *6* (4), 5115-5121.

19. Hussain, H.; Green, I. R.; Ahmed, I., Journey describing applications of oxone in synthetic chemistry. *Chemical Reviews* **2013,** *113* (5), 3329-3371.

20. Alavi Nikje, M. M.; Rafiee, A.; Haghshenas, M., Epoxidation of polybutadiene using in situ generated dimethyl dioxirane (DMD) in the presence of tetra-n-butyl ammonium bromide. *Designed Monomers and Polymers* **2006,** *9* (3), 293-303.

21. Li, W.; Fuchs, P. L., A new protocol for in situ dioxirane reactions: Stoichiometric in oxone and catalytic in fluorinated acetophenones. *Organic Letters* **2003,** *5* (16), 2853-2856.

22. Saeed, A.; Larik, F. A.; Lal, B.; Faisal, M.; El-Seedi, H.; Channar, P. A., Recent resurgence toward the oxidation of heteroatoms using dimethyldioxirane as an exquisite oxidant. *Synthetic Communications* **2017,** *47* (9), 835-852.

23. Baumstark, A. L.; Harden, D. B., Epoxidation of α,β-Unsaturated Carbonyl Compounds by Dimethyldioxirane. *Journal of Organic Chemistry* **1993,** *58* (26), 7615-7618.

24. Mikula, H.; Svatunek, D.; Lumpi, D.; Glöcklhofer, F.; Hametner, C.; Fröhlich, J., Practical and efficient large-scale preparation of dimethyldioxirane. *Organic Process Research and Development* **2013,** *17* (2), 313-316.

25. Lai, H.; Peng, X.; Li, L.; Zhu, D.; Xiao, P., Novel monomers for photopolymer networks. *Progress in Polymer Science* **2022,** *128,* 101529.

26. Park, H.-Y.; Yeo, J.-G.; Choi, J.; Choe, G.-B.; Kim, G.-N.; Koh, Y.-H.; Yang, S.; Jung, Y.-G., Ceramic green and fired body with a uniform microstructure prepared using

living characteristics of photo-curable cycloaliphatic epoxide: Applicability of cycloaliphatic epoxide in photo-polymerization-based 3D printing. *Journal of the European Ceramic Society* **2022,** *42* (2), 589-599.

27. Gachet, B.; Lecompère, M.; Croutxé-Barghorn, C.; Burr, D.; L'Hostis, G.; Allonas, X., Highly reactive photothermal initiating system based on sulfonium salts for the photoinduced thermal frontal cationic polymerization of epoxides: a way to create carbon-fiber reinforced polymers. *RSC Advances* **2020,** *10* (68), 41915-41920.
28. Höfer, M.; Liska, R., Photochemistry and initiation behavior of phenylethynyl onium salts as cationic photoinitiators. *Journal of Polymer Science Part A: Polymer Chemistry* **2009,** *47* (13), 3419-3430.
29. Crivello, J. V.; Lam, J. H. W., Photoinitiated cationic polymerization with triarylsulfonium salts. *Journal of Polymer Science: Polymer Chemistry Edition* **1979,** *17* (4), 977-999.
30. Crivello, J. V.; Lam, J. H. W., Diaryliodonium salts. A new class of photoinitiators for cationic polymerization. *Macromolecules* **1977,** *10* (6), 1307-1315.
31. Yagci, Y.; Jockusch, S.; Turro, N. J., Photoinitiated polymerization: Advances, challenges, and opportunities. *Macromolecules* **2010,** *43* (15), 6245-6260.
32. Sangermano, M.; Roppolo, I.; Chiappone, A., New Horizons in Cationic Photopolymerization. *Polymers* **2018,** *10* (2).
33. Pierau, L.; Elian, C.; Akimoto, J.; Ito, Y.; Caillol, S.; Versace, D.-L., Bio-sourced monomers and cationic photopolymerization–The green combination towards eco-friendly and non-toxic materials. *Progress in Polymer Science* **2022,** *127*, 101517.

34. Hu, Y.; Yang, Z.; Gao, Y.; Nie, J.; Sun, F., Synthesis and properties of bio-based cationic photopolymerizable polysiloxane oxacyclobutanes based on nopol. *Progress in Organic Coatings* **2022,** *163*, 106681.

35. Pawlik, H.; Prociak, A., Influence of Palm Oil-Based Polyol on the Properties of Flexible Polyurethane Foams. *Journal of Polymers and the Environment* **2012,** *20* (2), 438-445.

36. Wang, X.; Soucek, M. D., Investigation of non-isocyanate urethane dimethacrylate reactive diluents for UV-curable polyurethane coatings. *Progress in Organic Coatings* **2013,** *76* (7-8), 1057-1067.

37. Gama, N.; Ferreira, A.; Barros-Timmons, A., Polyurethane Foams: Past, Present, and Future. *Materials* **2018,** *11* (10), 1841.

38. Huang, S.; Xiao, J.; Zhu, Y. a.; Qu, J., Synthesis and properties of spray-applied high solid content two component polyurethane coatings based on polycaprolactone polyols. *Progress in Organic Coatings* **2017,** *106*, 60-68.

39. Fuensanta, M.; Jofre-Reche, J. A.; Rodríguez-Llansola, F.; Costa, V.; Iglesias, J. I.; Martín-Martínez, J. M., Structural characterization of polyurethane ureas and waterborne polyurethane urea dispersions made with mixtures of polyester polyol and polycarbonate diol. *Progress in Organic Coatings* **2017,** *112* (April), 141-152.

40. Barbhuiya, M.; Bhunia, S.; Kakkar, M.; Shrivastava, B.; Tiwari, P.; Gupta, S., Fine needle aspiration cytology of lesions of liver and gallbladder: An analysis of 400 consecutive aspirations. *Journal of Cytology* **2014,** *31* (1), 20-24.

41. Bello, D.; Herrick Christina, A.; Smith Thomas, J.; Woskie Susan, R.; Streicher Robert, P.; Cullen Mark, R.; Liu, Y.; Redlich Carrie, A., Skin Exposure to Isocyanates: Reasons for Concern. *Environmental Health Perspectives* **2007,** *115* (3), 328-335.

42. Merenyi, S., *REACH: Regulation (EC) No 1907/2006: Consolidated version (June 2012) with an introduction and future prospects regarding the area of Chemicals legislation*. GRIN Verlag: 2012; Vol. 2.

43. Maisonneuve, L.; Lamarzelle, O.; Rix, E.; Grau, E.; Cramail, H., Isocyanate-Free Routes to Polyurethanes and Poly(hydroxy Urethane)s. *Chemical Reviews* **2015,** *115* (22), 12407-12439.

44. Khatoon, H.; Iqbal, S.; Irfan, M.; Darda, A.; Rawat, N. K., A review on the production, properties and applications of non-isocyanate polyurethane: A greener perspective. *Progress in Organic Coatings* **2021,** *154*, 106124.

45. Suryawanshi, Y.; Sanap, P.; Wani, V., Advances in the synthesis of non-isocyanate polyurethanes. *Polymer Bulletin* **2019,** *76* (6), 3233-3246.

46. Garipov, R. M.; Sysoev, V. A.; Mikheev, V. V.; Zagidullin, A. I.; Deberdeev, R. Y.; Irzhak, V. I.; Berlin, A. A., Reactivity of Cyclocarbonate Groups in Modified Epoxy–Amine Compositions. *Doklady Physical Chemistry* **2003,** *393* (1-3), 289-292.

47. Tomita, H.; Sanda, F.; Endo, T., Reactivity comparison of five- and six-membered cyclic carbonates with amines: Basic evaluation for synthesis of poly(hydroxyurethane). *Journal of Polymer Science Part A: Polymer Chemistry* **2001,** *39* (1), 162-168.

48. Tomita, H.; Sanda, F.; Endo, T., Model reaction for the synthesis of polyhydroxyurethanes from cyclic carbonates with amines: Substituent effect on the reactivity and selectivity of ring-opening direction in the reaction of five-membered cyclic carbonates with amine. *Journal of Polymer Science Part A: Polymer Chemistry* **2001,** *39* (21), 3678-3685.

49. Lombardo, V. M.; Dhulst, E. A.; Leitsch, E. K.; Wilmot, N.; Heath, W. H.; Gies, A. P.; Miller, M. D.; Torkelson, J. M.; Scheidt, K. A., Cooperative Catalysis of Cyclic Carbonate Ring Opening: Application Towards Non-Isocyanate Polyurethane Materials. *European Journal of Organic Chemistry* **2015,** *2015* (13), 2791-2795.

50. Yuen, A.; Bossion, A.; Gómez-Bengoa, E.; Ruipérez, F.; Isik, M.; Hedrick, J. L.; Mecerreyes, D.; Yang, Y. Y.; Sardon, H., Room temperature synthesis of non-isocyanate polyurethanes (NIPUs) using highly reactive N-substituted 8-membered cyclic carbonates. *Polymer Chemistry* **2016,** *7* (11), 2105-2111.

51. Silbert, S. D.; Serum, E. M.; Lascala, J.; Sibi, M. P.; Webster, D. C., Biobased, Nonisocyanate, 2K Polyurethane Coatings Produced from Polycarbamate and Dialdehyde Cross-linking. *ACS Sustainable Chemistry & Engineering* **2019,** *7* (24), 19621-19630.

52. Gérard, D.; Méchin, F.; Saint-Loup, R.; Fleury, E.; Pascault, J.-P., Study of the carbamate/aldehyde reaction, a new pathway towards NIPU materials. *Progress in Organic Coatings* **2022,** *165*, 106728.

53. Argyropoulos, J. N.; Anderson, J. R.; Kamber, N. E.; Ortiz, R. S., Ambient temperature curable isocyanate-free compositions for preparing crosslinked polyurethanes. Google Patents: 2018.

54. Anderson, J. R.; Spilman, G. E.; Popa, P. J.; Argyropoulos, J. N., Crosslinkable composition, a method of making the same and a crosslinked composition produced therefrom. Google Patents: 2017.

55. Schubert, K.; Bier, W.; Linder, G.; Herrmann, E.; Koglin, B.; Menzel, T., Method of producing dispersions and carrying out of chemical reactions in the disperse phase. Google Patents: 2001.

56. Honarkar, H., Waterborne polyurethanes: A review. *Journal of Dispersion Science and Technology* **2018,** *39* (4), 507-516.

57. Kwak, Y. S.; Park, S. W.; Kim, H. D., Preparation and properties of waterborne polyurethane-urea anionomers - Influences of the type of neutralizing agent and chain extender. *Colloid and Polymer Science* **2003,** *281* (10), 957-963.

58. Santamaria-Echart, A.; Fernandes, I.; Barreiro, F.; Corcuera, M. A.; Eceiza, A., Advances in waterborne polyurethane and polyurethane-urea dispersions and their eco-friendly derivatives: A review. *Polymers* **2021,** *13* (3), 1-32.

CHAPTER 2. COMPARISON OF EPOXIDATION METHODS FOR BIOBASED OILS: DIOXIRANE INTERMEDIATES GENERATED FROM OXONE VERSUS PERACID DERIVED FROM HYDROGEN PEROXIDE*

2.1. Abstract

Epoxidized oils are typically synthesized using hydrogen peroxide, as well as acetic acid or other acid equivalents. This synthesis requires heating, catalysts, and generates acidic waste. Recently, advances have been made in the process of using Oxone (potassium peroxymonosulfate) and ketones to generate *in situ* dioxiranes to epoxidize alkenes. The dioxirane method has allowed for room temperature reactions and can eliminate the use of peroxides and acids in the traditional epoxidation method. This study focuses on the epoxidation of soybean oil, hempseed oil and sucrose soyate using *in situ* generated dioxiranes. Parameters that may influence the degree of conversion of the reaction, such as molar ratios and addition rates, were studied. The data shows that optimum reaction conditions are reached when molar ratios of Oxone and unsaturation are 1.6:1 and Oxone addition rate is 1ml/min. As a comparison, epoxidations using the acetic acid/hydrogen peroxide method were carried out and cured materials were prepared from the epoxidized compounds. Negligible differences were identified in the materials prepared between both synthetic pathways. An environmental sustainability assessment using green chemistry principles was also conducted for both methods to evaluate their safety and efficiency with respect to multiple criteria including minimizing waste generation and energy consumption.

*The material included in this chapter was co-authored by Raul A Setien, Shokoofeh Ghasemi, Ghasideh Pourhashem, and Dean Webster. Raul Setien had the primary responsibilities of synthesis, preparing the crosslinked thermosets, drafting and revising all versions of this chapter. Shokoofeh Ghasemi had the primary responsibilities of carrying out the safety and environmental sustainability assessment Published article can be found at DOI:10.1002/pi.6193

The analysis shows that although the peracid method is atom economic and generates less waste, the dioxirane method offers better occupational safety and requires less energy, demonstrating the tradeoffs involved with either pathway if one is to be selected.

2.2. Introduction

Concerns for limiting the use of petroleum-based sources for the fabrication of thermosetting resins in polymer and coatings applications have been rising over the course of the past few years.[1] As a result, there is a rise in the need of development of biobased resins to potentially replace petroleum-based resins. An important class of these resins include epoxy functionalized resins. Epoxides are cyclic ethers in which the structure consists of an oxygen atom within a 3 membered ring. Epoxy resins lead to a vast array of materials having desirable properties such as good overall mechanical properties, good adhesion to substrates, as well as heat and chemical resistance.[2, 3] Epoxides can be used in the synthesis of resins containing other reactive groups such as hydroxyls, cyclic carbonates or (meth)acrylates.[4-6] Additionally, the uses of epoxy and epoxy-derived resins extend to applications in areas such as electronic materials, biomedical systems, and the aerospace industry.[7-10]

Bio-based resins derived from renewable resources are materials which have amassed a considerable interest. These materials are usually derived from either fats or oils, specifically vegetable oils.[11, 12] Not only are these vegetable oils considered inexpensive and renewable sources, but are fairly versatile given that the structures of these oils contain unsaturated fatty acids which can be functionalized through a variety of different methods, one of the most common being epoxidation.[13] The degree of unsaturation and types of fatty acids in the oils can alter the properties of oils greatly.[12, 14-19] As a result, there is a great deal of literature exploring the uses and applications of bio-based resins derived from vegetable oils. [20-24]

Another approach to altering the properties of materials derived from vegetable oils includes the use of fatty acid esters vegetable oils to synthesize resins with specific characteristics. An example of consists of using sucrose esters of unsaturated fatty acids derived from soybean oil to synthesize sucrose soyate.[25] The sucrose core along with highly branched long carbon chain structure gives sucrose soyate unique mechanical properties when compared to soybean oil. The Webster group has extensively researched the many different applications of this type of molecule and its functional derivatives in comparison to other vegetable oil based starting materials.[20, 21, 26-29] Traditionally, these epoxidized vegetable oil-based resins are synthesized using a peracids generated *in situ* to undergo epoxidation.[30] This process includes the use of hydrogen peroxide, an ion exchange resin and acetic acid in order to generate peracid, which is then used to convert unsaturated sites into oxirane rings (Scheme 2.1).

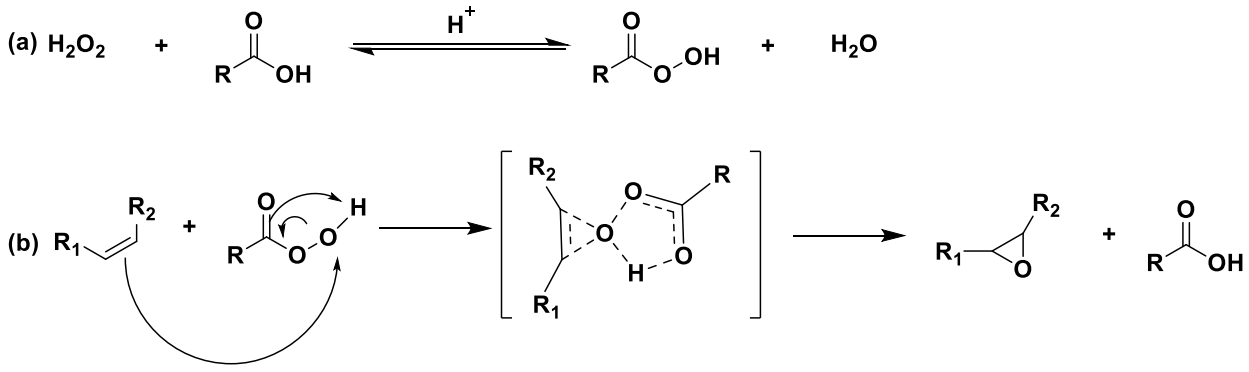

Scheme 2.1: Proposed mechanism of epoxidation of unsaturated sites utilizing peracids generated in situ with hydrogen peroxide and a source of carboxylic acids. (a) outline the generation of peracid, (b) outlines the consumption of peracid to yield the epoxidized products.

While the process itself is an improvement to older methods that utilized strong mineral acids, there are still some concerns that need to be addressed. The use of hydrogen peroxide in the synthesis raises some concerns regarding safety. Also, the waste that is generated from these reactions often requires additional reagents in order to properly neutralize and be disposed. Other

concerns stem from the reaction itself being exothermic which makes temperature control an issue which can then consequently result in unwanted side products to be generated.

Dioxiranes are an attractive and relatively new class of oxidants that have been gaining attention due to their epoxidation capabilities at room temperature and mild reaction conditions.[31-37] There is a variety of publications in literature that discuss and promote the use of oxone for the *in-situ* generation of dioxirane intermediates as a safer environmentally friendly oxidant.[35, 38-40] The dioxirane intermediates are generated in situ using Oxone (peroxymonosulfate) and a source of ketones. The dioxirane intermediates then epoxidize the unsaturated sites in a biphasic system (Scheme 2.2). Literature[34, 41] states that the dioxirane intermediates are more selective towards cis alkenes. In the case of oils, the alkenes are present in the cis configuration. In Addition, the synthesis can be limited to using a simple solvent system of water and acetone. Previous works have explored the epoxidation of fatty acid derivatives utilizing dioxirane intermediates.[42-46] However, more work is required in order to expand our understanding of how this reaction functions with different vegetable oils. Additionally, further work needs to be done to properly compare both synthetic methods to determine if there are any differences between the products obtained from both methods and to assess the safety and environmental issues of the two methods.

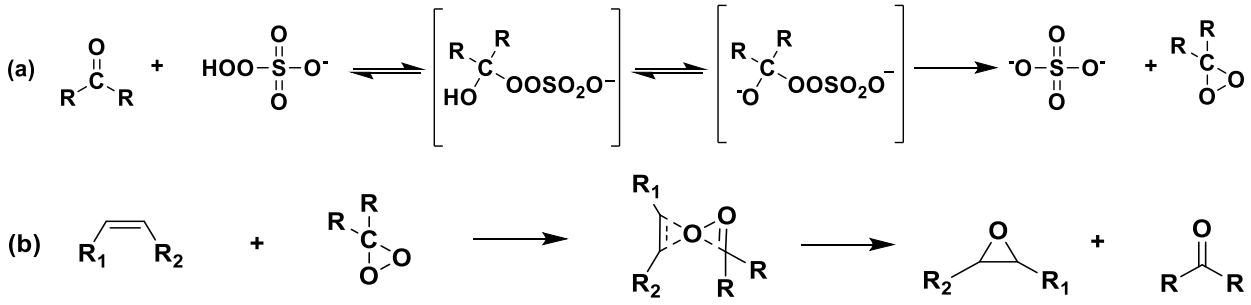

Scheme 2.2: Proposed reaction scheme for the epoxidation of unsaturated sites utilizing dimethyldioxirane intermediates generated *in situ* utilizing Oxone. (a) outlines the generation of dimethyldioxirane in *In situ* from a source of ketones, (b) outlines the epoxidation of unsaturated sites utilizing the dimethyldioxirane intermediate.

To address these issues, this study was designed to investigate the parameters that affect the epoxidation of unsaturated sites utilizing dimethyl dioxirane intermediates generated from Oxone. Additionally, thermosets and coatings made from the epoxidized resins synthesized using the two different methods are compared. Resins synthesized include epoxidized soybean oil, epoxidized hempseed oil, and epoxidized sucrose soyate. The two methods of epoxidation were compared using the principles of green chemistry.

2.3. Experimental

2.3.1. Materials

Sodium bicarbonate was purchased from Alfa Aesar. Acetic acid, magnesium sulfate, and sodium chloride were purchased from VWR while Amberlite® IR 120H, Oxone, sodium chloride, chloroform-d, acetone, and hexane were purchased from Sigma Aldrich. Deionized water was used for all the procedures that require water. For iodine value determination, sodium thiosulfate, chloroform, iodine solution according to Wijs, 10% wt potassium iodine solution and starch indicator solution 1%wt were used. Iodine solution according to Wijs was purchased from Acros Organics. Sodium thiosulfate 0.1N, starch indicator solution 1%, and 10% wt potassium iodide solution were purchased from VWR. Hempseed oil was provided by Healthy Oilseeds, Carrington, North Dakota. The hempseed oil was further refined by the NDSU Agricultural Engineering Department. Sucrose Soyate was provided by Procter and Gamble Chemicals. Soybean oil (Kirkland Signature Soybean Oil) was purchased from Costco. The iodine values of the oils were determined using a Wijs solution method based on AOCS method Tg 1a-64. The measured iodine values were as follows: hempseed oil, 160-163, sucrose soyate, 127, and soybean oil, 127. For epoxy anhydride thermosets, methylhexahydrophthalic anhydride (MHHPA) was used as the crosslinker and BV-CAT 7 was used as the catalyst. Both reagents were provided by Broadview

Chemicals. For epoxy-acid thermosets, the crosslinker, citric acid, was purchased from Sigma-Aldrich while methanol was purchased from VWR. Except as otherwise noted, all reagents were used as received without additional purification.

2.3.2. Epoxidation Utilizing Dimethyldioxirane Intermediates

A 250 mL 3 neck round bottom flask equipped with a mechanical stirrer was charged with a predetermined amount of oil (60 g), sodium bicarbonate (201 g) and acetone (693 g). A separate 500 mL beaker contained a predetermined amount of Oxone (184 g) dissolved in deionized water (1,115 mL). The reaction was stirred using an Arrow 1750 electric stirrer at ~340 rpmwhile the Oxone solution was slowly added to the reaction vessel via an FMI piston pump. The stirring was stopped when the addition of the Oxone was completed, approximately 18 hrs. The contents of the reaction flask were transferred to a separatory funnel, dissolved in hexane, and washed using a brine solution. The organic layer was separated and dried using magnesium sulfate overnight. Once dried, the magnesium sulfate was removed using vacuum filtration and the hexane was removed utilizing a rotary evaporator.

2.3.3. Epoxidation Utilizing Peroxyacid Intermediates

The molar ratios of reactants and reaction procedures were based of previous work.[47] A 250 mL 4 neck round bottom flask equipped with a mechanical stirrer, addition funnel, condenser, and thermocouple was placed in a heating mantle and charged with a predetermined amount of oil , Amberlite® IR 120H , and acetic acid. The molar ratios include (acetic acid:unsaturation) being (0.44:1) and (hydrogen peroxide:unsaturation) being (1.78:1). Amberlite® IR 120H is used at 17.3% based on the weight of sucrose soyate. For example, the epoxidation of 60 g of sucrose soyate would require 7.5 g of acetic acid, 34.6 g of hydrogen peroxide, and 10.4 g of Amberlite® IR 120H. The addition funnel was equipped with a nitrogen gas inlet and charged with a

predetermined amount of 50% wt hydrogen peroxide (47 g). The reaction was slowly heated to 60 ºC, stirred at ~340 rpm, and the hydrogen peroxide was slowly added to the reaction. Once the reaction was completed, approximately 5 hrs. the contents of the reaction vessel were transferred to a separatory funnel and were allowed to separate. The bottom layer was discarded and neutralized. The remaining contents of the separatory funnel were dissolved in hexane and neutralized utilizing a sodium bicarbonate solution. Once neutralized, the contents were washed with brine and separated. The remaining organic layer was dried using magnesium sulfate overnight. Once dried, the magnesium sulfate was removed using vacuum filtration and the hexane was removed utilizing a rotary evaporator.

2.3.4. Resin Characterization

Solids (non-volatile) content of the synthesized resins was determined in accordance to ASTM D 2369. The viscosity of the synthesized resins was determined at utilizing a Brookfield DV-II+ Pro viscometer with a HA/HB-1 spindle. Proton nuclear magnetic resonance spectroscopy (^{1}H NMR) was performed utilizing a Bruker system, Ascend 400 MHz magnet with an Avance III HD console (Bruker BioSpin Corporation, Billerica, Massachusetts, USA). The solvent used was $CDCl_3$. The conversion of unsaturated sites to epoxidized sites was determined by examining the Iodine value of the oils before and after epoxidation. The degree of unsaturation was determined using iodine value following AOCS method Tg 1a-64. The iodine value was used in order to calculate conversion (%) using eq 2.1:

$$Conversion\ (\%) = \frac{IV_a - IV_b}{IV_a} \times 100 \qquad (2.1)$$

Where IV_a is the determined iodine value before epoxidation and IV_b is the determined iodine value after epoxidation. Epoxy equivalent weight of the resins was determined following ASTM D1652. This value was used in the determination of percent epoxide using eq 2.2:

$$\frac{43 \times 100}{epoxy\ equivalent\ weight} = percent\ epoxide \quad (2.2)$$

2.3.5. Preparation of Epoxy-Anhydride Cured Thermosets

The epoxidized oils and epoxidized sucrose soyate synthesized were used to prepare epoxy anhydride coatings and thermosets. The anhydride used was MHHPA with BV-Cat 7 as the catalyst. The anhydride: epoxy molar ratios chosen for the formulations were 0.5, 0.75 and 1.0, while the catalyst amount was kept at 5% total weight. Samples were mixed in a Flack-tek mixer at 3500 RPM for 2 minutes. For thermosets, the formulations were poured in a silicone mold. The dimensions for the mold are as follows: width 12.8 cm, height 17.5 cm, thickness 3.2 cm. For coatings, the coatings were drawdown using a drawdown bar at 8 mils on cleaned cold rolled steel panels and glass panels. The curing conditions for both the coatings and the thermosets were 48 h at 80°C.

2.3.6. Preparation of Epoxy Acid Cured Coatings

The epoxy/acid/ formulation ratio consisted of the following for all epoxidized resins (1 : 1.0), (1 : 0.8) and (1 : 0.5). The acid : water : methanol ratio for all formulations consisted of (1 : 1.5 :0.5). For an example, an epoxy acid cured coatings with and epoxy:acid ratio of (1 : 1.0) and a EEW of 246 would contain 1.7 g of epoxy resin, 0.44 g of citric acid, 0.18 g of deionized water, and 0.11 g of methanol. The citric acid was dissolved in DI-water and methanol using a pressure vial at 75°C. Once the citric acid had dissolved, a predetermined amount of citric acid solution and designated epoxidized oil was poured into a pressure vial. The precuring conditions varied depending on the epoxidized oil being utilized and are as follows. ESBO (epoxidized soybean oil) containing formulations were precured for 1 hr at 80°C, ESS (epoxidized sucrose soyate) containing formulations were precured for 30 min at 80°C, and ESHO (Epoxidized hempseed oil) containing formulations were precured for 15 min at 80°C. The precured formulations were coated

on cleaned cold-rolled steel panels and cleaned glass panels using an 8 mil drawdown bar. The curing conditions were as follows, 75 ºC for 3h, 120 ºC for 1h, and 150 º C for 2h. The steel panel coatings were used for the determination of coatings properties while the coatings on the glass panels were removed and used for thermal analysis.

2.3.7. Coatings Characterization

Coating thickness was measured utilizing a Byko-Test 8500 coating thickness gauge. König pendulum hardness and pencil hardness were used to determine the harness of the coatings following ASTM D4366 and D3363, respectively. Coating adhesion to the substrate was determined via cross hatch adhesion following ASTM D 3359. The flexibility of the coatings was measured using a conical mandrel bend following ASTM D 522. The rapid deformation of the coatings was tested using a reverse impact test which follows ASTM D 2794. MEK double rubs was used to test the solvent resistance of the coatings. The method used a modified version of ASTM D 5402 which utilized a 26-ounce hammerhead wrapped in 6 layers of cheesecloth saturated in methyl ethyl ketone. The MEK soaked cloth was then placed at the base of the coating and rubbed back and forth until the substrate was exposed. The cheesecloth was rewet every 50 double rubs.

2.3.8. Thermal Gravimetric Analysis

The thermal decomposition of the thermosets was analyzed using a Q500 thermogravimetric system (TA Instruments) with the use of platinum pans. The samples were heated from room temperature to 600 ºC with a heating rate of 10º C/min.

2.3.9. Differential Scanning Calorimetry

The glass transition temperatures (T_g) of the coatings were determined using a DSC Q1000 (TA Instruments) using standard aluminum DSC pans with heating and cooling rates of 10°C/min at a heat/cool/heat cycle from -50°C to 180°C under nitrogen atmosphere.

2.3.10. Dynamic Mechanical Analysis

Dynamic mechanical analysis was carried out using a Q800 DMA (TA Instruments) operating at 15% amplitude and a heating rate of 3 °C/min from -50 °C to 180 °C (single cantilever mode). The storage modulus (E′) in the rubbery plateau region was determined at 60 °C above the T_g, which was calculated by determining the tan delta peak, and used to calculate the crosslink density (ν_e). Eq. 2.3 from the rubber elasticity theory was used to calculate the crosslinking density using the storage modulus:

$$E' = 3\nu_e RT \tag{2.3}$$

where E′ is the storage modulus in the rubbery plateau region, R is the gas constant, and T is the absolute temperature.

2.3.11. Safety and Environmental Sustainability Assessment

To ensure pollution prevention and minimize health and environmental risks of novel chemicals and processes, using indicators and metrics are essential. Such metrics allow for comparing alternative pathways and solutions to evaluate their “greenness” to support decision-making.[48] The principals for green chemistry and green engineering are well known for design of chemical products and processes that utilize resources (e.g. raw materials, energy) efficiently and reduce waste and toxic/hazardous chemicals use.[49] Here, the environmental sustainability and occupational safety of the two studied pathways for epoxidizing hempseed oil were assessed for their adherence to green chemistry principles.[50] Six principles applicable to these syntheses were

used including waste prevention, atom economy, safer solvents and auxiliaries, design for energy efficiency, catalysis and inherently safer chemistry for accident prevention. One of the most important steps in making organic reactions more environmentally sustainable is to maximize the efficiency of raw materials utilization and to minimize the waste generation. Waste prevention, here, was measured by E(nvironmental)-factor – mass of waste/mass of product, usually expressed as kg/kg – for assessing the environmental impact of manufacturing processes. A higher E-factor means more waste and, consequently, greater negative environmental impact is generated.[51] Atom economy (AE) is another effective metric which is widely used to evaluate the efficiency of a chemical reaction and greenness of a synthesis method. In an ideal reaction, all atoms of raw materials will appear in the desired product.[52] AE is calculated by dividing the molecular weight of the desired product by the sum of the molecular weights of all substances produced in the stoichiometric equation and expressed as a percentage.[53] Other principles were used as qualitative metrics for comparing the two synthetic pathways for epoxidizing hemp seed oil. In "safer solvents and auxiliaries" principle for example, the object is to eliminate and minimize the use of auxiliaries such as solvent whenever possible, but in many cases, the progress of the reaction is strongly dependent on the solvent. Therefore, for choosing solvent and other auxiliaries, it is necessary to consider the energy requirements, toxicity, life cycle environmental impacts and safety concerns.[50]

2.4. Results and Discussion

2.4.1. Synthesis of Epoxidized Oils

The first stage of this study was carried out to determine the optimal molar ratio of Oxone to moles of unsaturation and the optimum addition rate of Oxone solution using soybean oil. First, a series of epoxidation reactions were carried out where the ratio of Oxone to unsaturated groups was varied from 0.3 to 3.0 moles. By examining the NMR spectra (Figure 2.1), it is apparent how

the Oxone ratio affects the unsaturated site conversion to epoxy. The peaks at ~5.38 ppm show the olefin group of the unsaturated fatty acid chains in the soybean oil. Meanwhile the peaks at 4.18, 4,33 and 5.30 correspond to the protons in the glycerol backbone. Upon successful epoxidation, the spectra show the appearance of peaks at around 2.95-3.14 ppm due to the presence of the oxirane sites. Examination of the ^{1}H NMR spectra indicates that the reactions that contained less than 1.6 molar amount of Oxone contained unconverted saturated sites. At molar amounts of 1.6 and above, the conversion of unsaturation to epoxide appears to be close to completion.

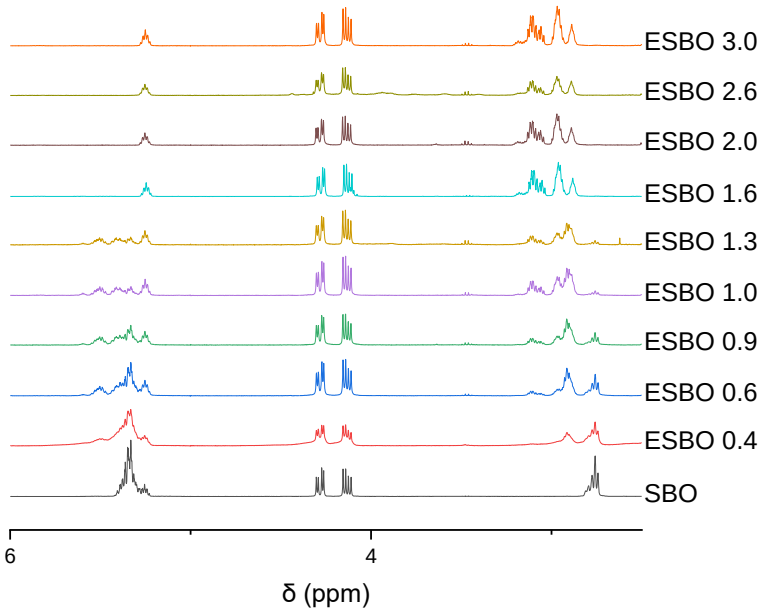

Figure 2.1: ^{1}H NMR spectra of SBO (soybean oil) and ESBO (epoxidized soybean oil) utilizing different moles of Oxone to moles of unsaturation. As the amount of Oxone increases, the peaks corresponding to the unsaturated sites (~5.38 ppm) decrease while the peaks corresponding to the oxirane sites (2.95-3.14) increase.

In order to supplement our understating of how varying Oxone ratios affect the degree of epoxidation in the yielded product, epoxy titrations and conversion (%) via iodine value before and after epoxidation were used to further analyze the epoxidized soybean oil (Table 2.1). The epoxy content of the epoxidized oil increased as the amount of Oxone increased. Once the amount

reached 1.6, the epoxy content began to plateau. The same trend can be observed by the conversion. The higher amount of Oxone yielded higher conversion. Once the Oxone amount reaches 1.6, the conversions plateau. From the ^{1}H NMR and the titration experiments, we can conclude that the ratio of moles of Oxone to moles of unsaturation is optimized at 1.6 : 1. Any further increase of amount of Oxone past 1.6 mol does not contribute further to epoxidation and can be considered wasteful. As a result, the addition rate studies focused on this specific concentration ratio.

Table 2.1: Synthesis composition of epoxidized oils used in this study. All synthesis ratios contain 1 mol of unsaturation with changing concentrations of Oxone. Oils consist of soybean oil (SBO) Hempseed oil (HSO) and sucrose soyate (SS). Numbers after oil name represents Oxone molar amount.

Name	Oil	Oxone (mol)	Oxone Addition Rates (ml/min)	Percent Epoxide (%)	Conversion (%)
ESBO 0.4	SBO	0.4	0.5	5.5	21.0
ESBO 0.6	SBO	0.6	0.5	8.8	36.0
ESBO 0.9	SBO	0.9	0.5	10.3	55.0
ESBO 1.0	SBO	1.0	0.5	13.6	70.0
ESBO 1.3	SBO	1.3	0.5	15.5	79.0
ESBO 1.6	SBO	1.6	0.5	19.2	98.0
ESBO 2.0	SBO	2.0	0.5	19.0	98.0
ESBO 2.6	SBO	2.6	0.5	18.7	98.0
ESBO 3.0	SBO	3.0	0.5	18.7	97.0
EHSO 1.0	HSO	1.0	1.0	19.8	70.0
EHSO 1.6	HSO	1.6	1.0	21.4	98.0
EHSO 3.0	HSO	3.0	1.0	21.5	97.0
ESS 1.0	SS	1.0	1.0	9.4	57.0
ESS 1.6	SS	1.6	1.0	18.5	95.0
ESS 2.0	SS	2.0	1.0	18.5	96.0
ESS 2.6	SS	2.6	1.0	18.1	95.0
ESS 3.0	SS	3.0	1.0	18.1	97.0

Literature has shown that Oxone is susceptible to decomposition if the concentration of dimethyldioxirane in the medium is too high.[54] Thus, it is imperative that the addition rate of Oxone solution is investigated so that an optimum flow rate for scale up is achieved. Starting with the data from the varying Oxone ratios, the addition rate of Oxone was explored. The addition rate investigated ranged from 0.5 – 10 (ml/min) using a consistent mole ratio of Oxone to unsaturation for all addition rates (1.6 : 1). Comparison of the NMR spectra using different Oxone addition rates shows that a conversion near completion can be achieved when the Oxone addition rate is set to 1 ml/min (Figure 2.2). The EEW and conversion values also show that good conversion can be achieved at 1 ml/min (Table 2.2).

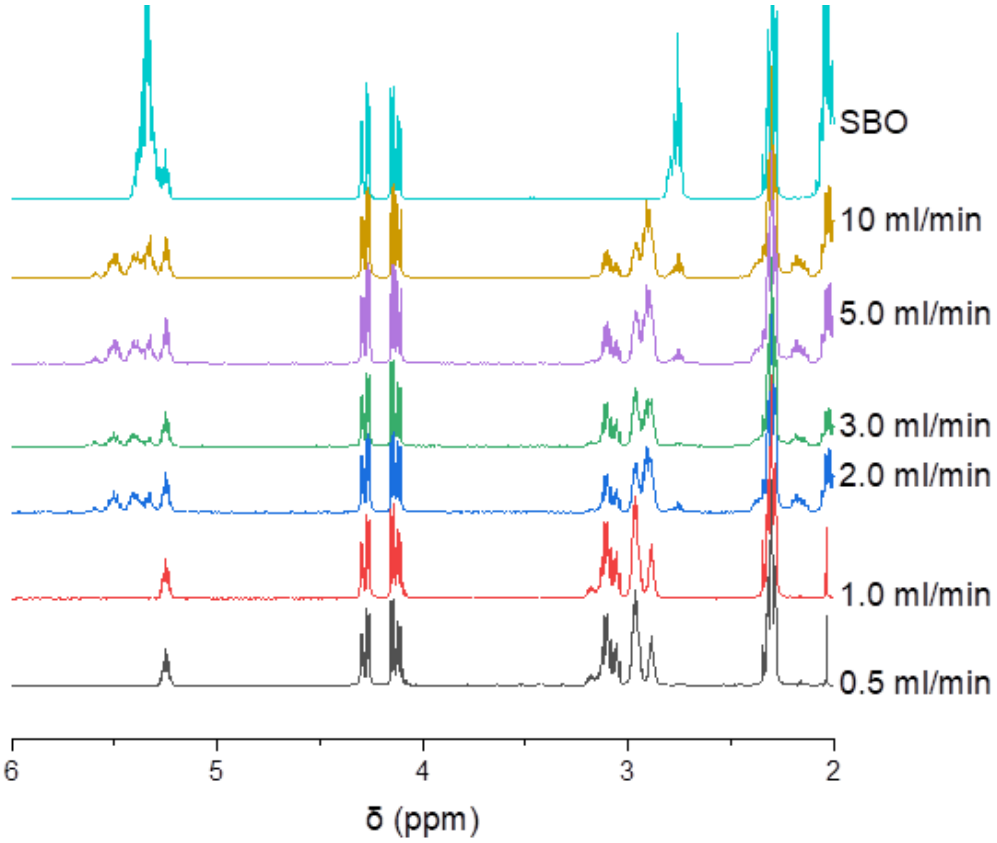

Figure 2.2: ^{1}H NMR spectra of synthesized ESBO utilizing different addition rates of Oxone. As the amount of Oxone increases, the peaks corresponding to the unsaturated sites (~5.38 ppm) decrease while the peaks corresponding to the oxirane sites (2.95-3.14) increase.

Table 2.2: Epoxy content and conversion (%) of different addition rates of Oxone using SBO. Molar ratios used coincided with those used in ESBO 1.6.

Addition Rate (ml/min)	Percent Epoxide (%)	Conversion (%)
0.5	20.9	95.0
1	18.1	96.0
2	17.8	94.0
3	16.7	85.0
5	14.4	78.0
10	12.5	70.0

Having established the best conditions for the ESBO synthesis utilizing dimethyl dioxirane intermediates, the procedure was adapted for the synthesis EHSO and ESS. The ^{1}H NMR spectra (Figure 2.3) show a similar trend as the ESBO NMR spectra (Figure 2.1) given that the conversion of unsaturated sites to oxirane sites appears to be complete when the Oxone molar ratios are at 1.6 mol and above for both EHSO and ESS synthesis. Additionally, the epoxy content and conversion (%) (Table 2.1) for EHSO and ESS support this statement given that the EEW and conversion (%) seems to plateau at Oxone molar ratios of 1.6 and above for all of the oils.

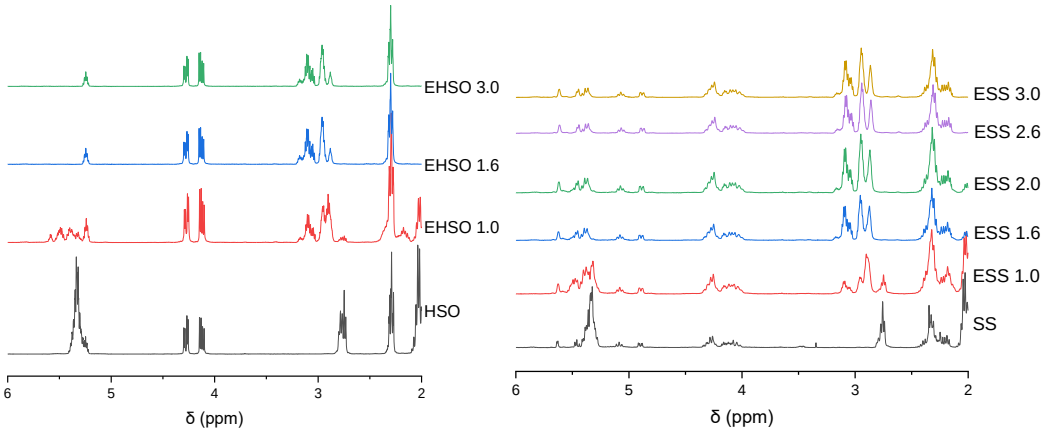

Figure 2.3: ^{1}H NMR spectra of synthesized EHSO (left) and ESS (right) utilizing different mole ratios of Oxone. For EHSO, as the amount of Oxone increases, the peaks corresponding to the unsaturated sites (~5.38 ppm) decrease while the peaks corresponding to the oxirane sites (2.95-3.14) increase. For ESS, the peaks corresponding to the unsaturated sites (~5.38 ppm) decrease while the peaks corresponding to the oxirane sites (2.95-3.14) increase.

Given that the overall goal of this study is to compare both the dimethyldioxirane and the peracid synthesis methods, the epoxidized oils were also synthesized using the peracid method and the resins were compared with resins made utilizing the dimethyl dioxirane method. Table 2.3 compares the characteristics of the epoxidized resins made by each method and illustrates the similarities between the resins synthesized using both methods. Resins synthesized using either method have similar properties with negligible differences. The resins were then used to formulate crosslinked thermosets and coatings to determine if there are any differences in the properties of the cured materials.

Table 2.3: Resin characteristics of both dioxirane and peracid synthesized resins.

Synthesis Method	**Dioxirane**			**Peracid**		
Resin Synthesized	ESBO	EHSO	ESS	ESBO	EHSO	ESS
Percent epoxy	17.9	21.4	18.5	17.5	22.2	18.1
Conversion (%)	96	99	97	98	99	98
Percent Solids (%)	98.7	97.7	96.0	98.6	97.5	99.1
Viscosity (mPa•s)	438	683	2350	423	721	2451

2.4.2. Crosslinking Resins

While crosslinking of bio-based resins has been previously studied, it is a goal of this study to show that the resins synthesized utilizing the dioxirane method do not compromise the properties of thermoset coatings when compared to materials made from epoxidized oils using the peracid method. The following section will highlight the properties of the cured resins via the epoxy-anhydride reaction and epoxy-acid reactions.

2.4.3. ATR-FTIR of Epoxy-Anhydride Coatings

ATR-FTIR was used to confirm that the coatings were fully cured (Figure 2.4). The coatings made utilizing the epoxy-anhydride reaction at a 1:1 ratio were tested in order to confirm that the reaction was undergoing to its full extent. For all of the epoxidized resins, ESBO, ESS, and ESHO, the ATR-FTIR shows that the systems are fully crosslinked. A first indication is the carbonyl and carbonyl ester peaks overlap at ~1740 cm^{-1}. The other indication is the lack of anhydride carbonyl peaks at 1857 cm^{-1} and 1780 cm^{-1} in the ATR-FTIR spectra for all coatings. The anhydride carbonyl peaks would only be present if unreacted anhydride were present in the systems.

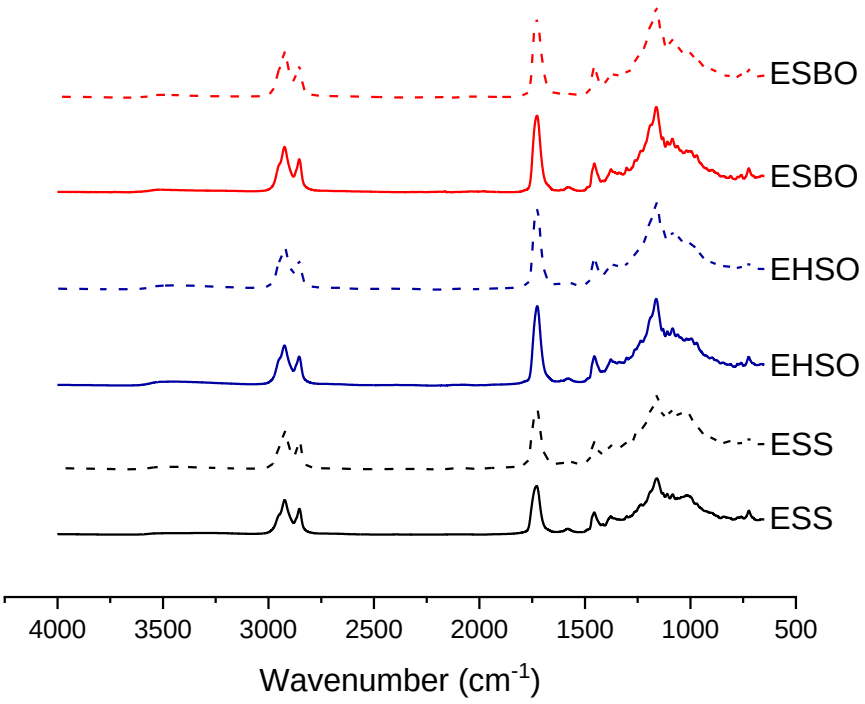

Figure 2.4: FTIR-ATR analysis of epoxy-anhydride crosslinked coatings. Dashed lines indicate the resins used were synthesized via the dioxirane method, while the solid lines indicate that the resins used were synthesized via the peracid method. Line color coding is as follows: red, ESBO, blue, EHSO, and black, ESS. ATR analysis shows no difference between the incorporation of epoxidized resins via the different synthetic pathways.

2.4.4. Epoxy-Anhydride Coatings

The formulations for the MHHPA crosslinked coatings and their properties are shown in Table 2.4. Regarding the ESBO coatings, the data exhibits a clear trend in the increase of coating properties (e.g. hardness) as the amount of MHHPA is increased. In general, the coating systems were very ductile, however such properties are expected from ESBO based epoxy coatings due to the long carbon chain fatty acids in the resin. A similar trend was observed with the EHSO coatings, however the coatings themselves were much harder and yield higher MEK double rubs. This property can be explained using the fact that the EHSO resins contained a lower EEW number due to the higher degree of unsaturation of the hempseed oil which would then correlate to the crosslinked coatings containing a higher degree of crosslinking compared to ESBO and thus the coatings contain better solvent resistance and higher mechanical properties. However, EHSO still contains the long carbon chain fatty acids hence the coatings retained some of their ductile properties. The ESS coatings exhibited properties of a highly crosslinked coatings. The ESS coatings contained high MEK double rubs and gave relatively hard coatings. However, the coatings were not as ductile due to the highly branched nature of the ESS molecule and thus the impact resistance of the coatings with the higher concentration of MHHPA was lower. Upon examination of the properties between the dioxirane coatings and the peracid coatings, the data shows that there are negligible differences between the coatings made from the resins synthesized via the two different epoxidation methods.

Table 2.4: Comparison of MHHPA crosslinked coatings.

Coatings Properties	(Epoxy:anhydride ratio)	Dioxirane			Peracid		
		ESBO	EHSO	ESS	ESBO	EHSO	ESS
Pencil Hardness	1 : 0.50	<8B	<8B	<8B	<8B	<8B	<8B
	1 : 0.75	<8B	3B	6B	<8B	3B	6B
	1 : 1.00	<8B	B	HB	<8B	B	HB
Adhesion	1 : 0.50	3B	5B	5B	3B	5B	5B
	1 : 0.75	5B	5B	5B	5B	5B	5B
	1 : 1.00	5B	5B	5B	5B	5B	5B
MEK Double Rubs	1 : 0.50	46	90	130	52	96	112
	1 : 0.75	76	232	372	79	250	380
	1 : 1.00	86	302	380	84	311	386
Reverse Impact (in·lb)	1 : 0.50	168.6	168.6	168.6	168.6	168.6	168.6
	1 : 0.75	168.6	168.6	125.4	168.6	168.6	125.4
	1 : 1.00	168.6	168.6	66.64	168.6	168.6	62.72
Mandrel Bend	1 : 0.50	Pass	Pass	Pass	Pass	Pass	Pass
	1 : 0.75	Pass	Pass	Pass	Pass	Pass	Pass
	1 : 1.00	Pass	Pass	Pass	Pass	Pass	Pass
König Hardness (sec)	1 : 0.50	11	16	22	13	12	19
	1 : 0.75	31	77	108	27	50	105
	1 : 1.00	55	157	144	56	150	152

2.4.5. Thermal Properties of MHHPA Crosslinked Systems

The thermal properties of the MHHPA crosslinked systems were examined and are highlighted in Table 2.5. The $T_{5\%}$ (ºC) of the systems were all on the higher end, above 200 °C. However, there is no clear trend on the systems' $T_{5\%}$ (ºC), the irregularities could be contributed to the residual solvent of the varying percent solids of the overall resin synthesis. The DSC shows a clear increase in glass transition temperature as the concentration of anhydride increases. This result can be attributed to the higher degree of crosslinking present in the system. The glass transition of the epoxy-anhydride thermosets obtained using DMA exhibit a much higher glass

transition than the DSC counterparts due to the different measurement methods and utilizes the tan delta of the thermoset to detect the glass transition. Figure 2.5 shows how the DMA curves of the thermosets overlap. This data helps illustrate how there is a negligible difference between the resins made utilizing the peracid method or the dimethyldioxirane method. While the glass transition data shows a clear trend of increasing glass transition as the concentration of anhydride increases, the storage modulus in the rubbery plateau and the crosslinking density do indicate some differences between the thermosets. However, these differences are believed to be due to minor variations in the network formation of the thermoset samples causing the storage modulus and the crosslinking density to vary.

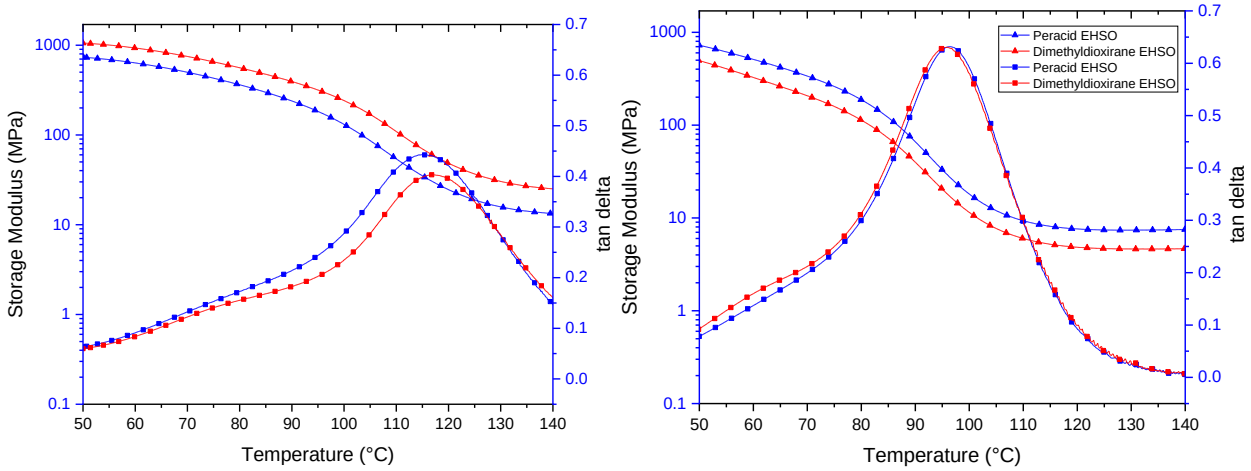

Figure 2.5: Example DMA curves of epoxy:anhydride thermosets from Table 5. Left corresponds to ESS resins at (1:1) epoxy:anhydride ratio. Right corresponds to EHSO resins at (1:1) epoxy anhydride ratio. DMA curves illustrate that there is a negligible difference between the incorporation of epoxidized resins via the different synthetic pathways.

Table 2.5: Comparison of MHHPA crosslinked coatings.

Thermal Property	(Epoxy:anhydride ratio)	Dioxirane			Peracid		
		ESBO	EHSO	ESS	ESBO	EHSO	ESS
$T_{5\%}$ (ºC)	1 : 0.50	291.16	266.38	279.91	278.52	279.18	266.63
	1 : 0.75	277.76	285.69	202.10	277.76	279.43	275.53
	1 : 1.00	259.65	230.05	210.75	232.61	269.49	285.81
T_g (ºC) (DSC)	1 : 0.50	-22.37	-6.33	24.47	-5.33	-5.33	27.79
	1 : 0.75	14.43	17.26	54.08	15.35	4.72	56.19
	1 : 1.00	16.57	42.17	72.79	13.42	47.91	67.37
T_g (ºC) (DMA)	1 : 0.50	28.85	52.44	62.36	26.08	41.65	56.45
	1 : 0.75	55.98	77.18	97.65	56.05	78.18	84.40
	1 : 1.00	73.33	96.04	117.08	78.67	96.46	115.59
E′ (MPa) at Tg+60 °C	1 : 0.50	2.61	7.63	20.97	4.88	7.52	9.25
	1 : 0.75	6.54	5.04	20.07	8.76	5.89	14.41
	1 : 1.00	4.71	4.88	26.25	9.79	7.96	14.56
v_e (mol/m^3)	1 : 0.50	288.97	793.35	2126.54	544.32	804.43	952.47
	1 : 0.75	674.09	492.83	1868.49	902.97	573.93	1384.14
	1 : 1.00	465.14	456.03	2338.34	953.46	743.03	1301.31

2.4.6. Citric Acid Crosslinked Coatings

The other method of crosslinking the epoxidized resins consisted of using citric acid to crosslink the epoxidized oils. The coatings properties of the crosslinked resins yielded similar trends to those of the anhydride cured coatings, but with different properties (Table 2.6). The coatings made using ESBO were very ductile as they contained low König hardness, high reverse impact and low pencil hardness. This property can be attributed to the long carbon chains in the ESBO structure. The solvent resistance of the coatings was adequate, however the coatings exhibited a downward trend in solvent resistance as the amount of citric acid concentration increased. This trend may be due excess citric acid left unreacted or insolubilized in the coating

thus having a negative effect on the coatings properties. The EHSO yielded the hardest coatings out of the other two epoxidized resins. The EHSO coatings surpassed the other two resins in pencil hardness and König hardness while still passing the mandrel bend test. Again, this property can be attributed to the coating retaining its flexibility due to the long carbon chain structure of the EHSO but its hardness and high solvent resistance is provided by the higher degree of epoxy groups in the resin. The ESS gave relatively good coatings. While the coatings did not contain the same hardness as the EHSO coatings, the lower concentrations did contain high solvent resistance. The coatings with higher concentrations of citric acid did fail the mandrel bend test, meaning the coatings do not perform well under slow deformation. This property can again be attributed to the fact that the ESS structure is highly branched and has a high degree of functional groups per molecule resulting in a high crosslink density that makes them more suspectable to damage due to deformation. Finally, in comparing the properties of the peracid synthesized resins and the dioxirane synthesized resins we see negligible differences between the two coating sets further illustrating that there are potentially no distinguishable differences between the resins produced from the two different synthesis methods.

Table 2.6: Comparison of Citric Acid crosslinked coatings.

Coatings Properties	Epoxy: Acid ratio	Dioxirane			Peracid		
		ESBO	EHSO	ESS	ESBO	EHSO	ESS
Pencil Hardness	1 : 0.50	4B	H	5B	4B	H	3B
	1 : 0.80	4B	H	B	4B	H	B
	1 : 1.00	5B	2H	HB	5B	2H	HB
Adhesion	1 : 0.50	5B	4B	5B	5B	4B	5B
	1 : 0.80	5B	5B	5B	5B	5B	5B
	1 : 1.00	5B	5B	5B	5B	5B	5B
MEK Double Rubs	1 : 0.50	250	320	>400	233	312	>400
	1 : 0.80	178	>400	>400	180	>400	>400
	1 : 1.00	145	>400	>400	100	>400	>400
Reverse Impact (in·lb)	1 : 0.50	168.6	27.49	70.56	168.6	27.49	70.56
	1 : 0.80	168.6	11.76	19.6	168.6	11.76	19.6
	1 : 1.00	168.6	7.84	11.76	168.6	5.88	11.76
Mandrel Bend	1 : 0.50	Pass	Pass	Pass	Pass	Pass	Pass
	1 : 0.80	Pass	Pass	Fail (5cm)	Pass	Pass	Fail (5cm)
	1 : 1.00	Pass	Pass	Fail (5cm)	Pass	Pass	Fail (3cm)
König Hardness (sec)	1 : 0.50	13	74	49	13	85	50
	1 : 0.80	16	109	105	18	114	105
	1 : 1.00	22	116	109	24	128	112

2.4.7. Thermal Properties Citric Acid Cured Coatings

The thermal properties of the citric acid coatings (Table 2.7) were determined using TGA and DSC. The $T_{5\%}$ of the coatings showed a clear trend where the coatings with higher concentrations of citric acid contained lower thermal decomposition than those of lower concentrations. The results imply there may be some unreacted citric acid in the systems and thus the lower thermal decomposition is observed. The glass transition temperatures of the systems show an increase of glass transition as the amount of citric acid is increased, which is indicative of a higher crosslink density network.

Table 2.7: Comparison of citric acid crosslinked systems.

Thermal Property	(Epoxy:Acid ratio)	Dioxirane			Peracid		
		ESBO	EHSO	ESS	ESBO	EHSO	ESS
$T_{5\%}$ (ºC)	1 : 0.5	289.17	272.15	277.34	277.63	269.97	278.79
	1 : 0.8	264.40	260.09	263.63	262.73	259.55	236.46
	1 : 1.0	254.09	260.96	259.02	255.82	249.53	258.85
T_g (ºC) (DSC)	1 : 0.5	-6.30	12.43	10.04	-8.93	11.42	10.79
	1 : 0.8	1.78	10.07	11.76	-0.2	9.52	14.78
	1 : 1.0	6.19	16.24	13.45	5.91	14.32	12.92

2.4.8. Safety and Sustainability Evaluation

The safety and sustainability of the two methods for epoxidizing hemp seed oil were evaluated based on their adherence to green chemistry principles (Table 2.8). For some principles, the peracid method performed environmentally better than the dioxirane method and in others the dimethyldioxirane method could be considered more sustainable. In waste minimization, the peracid method displayed a lower E-factor which means less waste is generated in this pathway. The peracid method has also higher AE, which demonstrates higher efficiency of this method for maximizing the incorporation of reactants' atoms in the final product. However, in energy consumption, the dimethyldioxirane method is more efficient because the peracid method, while requiring initial heating, comprises a highly exothermic reaction, which requires a large amount of energy for lowering and controlling the reaction temperature. Besides, this exothermic reaction via peracid method can be unsafe while increasing the likelihood of chemical accidents happening. Additionally, the oxidant used in dimethyldioxirane method, oxone, is much safer to work with than hydrogen peroxide. Hydrogen peroxide is a strong oxidizer and requires special handling precautions. As catalytic reagents are superior to stoichiometric reagents,[50] the peracid method is more desirable because, in this method, an ion exchange catalyst is used, which accelerates the rate of the reaction without being consumed and therefore, does not generate waste. In the

dioxirane method, however, the reaction proceeds at a very slow rate and it will take a longer time to be completed.

Table 2.8: Safety and sustainability comparison of epoxidation methods based on Green Chemistry Principles.

Principle	Dimethyldioxirane Method	Peracid Method
Waste Prevention E-factor (Kg/Kg)	9.7	3.1
Atom Economy (%)	8.5	65.8
Design for Energy Efficiency	Process requires lower energy.	Process requires higher energy.
Inherently Safer Chemistry for Accident Prevention	Safe	Not safe A highly exothermic reaction that has potential for chemical accidents.
Safer Solvents and Auxiliaries	Oxone is a safer oxidizer.	H_2O_2 is a strong oxidizer.
Catalysis	Stoichiometric reagents	Stoichiometric and catalyst reagents

However, such an assessment may have some shortcomings including assigning the same weight to all types of waste or disregarding the substances used in the workup of the reaction mixture. Thus, for a comprehensive assessment, other tools such as life cycle assessment (LCA)[55] and techno-economic analysis [56] could be supplemented to identify the most sustainable synthesis methods and help in identifying hotspots for improving the overall environmental, health and economic performance of the process.

2.5. Conclusion

The work done in the epoxidation of vegetable oil-based sources to replace petroleum-based epoxy resins is of importance. This study explored the use of Oxone to generate

dimethyldioxirane intermediates to epoxidize vegetable-oil based resins. The resins synthesized through the dimethyldioxirane method were compared to the resins synthesized using the peracid approach. The resins demonstrated similar properties with negligible differences. Crosslinking systems of the resins were tested and were found to result in similar networks with similar mechanical and thermal properties. While this new alternative approach (dioxirane) for epoxidizing vegetable oils provides a safer reaction, it generates more waste and has lower atom efficiency. Further work needs to be explored with regard to lowering solvent usage and decreasing reaction time of the dimethyldioxirane system. In addition, other methods to quantify the overall environmental impacts such as LCA can aid in providing a more comprehensive evaluation of the two pathways.

2.6. References

1. Babu, R. P.; O'Connor, K.; Seeram, R., Current progress on bio-based polymers and their future trends. *Progress in Biomaterials* **2013,** *2* (1), 8.
2. Chen, X.; Hou, J.; Gu, Q.; Wang, Q.; Gao, J.; Sun, J.; Fang, Q., A non-bisphenol-A epoxy resin with high Tg derived from the bio-based protocatechuic Acid:Synthesis and Properties. *Polymer* **2020,** *195*.
3. Xiong, G.; Kang, P.; Zhang, J.; Li, B.; Yang, J.; Chen, G.; Zhou, Z.; Li, Q., Improved adhesion, heat resistance, anticorrosion properties of epoxy resins/POSS/methyl phenyl silicone coatings. *Progress in Organic Coatings* **2019,** *135*, 454-464.
4. Yu, A. Z.; Rahimi, A.; Webster, D. C., High performance bio-based thermosets from dimethacrylated epoxidized sucrose soyate (DMESS). *European Polymer Journal* **2018,** *99*, 202-211.
5. Yu, A. Z.; Setien, R. A.; Sahouani, J. M.; Docken, J.; Webster, D. C., Catalyzed non-isocyanate polyurethane (NIPU) coatings from bio-based poly(cyclic carbonates). *Journal of Coatings Technology and Research* **2019,** *16* (1), 41-57.
6. Mora, A.-S.; Tayouo, R.; Boutevin, B.; David, G.; Caillol, S., Synthesis of biobased reactive hydroxyl amines by amination reaction of cardanol-based epoxy monomers. *European Polymer Journal* **2019,** *118*, 429-436.
7. Ho, T. H.; Wang, C. S., Modification of epoxy resins with polysiloxane thermoplastic polyurethane for electronic encapsulation: 1. *Polymer* **1996,** *37* (13), 2733-2742.
8. Lin, L. L.; Ho, T. H.; Wang, C. S., Synthesis of novel trifunctional epoxy resins and their modification with polydimethylsiloxane for electronic application. *Polymer* **1997,** *38* (8), 1997-2003.

9. Barua, S.; Dutta, N.; Karmakar, S.; Chattopadhyay, P.; Aidew, L.; Buragohain, A. K.; Karak, N., Biocompatible high performance hyperbranched epoxy/clay nanocomposite as an implantable material. *Biomedical Materials* **2014,** *9* (2), 025006-025006.

10. Kandare, E.; Kandola, B. K.; Myler, P., Evaluating the influence of varied fire-retardant surface coatings on post-heat flexural properties of glass/epoxy composites. *Fire Safety Journal* **2013,** *58*, 112-120.

11. Xia, Y.; Larock, R. C., Vegetable oil-based polymeric materials: Synthesis, properties, and applications. *Green Chemistry* **2010,** *12* (11), 1893-1909.

12. Zhang, C.; Garrison, T. F.; Madbouly, S. A.; Kessler, M. R., Recent advances in vegetable oil-based polymers and their composites. *Progress in Polymer Science* **2017,** *71*, 91-143.

13. Tan, S. G.; Chow, W. S., Biobased Epoxidized Vegetable Oils and Its Greener Epoxy Blends: A Review. *Polymer-Plastics Technology and Engineering* **2010,** *49* (15), 1581-1590.

14. Atimuttigul, V.; Damrongsakkul, S.; Tanthapanichakoon, W., Effects of oil type on the properties of short oil alkyd coating materials. *Korean Journal of Chemical Engineering* **2006,** *23* (4), 672-677.

15. Yalcin, H.; Toker, O. S.; Dogan, M., Effect of oil type and fatty acid composition on dynamic and steady shear rheology of vegetable oils. *Journal of Oleo Science* **2012,** *61* (4), 181-187.

16. Ataei, S.; Khorasani, S. N.; Neisiany, R. E., Biofriendly vegetable oil healing agents used for developing self-healing coatings: A review. *Progress in Organic Coatings* **2019,** *129* (December 2018), 77-95.

17. Bobade, S. K.; Paluvai, N. R.; Mohanty, S.; Nayak, S. K., Bio-Based Thermosetting Resins for Future Generation: A Review. *Polymer - Plastics Technology and Engineering* **2016,** *55* (17), 1863-1896.

18. Sawpan, M. A., Polyurethanes from vegetable oils and applications: a review. *Journal of Polymer Research* **2018,** *25* (8).

19. Fox, N. J.; Stachowiak, G. W., Vegetable oil-based lubricants-A review of oxidation. *Tribology International* **2007,** *40* (7), 1035-1046.

20. Ma, S.; Webster, D. C., Naturally Occurring Acids as Cross-Linkers To Yield VOC-Free, High-Performance, Fully Bio-Based, Degradable Thermosets. *Macromolecules* **2015,** *48* (19), 7127-7137.

21. Ma, S.; Kovash, C. S.; Webster, D. C., Effect of solvents on the curing and properties of fully bio-based thermosets for coatings. *Journal of Coatings Technology and Research* **2017,** *14* (2), 367-375.

22. Stemmelen, M.; Lapinte, V.; Habas, J. P.; Robin, J. J., Plant oil-based epoxy resins from fatty diamines and epoxidized vegetable oil. *European Polymer Journal* **2015,** *68*, 536-545.

23. Fernandes, F. C.; Kirwan, K.; Wilson, P. R.; Coles, S. R., Sustainable Alternative Composites Using Waste Vegetable Oil Based Resins. *Journal of Polymers and the Environment* **2019,** *27* (11), 2464-2477.

24. Mahendran, A. R.; Wuzella, G.; Aust, N.; Kandelbauer, A.; Müller, U., Photocrosslinkable modified vegetable oil based resin for wood surface coating application. *Progress in Organic Coatings* **2012,** *74* (4), 697-704.

25. Pan, X.; Sengupta, P.; Webster, D. C., Novel biobased epoxy compounds: epoxidized sucrose esters of fatty acids. *Green Chemistry* **2011,** *13* (4), 965.

26. Paramarta, A.; Webster, D. C., The exploration of Michael-addition reaction chemistry to create high performance, ambient cure thermoset coatings based on soybean oil. *Progress in Organic Coatings* **2017,** *108*, 59-67.

27. Paramarta, A.; Pan, X.; Webster, D. C., Highly functional acrylated biobased resin system for UV-curable coatings. *Radtech Report* **2013,** *1* (1), 26-32.

28. Pan, X.; Sengupta, P.; Webster, D. C., Novel biobased epoxy compounds: Epoxidized sucrose esters of fatty acids. *Green Chemistry* **2011,** *13* (4), 965-975.

29. Yu, A. Z.; Sahouani, J. M.; Setien, R. A.; Webster, D. C., Effect of nature and extent of functional group modification on properties of thermosets from methacrylated epoxidized sucrose soyate. *Reactive and Functional Polymers* **2018,** *128*, 29-39.

30. Milchert, E.; Malarczyk-Matusiak, K.; Musik, M., Technological aspects of vegetable oils epoxidation in the presence of ion exchange resins: a review. *Polish Journal of Chemical Technology* **2016,** *18* (3), 128-133.

31. Adam, W.; Curci, R.; Edwards, J. O., Dioxiranes: A New Class of Powerful Oxidants. *Accounts of Chemical Research* **1989,** *22* (6), 205-211.

32. Baumstark, A. L.; Harden, D. B., Epoxidation of α,β-Unsaturated Carbonyl Compounds by Dimethyldioxirane. *Journal of Organic Chemistry* **1993,** *58* (26), 7615-7618.

33. Charbonneau, L.; Foster, X.; Zhao, D.; Kaliaguine, S., Catalyst-Free Epoxidation of Limonene to Limonene Dioxide. *ACS Sustainable Chemistry and Engineering* **2018,** *6* (4), 5115-5121.

34. Curci, R.; Dinoi, A.; Rubino, M. F., Dioxirane oxidations: Taming the reactivity-selectivity principle. *Pure and applied chemistry* **1995,** *67* (5), 811-822.

35. Hashimoto, N.; Kanda, A., Practical and environmentally friendly epoxidation of olefins using Oxone. *Organic Process Research and Development* **2002,** *6* (4), 405-406.

36. Hussain, H.; Green, I. R.; Ahmed, I., Journey describing applications of oxone in synthetic chemistry. *Chemical Reviews* **2013,** *113* (5), 3329-3371.

37. Li, W.; Fuchs, P. L., A new protocol for in situ dioxirane reactions: Stoichiometric in oxone and catalytic in fluorinated acetophenones. *Organic Letters* **2003,** *5* (16), 2853-2856.

38. Mikula, H.; Svatunek, D.; Lumpi, D.; Glöcklhofer, F.; Hametner, C.; Fröhlich, J., Practical and efficient large-scale preparation of dimethyldioxirane. *Organic Process Research and Development* **2013,** *17* (2), 313-316.

39. Saeed, A.; Larik, F. A.; Lal, B.; Faisal, M.; El-Seedi, H.; Channar, P. A., Recent resurgence toward the oxidation of heteroatoms using dimethyldioxirane as an exquisite oxidant. *Synthetic Communications* **2017,** *47* (9), 835-852.

40. Alavi Nikje, M. M.; Rafiee, A.; Haghshenas, M., Epoxidation of polybutadiene using in situ generated dimethyl dioxirane (DMD) in the presence of tetra-n-butyl ammonium bromide. *Designed Monomers and Polymers* **2006,** *9* (3), 293-303.

41. Murray, R. W., Dioxiranes. *Chemical Reviews* **1989,** *89* (5), 1187-1201.

42. Von Czapiewski, M.; Rhein, M.; Meier, M. A. R., Fatty Acid Derived Renewable Platform Chemicals via Selective Oxidation Processes. *ACS Sustainable Chemistry and Engineering* **2018,** *6* (11), 15170-15179.

43. Sonnet, P. E.; Foglia, T. A., Epoxidation of natural triglycerides with ethylmethyldioxirane. *JAOCS, Journal of the American Oil Chemists' Society* **1996,** *73* (4), 461-464.

44. De Kruijff, G. H. M.; Goschler, T.; Derwich, L.; Beiser, N.; Türk, O. M.; Waldvogel, S. R., Biobased Epoxy Resin by Electrochemical Modification of Tall Oil Fatty Acids. *ACS Sustainable Chemistry and Engineering* **2019,** *7* (12), 10855-10864.

45. Armylisasa, A. H. N.; Hazirahb, M. F. S.; Yeonga, S. K.; Hazimaha, A. H., Modification of olefinic double bonds of unsaturated fatty acids and other vegetable oil derivatives via epoxidation: A review. *Grasas y Aceites* **2017,** *68* (1), 1-11.

46. Chen, J.; Soucek, M. D.; Simonsick, W. J.; Celikay, R. W., Epoxidation of partially norbornylized linseed oil. *Macromolecular Chemistry and Physics* **2002,** *203* (14), 2042-2057.

47. Monono, E. M.; Bahr, J. A.; Pryor, S. W.; Webster, D. C.; Wiesenborn, D. P., Optimizing Process Parameters of Epoxidized Sucrose Soyate Synthesis for Industrial Scale Production. *Organic Process Research and Development* **2015,** *19* (11), 1683-1692.

48. Cavani, F.; Centi, G.; Perathoner, S.; Trifirò, F., *Sustainable industrial chemistry: Principles, tools and industrial examples*. John Wiley & Sons: 2009.

49. Sheldon, R. A., Metrics of green chemistry and sustainability: past, present, and future. *ACS Sustainable Chemistry & Engineering* **2018,** *6* (1), 32-48.

50. Anastas, P. T.; Warner, J. C., *Green Chemistry: Theory and Practice*. Oxford University Press: New York, 1998.

51. Sheldon, R. A., The E factor 25 years on: the rise of green chemistry and sustainability. *Green Chemistry* **2017,** *19* (1), 18-43.

52. Freund, R.; Lächelt, U.; Gruber, T.; Rühle, B.; Wuttke, S., Multifunctional efficiency: extending the concept of atom economy to functional nanomaterials. *ACS Nano* **2018,** *12* (3), 2094-2105.

53. Tabone, M. D.; Cregg, J. J.; Beckman, E. J.; Landis, A. E., Sustainability metrics: life cycle assessment and green design in polymers. *Environmental Science & Technology* **2010,** *44* (21), 8264-8269.

54. Wallace, W. H.; Bushway, K. E.; Miller, S. D.; Delcomyn, C. A.; Renard, J. J.; Henley, M. V., Use of in situ-generated dimethyldioxirane for inactivation of biological agents. *Environmental Science & Technology* **2005,** *39* (16), 6288-6292.

55. Ghasemi, S.; Sibi, M. P.; Ulven, C. A.; Webster, D. C.; Pourhashem, G., A Preliminary Environmental Assessment of Epoxidized Sucrose Soyate (ESS)-Based Biocomposite. *Molecules* **2020,** *25* (12), 2797.

56. Shen, R.; Tao, L.; Yang, B., Techno-economic analysis of jet-fuel production from biorefinery waste lignin. *Biofuels, Bioproducts and Biorefining* **2019,** *13* (3), 486-501.

CHAPTER 3. CATIONIC PHOTOPOLYMERIZATION OF EPOXIDIZED SUCROSE SOYATE WITH THE ADDITION OF REACTIVE DILUENTS

3.1. Abstract

The use of a highly functional bio-based epoxy system, epoxidized sucrose soyate (ESS) in cationic photopolymerization was studied. Bio-based and petroleum-based reactive diluents were used in the formulations in different concentrations to study the overall changes in coatings properties as a function of composition. The viscosity of the formulations was observed utilizing a rheometer. Cured coatings formulations were characterized by FTIR-ATR. Thermal properties were determined using thermal gravimetric analysis and differential scanning calorimetry. Viscoelastic properties was determined with dynamic mechanical analysis. Coating properties were evaluated using ASTM methods of characterization. The coatings evaluation shows that incorperation of ESS and other epoxidized oils into a UV curable formulation produce coatings with high solvent resistance and incresed ductility when compared to their petroleum based alternatives. .

3.2. Introduction

Thermoset polymers are a class of polymers that are commonly used in industrial applications. Some of these applications include adhesives, coatings, sealants and fiber composites.[1] The conventional way for producing thermoset coatings is through crosslinking reactions of polymeric chains to create an irreversible interconnected 3D-network. These crosslinking reactions are usually driven by the application of heat to a coating formulation. An alternative method of crosslinking is utilizing ultraviolet radiation curing to initiate crosslinking reactions. The use of ultraviolet radiation to cure via electronic excitation and ionization can be

used to define UV curing.[2] UV curable resins have gained a significant amount of interest and have found some success in markets such as dental applications[3], protective coatings[4], and 3D-printing technologies.[5] This interest can be attributed to their fast-curing mechanisms, low viscosity, high solids, low VOC and low energy requirements.[6-8]

Two different pathways to achieve UV curable systems could be by free-radical curing or cationic photopolymerization. The initiation step in cationic polymerization involves the transfer of charged species. These charged species are strong acids generated from the photodecomposition of a photoinitiators that are sensitive to UV light (Scheme 3.1).[9, 10]

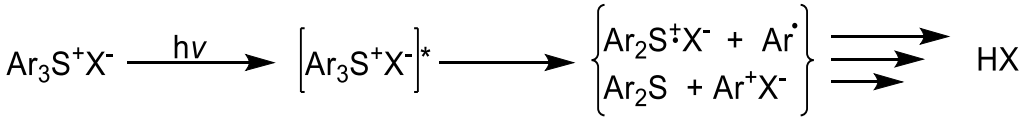

Scheme 3.1: General scheme of triarylsulfonium generating photoinitiators, where the X represents the counteranion.

A class of photoinitiators for cationic photopolymerization are onium salts which generate a very acidic molecular species when irradiated with UV light.[11] The salts contain a cationic an anionic moiety. The cationic moiety dictates how the photoinitiation controls the UV absorbing characteristic and the photosensitivity of the compound.[12] Meanwhile the counterion greatly influences the strength of the acid and the initiation efficiency.[13] As a result, there has been a great deal of research investigating the kinetics and the use of different onium salt as photoinitiators in UV curable formulations.[13-18]

In certain applications, cationic cured systems will typically have good adhesion to the substrate. In the cationic photopolymerization of epoxy (Scheme 3.2), oxygen inhibition is not an issue. Lower shrinkage occurs in cationically cured formulations and as a result the amount of internal stress that is present in the polymer-substrate interface is lower and thus adhesion is improved. However, polymerization reactions occurring during cationic photopolymerization can

be terminated in by water in the environment. Additionally, polymerization may take place after the source of the UV radiation is removed making and thus post thermal cure cycles can be implemented. Temperature has also been shown to influence conversion of epoxy photopolymerization.[19, 20] Liu found that an increase from 30 °C to 60 °C in the cationic photopolymerization of bisphenol A epoxy resins showed an increase in conversion up to 30%.[21]

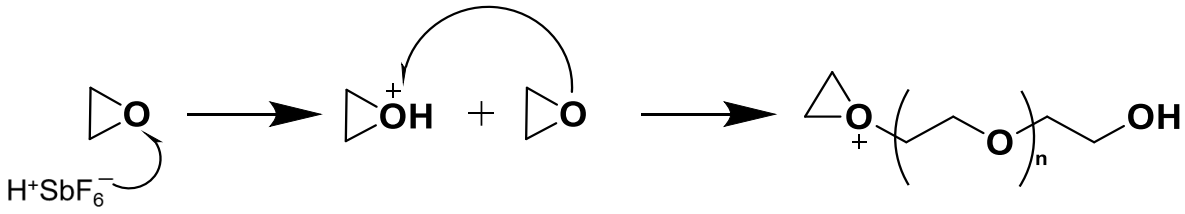

Scheme 3.2: General reaction scheme of cationic photopolymerization of epoxy groups.[4]

Naturally, an aspect of cationic photopolymerization that is being investigated is the use of biobased alternatives to act as substitutes for petrochemically derived epoxy resins. There have been many approaches to achieving this goal including the incorporation of bio-based sources such as epoxidized plant oils in UV curable formulations.[22-28] Epoxidized sucrose soyate is a bio-based epoxy resin that is derived from the that has been studied extensively by the Webster group.[29-35] The molecular structure contains high epoxy functionality along with long aliphatic carbon chains that contribute to flexibility while the sucrose core contributes to rigidity. Derivates of epoxidized sucrose soyate have been utilized in the application of UV curable technologies.[36-38] Silbert[38], explored the used of methacrylate and acrylate resins derived from epoxidized sucrose soyate for use in SLA 3D printing. The study concluded that biobased resins contained comparable properties, such as glass transition temperature, to commercial based resins such as Ebecryl 1290 and Ebecryl 220.

This study focuses on the use of epoxidized sucrose soyate (Figure 3.1) and additional diluents for use in cationic photopolymerization of bio-based thermoset coatings with the goal to

evaluate the potential for substituting petroleum-based sources with biobased epoxy resins. The diluents consisted of bio-based epoxidized soybean oil and petroleum based 3,4-Epoxycyclohexylmethyl 3,4-epoxycyclohexanecarboxylate and Epon 828 which is a difunctional bisphenol A/epichlorohydrin derived epoxy resin.

3.3. Experimental

3.3.1. Materials

Sodium bicarbonate was purchased from Alfa Aesar, Tewksbury, MA, USA. Acetic acid, hydrogen peroxide 50% in water, magnesium sulfate and sodium chloride were purchased from VWR, Aurora, CO, USA, while Amberlite® IR 120H, 3,4-Epoxycyclohexylmethyl 3,4-epoxycyclohexanecarboxylate (EEW 126 g/eq), Triarylsulfonium hexafluoroantimonate salts 50% in propylene carbonate, sodium chloride, and hexane were purchased from Sigma-Aldrich, Milwaukee WI, USA. Epon 828 (EEW 185 – 192 g/eq), a difunctional bisphenol A/epichlorohydrin derived epoxy resin, was purchased from Hexion, USA.

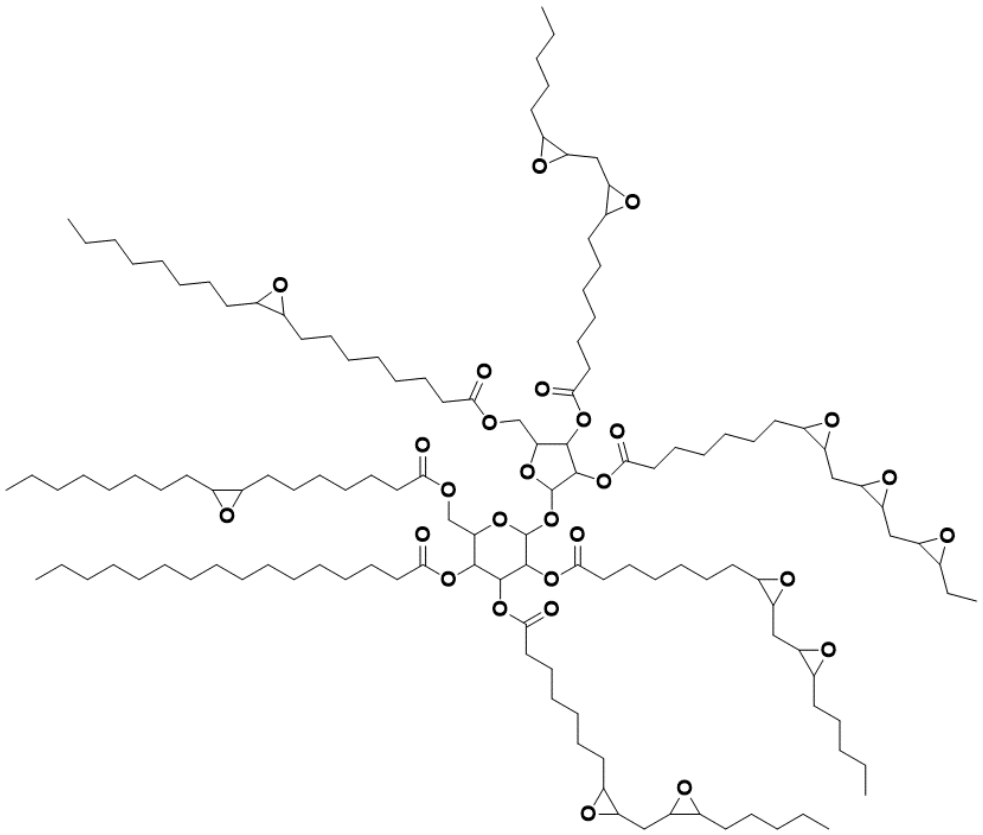

Figure 3.1: Structure of epoxidized sucrose soyate.

3.3.2. Synthesis of Epoxidized Vegetable Oil Based Resins

The molar ratios for the reactants for the synthesis of epoxidized sucrose soyate and epoxidized soybean oil has been studied in depth in previous work.[39-41] A 1L round bottom flask was charged with vegetable oil, Amberlite® IR 120H and acetic acid. The molar ratios of the reactants are as follows. Acetic acid:unsaturation equal to 0.44:1 and hydrogen peroxide:unsaturation equal to 1.78:1. Amberlite® IR 120H amount was 17.3% based on percent by weight of vegetable oil. Then, the flask and its contents were equipped with a mechanical stirrer, addition funnel, condenser, and a thermocouple. Hydrogen peroxide 50% wt was added to the addition funnel and a nitrogen inlet was equipped to it. A heating mantle was used as the source of heat. The reaction was heated slowly to 60 °C with stirring while the hydrogen peroxide was added in dropwise addition. The addition rate was varied to maintain the exothermic nature of the

reaction under control and to maintain the reaction at 60 °C. The reaction was completed in approximately 5 h. The contents of the reaction were then transferred to a separatory funnel and were allowed to separate. The aqueous layer was discarded and neutralized. The remaining organic layer is then dissolved in hexane and neutralized with an aqueous sodium bicarbonate solution. The aqueous layer is once again separated and discarded. The remaining organic layer is washed and separated 3 times using a brine solution. Once the organic layer is collected, it is dried overnight using magnesium sulfate. The magnesium sulfate is removed from the product utilizing vacuum filtration and the hexane is removed using a rotary evaporator.

3.3.3. Epoxy Equivalent Weight Determinations

The epoxy equivalent weight (EEW) of synthesized resins was determined following ASTM D1652. For purchased epoxy resins (3,4-Epoxycyclohexylmethyl 3,4-epoxycyclohexanecarboxylate, Epon 828), EEW given in the technical data sheet was used.

3.3.4. Coatings Formulations

The compositions used in the coating formulations are highlighted in Table 3.1 and the structure of the reagents used in the coating formulations are illustrated in Figure 3.2. Reagents were mixed utilizing a Flack teck high speed mixer at 3500 RPM for 3 min. All formulations contained 1% triarylsulfonium hexafluoroantimonate salts (TSHA) by total mass of the formulation. Formulations were then drawn down on iron phosphated steel panels, Q-lab S-36-I, utilizing an 8 mil drawdown bar. The drawdowns were then irradiated with UV light for 10 seconds using a UV radiation using a Fusion LC6B Benchtop Conveyer with an F300 Lamp. The approximate irradiation exposure intensities were 1606 mW/ cm2 (UVA), 383 mW/ cm2(UVB), 71 mW/ cm2 (UVC), 1334 mW/cm2 (UVV).

Table 3.1: Table illustrating the formulations compositions and the entry name corresponding to each formulation.

Diluent Name	ESS (%)	Diluent (%)	Entry Name
Epoxidized Soybean Oil	89	10	ESBO-10
Epoxidized Soybean Oil	79	20	ESBO-20
Epoxidized Soybean Oil	69	30	ESBO-30
Epoxidized Soybean Oil	59	40	ESBO-40
Epoxidized Soybean Oil	49	50	ESBO-50
3,4-Epoxycyclohexylmethyl 3,4-epoxycyclohexanecarboxylate	89	10	ECC-10
3,4-Epoxycyclohexylmethyl 3,4-epoxycyclohexanecarboxylate	79	20	ECC-20
3,4-Epoxycyclohexylmethyl 3,4-epoxycyclohexanecarboxylate	69	30	ECC-30
Epon 828	89	10	Epon-10
Epon 828	79	20	Epon-20
Epon 828	69	30	Epon-30

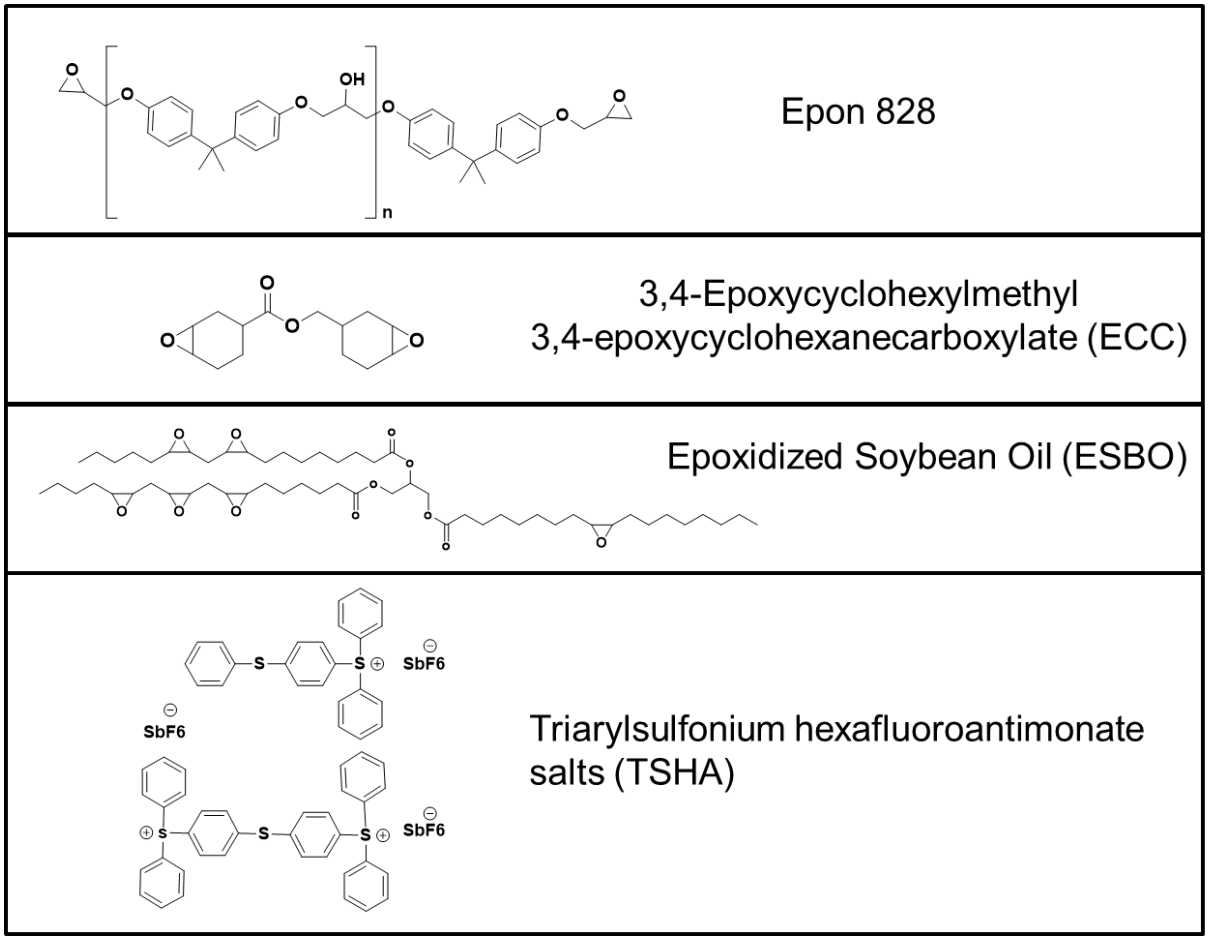

Figure 3.2: Structures of reactive diluents and catalyst used in coatings formulations.

3.3.5. Characterization of Formulations

FTIR spectra of the formulations was done utilizing a Thermo Scientific Nicolet 87000 with a DTGS KBr detector with a nitrogen blanket. The absorption spectra of the samples were collected by transferring a sample of the formulations to a potassium bromide crystal optic disc (25mm x 4mm) using 32 scans at $4cm^{-1}$ resolution. Viscosity of the formulations was recorded utilizing an ARES G2 Rheometer using 0.1 rads to 100 rads with 1% strain at a temperature of 25°C. Photo and thermal dynamic scanning calorimetry (DSC) was done on a TA instruments Q1000 DSC to determine the heat of enthalpy of the formulations. Samples were then subjected to a DSC heat cycle to determine the remaining heat of enthalpy. Photo DSC was done in

isothermal conditions at a temperature of 30 °C using the photocalorimetry accessory. Samples were then irradiated with UV light for 15 seconds twice. Thermal DSC of the samples were done subsequential to the photo DSC experiments 0° C to 250° C at a ramp rate of 10 °C/min for 1 cycle.

3.3.6. Characterization of Coatings

FTIR-ATR spectra of the cured coatings were collected utilizing a Thermo Scientific Nicolet 87000 equipped with a Smart iTR attenuated total reflectance accessory (ATR). The cured coatings were placed on top of the diamond with ZnSe lens where the absorption spectrum was collected using 32 scans at $4cm^{-1}$ resolution. The reflectance was then converted to absorbance using delta software. A TA instruments Q1000 DSC was utilized using a heating and cooling rate 10 °C/ min for a heat/cool/heat cycle ranging from -30 °C to 280 °C. Glass transition determined by DSC was measured by the point of intersection of the bisector of the angle between the tangents of the measurement curve.

DMA was carried out on a Q800 (TA Instruments) dynamic mechanical analyzer with a film tension clamp using samples with approximate dimensions (l,w,h) of 18 x 5 x 0.1 mm. Films were cut out of the steel substrate and cut to size using a film cutter. The instrument operated at 1Hz with a starting temperature of -40 °C. The heat ramp consisted of 3 °C/min to a max temperature of 150°C. The peak in tan δ measurement was used to determine glass transition. Storage modulus above 60 C of the glass transition was used to calculate crosslink density utilizing Equation 3.1.

$$E' = 3v_e RT \tag{3.1}$$

Where E' is the storage modulus 60 °C above glass transition, υ_e is crosslink density, R is the gas law constant and T is the absolute temperature.

Thermal Degradation was determined utilizing a TA instruments Q500 thermogravimetric analysis (TGA) system using heating a heat ramp of 10 °C/min from 30 to 600 °C in a nitrogen blanket.

Coating's properties were evaluated in accordance with ASTM procedures. Hardness was determined using both pencil hardness following ASTM D 3363 and König pendulum hardness following ASTM D 4366. Coating thickness was determined for cured coatings using a BYKI-Test 8500 coating thickness gauge. Crosshatch adhesion was determined to characterize coating adhesion to the substrate using a Gardco® crosshatch paint adhesion test kit following ASTM D 3359. Slow deformation using a conical mandrel bend measured flexibility following ASTM D 522. Reverse impact was used to measure flexibility under rapid deformation using ASTM D 2794 MEK Double rubs were done following a modified version of ASTM D 5402. Modifications include utilizing six layers of methyl ethyl ketone-soaked cheese cloth wrapped and tied around a 26-ounce hammerhead. The coating was rubbed back and forth with the hammer from the top of the coating to the base of the coating. Failure was reached when the substrate was exposed in the middle of the coating. The cloth was re-soaked in methyl ethyl ketone every 50 rubs.

3.4. Results and Discussion

3.4.1. Viscosity

Generally, formulations for UV curing applications do not use solvents. Thus, viscosity is an important parameter to explore when taking into consideration the application of the coatings to substrates. Figure 3.3 illustrates the different viscosities of the diluents and the formulations. Epoxidized sucrose soyate (ESS) has a viscosity 2.52 Pa•s. The starshaped structure of ESS along with its high functionality and sucrose core contributes to its relatively high viscosity.[42] As such, it is expected that overall formulation viscosities will decrease when diluents are added that have

a viscosity lower than 2.52 Pa•S. This trend is the case with the formulations which utilized ESBO and ECC as a reactive diluent since the overall viscosity decreased for the formulations as the concentration of the diluents increased. These results are not surprising since both the ESBO and ECC are considered low viscosity diluents for cationic systems with ESBO having a viscosity of 0.45 Pa•S and ECC having a viscosity of 0.35 Pa•S.

The Epon 828 diluent has the opposite effect when compared to the other two diluents. This effect can be explained since the viscosity of the diluent having the largest viscosity is Epon 828 at 11.24 Pa•s. Additionally, the aromatic structure along with repeating units and the hydroxyl functionality that is present in the molecular structure will contribute to an increase in viscosity. As a result, having a higher amount of Epon 828 in the formulation will increase its overall viscosity.

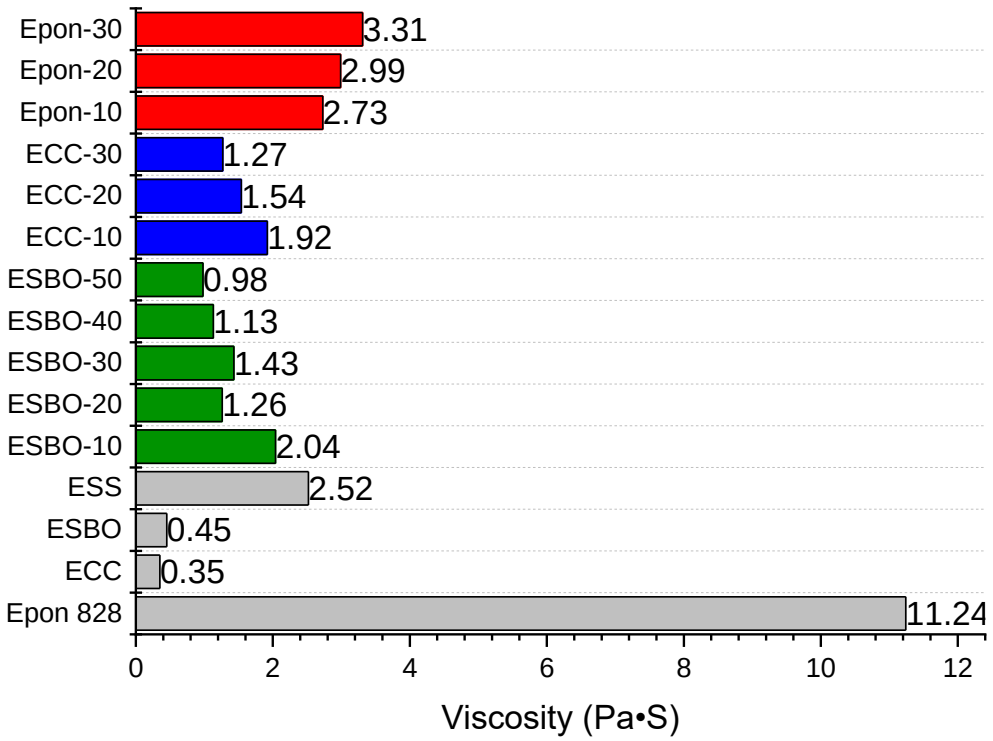

Figure 3.3: The viscosities of the uncured formulations and the diluents.

3.4.2. FTIR-ATR Analysis

FTIR and ATR spectra of uncured and cured formulations were taken to confirm that the reactions had undergone curing. Figure 3.4 shows the comparison of the uncured FTIR and the cured ATR spectra. The FITR ATR comparison exhibits a change in intensity in the 3500-3400 cm^{-1}, 1280-1230 cm^{-1}, 880-750 cm^{-1}, and 1140-1070 cm^{-1} range. Referring back to Scheme 3.2, one can see that the polymer chain as undergoes a nucleophilic attack from the hydroxyl group to produce a protonated ether. The increase in intensity at 3500-3400 cm^{-1} are due to the hydroxyl functionality that forms as the polymer chains approach the termination step. Similarly, the change in intensity for 1280-1230 cm^{-1} and 1140-1070 cm^{-1} can be attributed to the increase in the ether species that are formed as the epoxide rings open, and the polymer chain grows. These changes can be observed in all the coating formulations. The epoxy peaks are difficult to evaluate in these formulations. Typically a decrease in the peaks corresponding to epoxies would the observed around 880-750.[43, 44] While this decrease in intensity is observed to some degree in the formulations containing ESBO and ECC, there appears to be an increase in intensity at 831cm^{-1} in the formulations containing Epon 828 as a reactive diluent. The ring opening polymerization of Epon 828 increases the amount of linear ether groups being adjacent to aromatic structures. This overlap makes it difficult to differentiate between the epoxy groups and the linear aliphatic ethers while also explaining why the issue is not as prominent in the ECC or ESBO formulations since there are no aromatic groups that are participating in the crosslinking reaction. Overall, the FTIR indicates that crosslinking reactions are successfully occurring in the formulated systems.

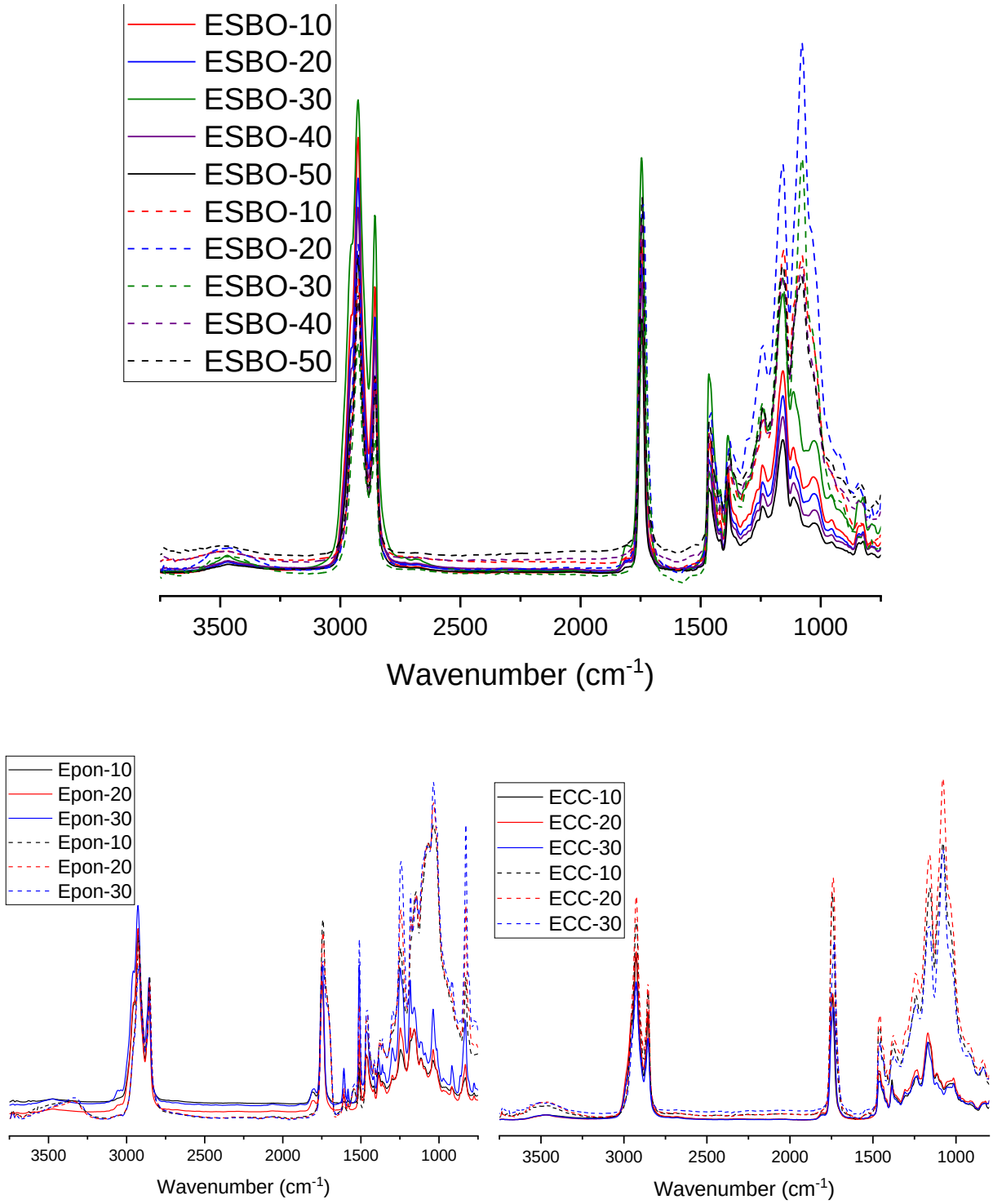

Figure 3.4: ATR and FTIR spectra of the uncured and cured formulations. Top represents the formulation containing ESBO as a diluent. Bottom left represents the formulation containing Epon 828 as a diluent. Bottom right represents the formulations containing ECC as a diluent. The solid lines represent the FTIR spectra for the uncured formulation while the dashed lines represent the ATR spectra of the cured formulations.

3.4.3. Thermal Properties

Thermal properties of the cured samples were taken and are summarized in Table 3.2. Measurement of thermal properties gives a good indication of the extent of reactivity from the crosslinked species. It is well known that structure and neighboring substituents play a key role on the rate of polymerization of ring opening cationic photopolymerization of epoxies. Thus, it is expected that thermal data will vary with formulation composition. Thermogravimetric analysis shows that the thermal degradation (Td %5) of the samples occurs at approximately 300 °C with the exception of ECC-30. This range of thermal degradation is a similar effect was reported in literature[45, 46] where a decrease in thermal degradation temperature is observed when the presence of ester groups in the structure increases. The thermal degradation can be ascribed by the ester groups being prone to β-elimination under high temperatures. Glass transition temperature (Tg) collected from DSC shows a wide range of glass transition temperatures in the formulations. For the formulations containing ESBO the higher the concentration of ESBO the lower the glass transition of the coatings. In conjunction with the overall lower functionality of the ESBO molecule, the long aliphatic carbon chains of the ESBO as well as the glycerol ester center that is present in the molecule as opposed to the cyclic sucrose core that is present in ESS will decrease the glass transition of the cured coating . These long fatty acid chains lead to higher free volume in the cured species thus, lower glass transition is observed. When using ECC as a diluent the opposite effect can be observed. As the concentration of ECC increased, the glass transition temperature of the coating increased. This effect is due to the small molecular weight and cycloaliphatic structure of the ECC participating in the crosslinking reaction yielding short rigid molecular chains which contribute to yielding a product with higher glass transition. Additionally it has been reported by Crivello[47] that structures containing epoxycyclohexene groups, such as

ECC, contain higher reactivity in photoinitiated cationic polymerization and thus a higher glass transition is observed. As an example, Udagawa[48] reported glass transition temperatures of ECC thermosets above 160°C. Formulations containing Epon 828 exhibited a similar trend as ECC. For similar reasons as the amount of Epon 828 increased, the overall glass transition of the coating increased. However, the formulations containing Epon 828 as a diluent had a lower glass transition than the ones containing ECC. This effect is due to the structural differences in the chemical compounds. Epon 828 contains neighboring ether substituents which can stabilize the secondary oxonium ion species through hydrogen bonding and as a result causes a slowdown in the polymerization kinetics. As a result, thermal energy is required to overcome the activation energy of these types of epoxy monomer.[49]

Table 3.2: Thermal properties of cured coatings.

Entry	TGA (Td %5) (°C)	DSC (Tg Cycle 2) (°C)	DMA (Tg Tan Delta) (°C)	E′ (MPa) at Tg +60°C	v_e (mol/m^3)
ESBO-10	320.2	29.82	41.72	54.18	5800
ESBO-20	317	29.28	41.9	12.31	1317
ESBO-30	320.9	12.27	26.9	7.105	792
ESBO-40	316.3	10.58	22.41	15.29	1726
ESBO-50	312.8	7.98	20.64	0.048	5
ECC-10	311.5	45.7	57.94	76.18	7816
ECC-20	305.1	60.7	75.6	59.49	5840
ECC-30	288.7	70.2	89.15	33.14	3149
Epon-10	326.1	49.9	54.6	78.01	8073
Epon-20	323.9	62.6	59.09	130.3	13330
Epon-30	328.3	67.3	60.03	97.1	9910

The DMA graphs are illustrated in Figure 3.5. The glass transition based of off DMA indicate that as the concentration of ESBO increases, the glass transition decrease. Meanwhile, the

opposite effect is observed for the formulations containing ECC and Epon 828. This trend can be ascribed to the reasoning explained earlier regarding structure reactivity relationships. The viscoelastic properties which include the storage modulus and the crosslinking density show an interesting trend. For the ESBO coatings the storage modulus and the crosslinking density decrease as the amount of ESBO in the formulation is increased. This is a result of the amount of long aliphatic carbon chains from the ESBO and the triglyceride core that do not participate in the crosslinking reaction. Crosslinking density of the formulations with the ECC and EPON is generally much higher than those of the ESBO containing formulations. Again, this result is due to the smaller cyclic structures of those compounds contributing largely to the overall crosslinking density of the cured products.

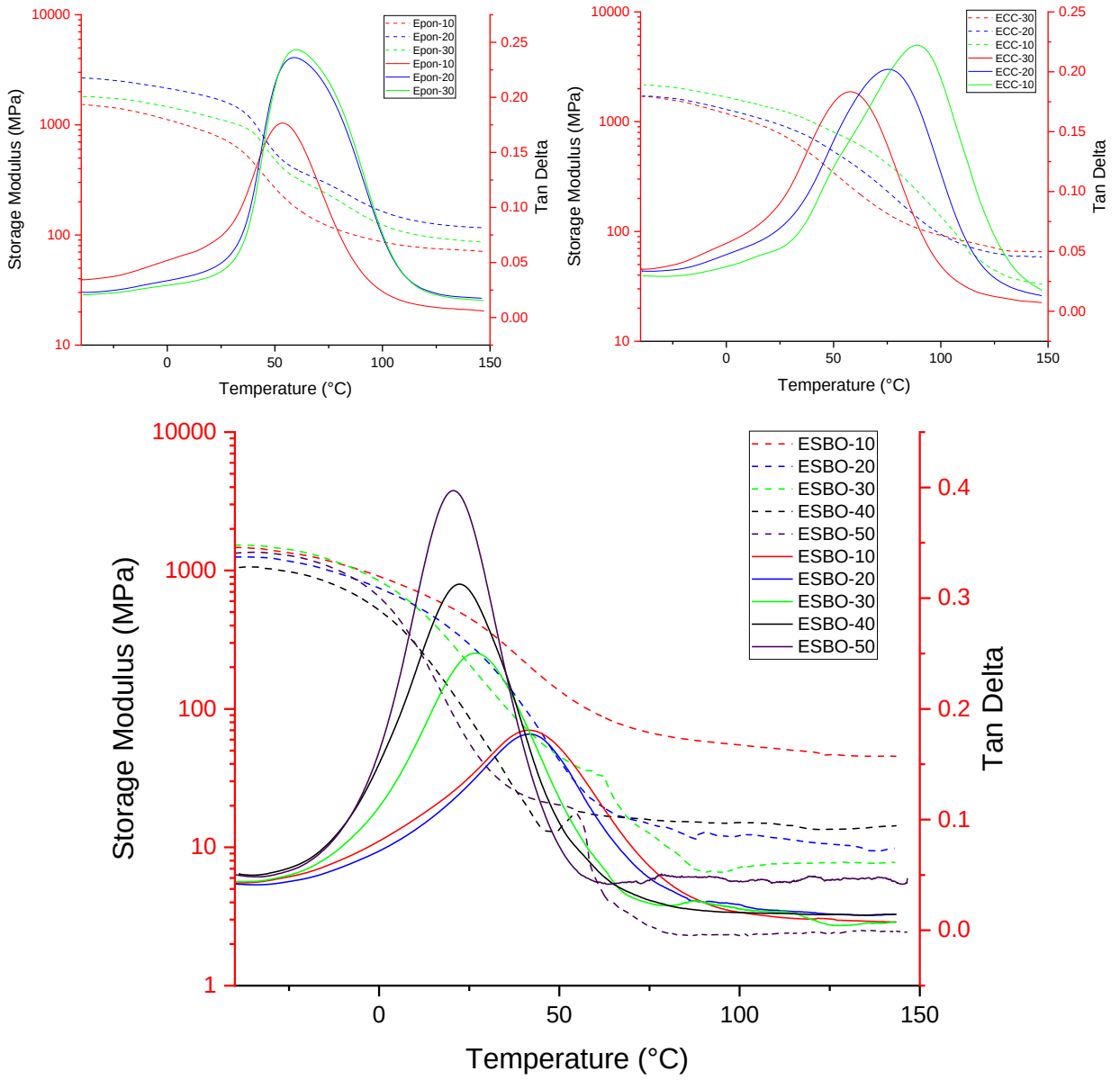

Figure 3.5: DMA curves of cured coating samples. Top left corresponds to formulations utilizing Epon 828 as a diluent. Top right corresponds to formulations utilizing ECC as a diluent. Bottom corresponds to formulations utilizing ESBO as a diluent. Solid lines are the tan delta measurements while the dashed lines graph the storage modulus.

3.4.4. Coatings Properties

Coating's properties exhibited a clear trend in diluent addition which is affirmed in conjunction to the thermal property data. Coatings characterization data is summarized in Table 3.3.

Table 3.3: Table displaying the coatings properties of cured formulations.

Entry Name	König (sec)	Thickness (µm)	Cross Hatch Adhesion	Pencil Hardness	Reverse Impact (in•lb)	Mandrel Bend	MEK DR's
ESBO-10	75	85	4B	2H	3.92	Fail	>400
ESBO-20	64	107	4B	HB	4.90	Fail	>400
ESBO-30	42	100	4B	3B	37.24	Pass	>400
ESBO-40	29	70	2B	<8B	26.46	Pass	266
ESBO-50	33	71	0B	<8B	39.20	Pass	194
ECC-10	110	90	4B	F	4.90	Fail	>400
ECC-20	117	98	4B	4H	4.90	Fail	>400
ECC-30	152	117	3B	F	4.90	Fail	>400
Epon-10	64	41	3B	B	3.92	Fail	>400
Epon-20	62	59	2B	B	<3.92	Fail	>400
Epon-30	77	60	2B	HB	<3.92	Fail	>400

In general, all coatings exhibited excellent solvent resistance with MEK double rubs over 400. A negative impact on solvent resistance can be observed for the formulations containing ESBO as the ESBO weight percentage increases above 30%. Coating hardness has an overall increase in hardness as the ECC and Epon in the formulations increase. Crosshatch adhesion is average for most of the coatings. However, it is important to note that the use of phosphated steel panels aid the overall coating to substrate adhesion. Resistance to deformation via mandrel bend and reverse impact show that the coatings are fairly brittle. Only the formulations containing the higher content of ESBO begun to exhibit some form of ductibility.

3.4.5. Thermal and Photo DSC of Uncured Formulation

The thermal and photo DSC of the uncured formulations show the change in enthalpy of the formulation as curing takes place. This data is summarized in Figure 3.6. The 15 sec exposure time is to simulate the amount of time coatings are exposed to UV lamp as the pass through on a conveyer belt. To our knowledge, the reaction kinetics of cationic photopolymerization of

epoxidized sucrose soyate has not been studied. As such, conversion percentages were calculated based on total area of the photo DSC and thermal DSC curves. The conversion of the ESBO formulation in photo DSC decreased as the ESBO content in the formulation increased. This occurrence can be attributed to vitrification within the coating. That is to say, as the curing process begins, the steric hindrance present as a result of the aliphatic carbon chains of the ESBO material prevent the epoxy rings from free movement and thus limit the extent of crosslinking. In addition to the steric hindrance caused by the aliphatic groups, the large size of the ESBO molecule negatively impacts the ability for the epoxy functional groups to react with each other with in the formulation.

The formulations containing ECC saw little to no change regarding as the concentration of ECC increased in the formulation. The formulations containing Epon 828 had the largest overall conversion due to UV radiation. A reasoning for this conversion could be due to the aromatic structure of the Epon 828 attributing to a higher absorption of the UV light.

The examination of the thermal DSC post photo DSC illustrates that the coating formulations are not undergoing full conversion. However, it is important to note that the reactions in the photo DSC are being carried out at a constant temperature. As opposed to in practice where the UV lamp and exotherms in the formulation contribute to secondary heating effects interacting with the formulation.

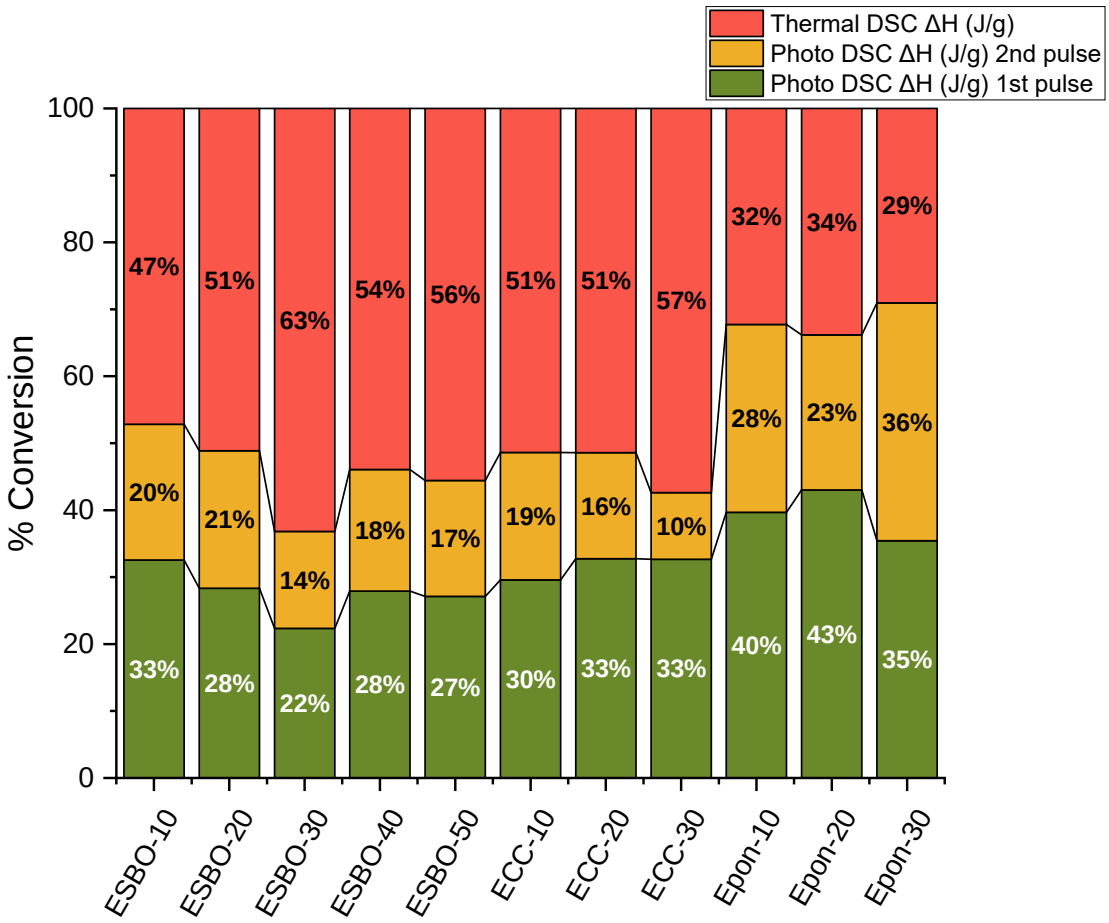

Figure 3.6: Conversion of cured samples based on the heat of enthalpy detected by photo DSC and Thermal DSC.

In literature, it has been shown that an increase in temperature from 30 °C to 60 °C can contribute to a large increase in conversion in the cationic photopolymerization of epoxy compounds. Using an infrared thermometer, one can observe that the coatings undergo a temperature change of 28 °C to 60 °C when following the proposed UV curing conditions implying that the coatings are exposed to a temperature change while simultaneously undergoing UV light radiation. An experiment designed around using photo DSC at different temperatures could be done to further understand the heating effects influence in the overall conversion of the coating systems.

3.5. Conclusion

A wide variety of coating formulations were produced in order to explore the feasibility of ESS in photocationic curing applications. Different reactive diluents consisting of aliphatic, cylic, and aromatic structres where studied at different concentrations to explore their effects on a ESS containing formulation. In conclusion, given the data collected from coatings and thermal characterization ESS could be a viable replacement for petroleum based materials such as Epon 828. Further exploration on the kinetic post cure cycles of the formulations could be carried out in future work.

3.6. References

1. Bobade, S. K.; Paluvai, N. R.; Mohanty, S.; Nayak, S. K., Bio-Based Thermosetting Resins for Future Generation: A Review. *Polymer - Plastics Technology and Engineering* **2016,** *55* (17), 1863-1896.
2. Davidson, R. S., *Exploring the science, technology and applications of UV and EB curing*. Sita Technology: 1999.
3. Vitale, A.; Sangermano, M.; Bongiovanni, R.; Burtscher, P.; Moszner, N., Visible light curable restorative composites for dental applications based on epoxy monomer. *Materials* **2014,** *7* (1), 554-562.
4. Sangermano, M.; Razza, N.; Crivello, J. V., Cationic UV-curing: Technology and applications. *Macromolecular Materials and Engineering* **2014,** *299* (7), 775-793.
5. Gonzalez, G.; Chiappone, A.; Roppolo, I.; Fantino, E.; Bertana, V.; Perrucci, F.; Scaltrito, L.; Pirri, F.; Sangermano, M., Development of 3D printable formulations containing CNT with enhanced electrical properties. *Polymer* **2017,** *109*, 246-253.
6. Crivello, J. V.; Reichmanis, E., Photopolymer materials and processes for advanced technologies. *Chemistry of Materials* **2014,** *26* (1), 533-548.
7. Sangermano, M., Advances in cationic photopolymerization. *Pure and Applied Chemistry* **2012,** *84* (10), 2089-2101.
8. Yagci, Y.; Jockusch, S.; Turro, N. J., Photoinitiated polymerization: Advances, challenges, and opportunities. *Macromolecules* **2010,** *43* (15), 6245-6260.
9. Gachet, B.; Lecompère, M.; Croutxé-Barghorn, C.; Burr, D.; L'Hostis, G.; Allonas, X., Highly reactive photothermal initiating system based on sulfonium salts for the

photoinduced thermal frontal cationic polymerization of epoxides: a way to create carbon-fiber reinforced polymers. *RSC Advances* **2020,** *10* (68), 41915-41920.

10. Höfer, M.; Liska, R., Photochemistry and initiation behavior of phenylethynyl onium salts as cationic photoinitiators. *Journal of Polymer Science Part A: Polymer Chemistry* **2009,** *47* (13), 3419-3430.
11. Crivello, J. V.; Lam, J. H. W., Diaryliodonium salts. A new class of photoinitiators for cationic polymerization. *Macromolecules* **1977,** *10* (6), 1307-1315.
12. Crivello, J. V., The discovery and development of onium salt cationic photoinitiators. *Journal of Polymer Science Part A: Polymer Chemistry* **1999,** *37* (23), 4241-4254.
13. Crivello, J. V.; Lam, J. H. W., Photoinitiated cationic polymerization with triarylsulfonium salts. *Journal of Polymer Science: Polymer Chemistry Edition* **1979,** *17* (4), 977-999.
14. Crivello, J. V., Cationic polymerization—iodonium and sulfonium salt photoinitiators. *Initiators—poly-reactions—optical activity* **1984**, 1-48.
15. Crivello, J. V.; Lee, J. L., Photosensitized cationic polymerizations using dialkylphenacylsulfonium and dialkyl (4-hydroxyphenyl) sulfonium salt photoinitiators. *Macromolecules* **1981,** *14* (5), 1141-1147.
16. Fouassier, J. P.; Burr, D.; Crivello, J. V., Photochemistry and photopolymerization activity of diaryliodonium salts. *Journal of Macromolecular Science—Pure and Applied Chemistry* **1994,** *31* (6), 677-701.
17. Sangermano, M.; Razza, N.; Crivello, J. V., Cationic UV-Curing: Technology and Applications. *Macromolecular Materials and Engineering* **2014,** *299* (7), 775-793.

18. Zhang, B.; Li, T.; Kang, Y., Synthesis and characterization of triarylsulfonium salts as novel cationic photoinitiators for UV-photopolymerization. *Research on Chemical Intermediates* **2017,** *43* (11), 6617-6625.

19. Bachmann, J.; Gleis, E.; Schmölzer, S.; Fruhmann, G.; Hinrichsen, O., Photo-DSC method for liquid samples used in vat photopolymerization. *Analytica Chimica Acta* **2021,** *1153*, 338268.

20. Lai, H.; Peng, X.; Li, L.; Zhu, D.; Xiao, P., Novel monomers for photopolymer networks. *Progress in Polymer Science* **2022,** *128*, 101529.

21. Liu, G.; Zhu, X.; Xu, B.; Qian, X.; Song, G.; Nie, J., Cationic photopolymerization of bisphenol A diglycidyl ether epoxy under 385 nm. *Journal of Applied Polymer Science* **2013,** *130* (5), 3698-3703.

22. Wu, J.; Qian, Y.; Sutton, C. A.; La Scala, J. J.; Webster, D. C.; Sibi, M. P., Bio-Based Furanic Di(meth)acrylates as Reactive Diluents for UV Curable Coatings: Synthesis and Coating Evaluation. *ACS Sustainable Chemistry & Engineering* **2021,** *9* (46), 15537-15544.

23. Xu, J.; Jiang, Y.; Zhang, T.; Dai, Y.; Yang, D.; Qiu, F.; Yu, Z.; Yang, P., Synthesis of UV-curing waterborne polyurethane-acrylate coating and its photopolymerization kinetics using FT-IR and photo-DSC methods. *Progress in Organic Coatings* **2018,** *122* (May), 10-18.

24. Wu, Q.; Hu, Y.; Tang, J.; Zhang, J.; Wang, C.; Shang, Q.; Feng, G.; Liu, C.; Zhou, Y.; Lei, W., High-Performance Soybean-Oil-Based Epoxy Acrylate Resins: "green" Synthesis and Application in UV-Curable Coatings. *ACS Sustainable Chemistry and Engineering* **2018,** *6* (7), 8340-8349.

25. Park, J.-W.; Shim, G.-S.; Lee, J.-G.; Jang, S.-W.; Kim, H.-J.; Choi, J.-N., Evaluation of UV Curing Properties of Mixture Systems with Differently Sized Monomers. *Materials (Basel)* **2018,** *11* (4), 509.

26. Dai, J.; Liu, X.; Ma, S.; Wang, J.; Shen, X.; You, S.; Zhu, J., Soybean oil-based UV-curable coatings strengthened by crosslink agent derived from itaconic acid together with 2-hydroxyethyl methacrylate phosphate. *Progress in Organic Coatings* **2016,** *97*, 210-215.

27. Chen, Z.; Chisholm, B. J.; Patani, R.; Wu, J. F.; Fernando, S.; Jogodzinski, K.; Webster, D. C., Soy-based UV-curable thiol–ene coatings. *Journal of Coatings Technology and Research* **2010,** *7* (5), 603-613.

28. Chen, Z.; Webster, D. C., Study of the effect of hyperbranched polyols on cationic UV curable coating properties. *Polymer International* **2007,** *56* (6), 754-763.

29. Ghasemi, S.; Sibi, M. P.; Ulven, C. A.; Webster, D. C.; Pourhashem, G., A Preliminary Environmental Assessment of Epoxidized Sucrose Soyate (ESS)-Based Biocomposite. *Molecules* **2020,** *25* (12), 2797.

30. Hosseini, N.; Webster, D. C.; Ulven, C., Advanced biocomposite from highly functional methacrylated epoxidized sucrose soyate (MAESS) resin derived from vegetable oil and fiberglass fabric for composite applications. *European Polymer Journal* **2016,** *79*, 63-71.

31. Ma, S.; Kovash, C. S.; Webster, D. C., Effect of solvents on the curing and properties of fully bio-based thermosets for coatings. *Journal of Coatings Technology and Research* **2017,** *14* (2), 367-375.

32. Paramarta, A.; Webster, D. C., The exploration of Michael-addition reaction chemistry to create high performance, ambient cure thermoset coatings based on soybean oil. *Progress in Organic Coatings* **2017,** *108*, 59-67.

33. Paramarta, A.; Webster, D. C., Bio-based high performance epoxy-anhydride thermosets for structural composites: The effect of composition variables. *Reactive and Functional Polymers* **2016,** *105*, 140-149.

34. Yu, A. Z.; Rahimi, A. R.; Webster, D. C., High performance bio-based thermosets from dimethacrylated epoxidized sucrose soyate (DMESS). *European Polymer Journal* **2018,** *99* (December 2017), 202-211.

35. Yu, A. Z.; Sahouani, J. M.; Setien, R. A.; Webster, D. C., Effect of nature and extent of functional group modification on properties of thermosets from methacrylated epoxidized sucrose soyate. *Reactive and Functional Polymers* **2018,** *128*, 29-39.

36. Yu, A. Z.; Sahouani, J. M.; Webster, D. C., Highly functional methacrylated bio-based resins for UV-curable coatings. *Progress in Organic Coatings* **2018,** *122*, 219-228.

37. Paramarta, B. A.; Webster, D. C., Highly Functional Acrylated Biobased Resin System for UV-Curable Coatings. **2013,** (1).

38. Silbert, S. D.; Simpson, P.; Setien, R.; Holthaus, M.; La Scala, J.; Ulven, C. A.; Webster, D. C., Exploration of Bio-Based Functionalized Sucrose Ester Resins for Additive Manufacturing via Stereolithography. *ACS Applied Polymer Materials* **2020,** *2* (7), 2910-2918.

39. Setien, R. A.; Ghasemi, S.; Pourhashem, G.; Webster, D. C., Comparison of epoxidation methods for biobased oils: dioxirane intermediates generated from Oxone versus peracid derived from hydrogen peroxide. *Polymer International* **2021,** *70* (5), 594-603.

40. Monono, E. M.; Bahr, J. A.; Pryor, S. W.; Webster, D. C.; Wiesenborn, D. P., Optimizing Process Parameters of Epoxidized Sucrose Soyate Synthesis for Industrial Scale Production. *Organic Process Research and Development* **2015,** *19* (11), 1683-1692.

41. Monono, E. M.; Webster, D. C.; Wiesenborn, D. P., Pilot scale (10kg) production and characterization of epoxidized sucrose soyate. *Industrial Crops and Products* **2015,** *74*, 987-997.

42. Pan, X.; Sengupta, P.; Webster, D. C., Novel biobased epoxy compounds: epoxidized sucrose esters of fatty acids. *Green Chemistry* **2011,** *13* (4), 965.

43. Noè, C.; Malburet, S.; Bouvet-Marchand, A.; Graillot, A.; Loubat, C.; Sangermano, M., Cationic photopolymerization of bio-renewable epoxidized monomers. *Progress in Organic Coatings* **2019,** *133*, 131-138.

44. Turco, R.; Tesser, R.; Vitiello, R.; Russo, V.; Andini, S.; Serio, M. D., Synthesis of Biolubricant Basestocks from Epoxidized Soybean Oil. *Catalysts* **2017,** *7* (10), 309.

45. Xia, Y.; Zhang, D.; Li, Z.; Lin, H.; Chen, X.; Oliver, S.; Shi, S.; Lei, L., Toughness modification of cationic UV-cured cycloaliphatic epoxy resin by hydroxyl polymers with different structures. *European Polymer Journal* **2020,** *127*, 109594.

46. Sangermano, M.; Tonin, M.; Yagci, Y., Degradable epoxy coatings by photoinitiated cationic copolymerization of bisepoxide with ε-caprolactone. *European Polymer Journal* **2010,** *46* (2), 254-259.

47. Crivello, J. V.; Liu, S., Photoinitiated cationic polymerization of epoxy alcohol monomers. *Journal of Polymer Science Part A: Polymer Chemistry* **2000,** *38* (3), 389-401.

48. Udagawa, A.; Yamamoto, Y.; Inoue, Y.; Chûjô, R., Physical Properties and Photoreactivity of Cycloaliphatic Epoxy Resins Cured by UV-Induced Cationic Polymerization. *Polymer Journal* **1991,** *23* (9), 1081-1090.

49. Bulut, U.; Crivello, J. V., Investigation of the Reactivity of Epoxide Monomers in Photoinitiated Cationic Polymerization. *Macromolecules* **2005,** *38* (9), 3584-3595.

CHAPTER 4. NOVEL WATERBORNE POLYURETHANE DISPERSIONS UTILIZING CYCLIC CARBONATES FOR NON-ISOCYANATE CROSSLINKING APPLICATIONS

4.1. Abstract

The feasibility of synthesizing novel non-isocyanate waterborne polyurethane dispersions utilizing 5 and 6 membered cyclic carbonates was investigated. The polyurethanes utilized a non-ionic internal emulsifier, m-PEG 750, at different concentrations to gain dispersibility in water. FTIR and NMR characterization expressed that the polyurethanes were synthesized successfully. The dispersions created using high shear were characterized for particle size and stability. Higher m-PEG content yielded smaller particle sizes and more stable dispersions. Thermoset coatings were prepared by crosslinking using a trifunctional amine under ambient and thermal curing conditions. The system based on the 6-membered cyclic carbonate became tack free in a much shorter time than the systems based on the 5-membered cyclic carbonates. Analysis using ATR-FTIR showed that the ambient cured systems were not fully reacted after 2 weeks of curing. When comparing the oven cured coatings, utilization of 6-membered cyclic carbonate yields products that cure faster, yield harder coatings, and have higher MEK solvent resistances than the formulations using 5-membered cyclic carbonates due to the higher reactivity.

4.2. Introduction

Polyurethanes are a class of polymers that are highly versatile and are used in a variety of different applications such as adhesives, foams for upholstery and automobile coatings.[1]A typical approach to synthesizing polyurethanes consists of utilizing isocyanate functional resins and hydroxyl functional species to yield the urethane linkages that make up the polyurethanes. However, this approach to creating polyurethane coatings has garnered significant concern due to

issues in human health from exposure to isocyanate functional species.[2, 3] Thus, there is a significant interest in developing new polyurethane technologies that minimize the use of isocyanates.

A relatively recent alternative approach is utilizing cyclic carbonates to develop non-isocyanate polyurethanes (NIPU). The cyclic carbonates undergo a ring opening polymerization pathway via step-growth polyaddition of cyclic carbonates with amines which can be exploited to produce crosslinked thermosets used for coatings applications.

Many different studies exist in the literature consisting of both synthesis and formulative work of non-isocyanate polyurethanes.[4-13] Burk proposed a synthesis for cyclic carbonates which consisted of utilizing diols and triphosgene as a means to achieve higher yields and replace the use of phosgene.[14] However, a more sustainable way to synthesize cyclic carbonates reaction that consist of 100% atom economy utilizes the use of epoxy resins at supercritical conditions with the addition of carbon dioxide and a metal based catalyst. [15-21] This method has been adapted in research work, including our group, and has allowed for applications of cyclic carbonate systems in coatings systems.[22-28] However, one of the main drawbacks of utilizing these systems in coatings comes from the low reactivity of the 5-membered cyclic carbonates with amines when compared to their isocyanate-hydroxyl counterparts. A study conducted by Lombardo[29] found success in utilizing a Lewis acid/base cooperative catalyst system to increase the reaction rate of the ring opening reaction of cyclic carbonates with amine.

Most the of the literature discussed pertains to 5-membered cyclic carbonate groups, however cyclic carbonates of higher ring sizes have been investigated as an alternative way to address the low reactivity of the cyclic carbonate-amine reaction. Literature shows that the reactivity of the cyclic carbonates can be expressed as such: 5-membered < 6-membered < 7-

membered < 8-membered.[30, 31] The difference between the reactivity is quite substantial, for example a 6-membered cyclic carbonate could potentially react with an amine 30 times faster than its 5-membered counterpart.[32]

The methods used in this study are based on methodology for producing WBPUD that have been published previously.[33] Harkal found that incorporating m-PEG as a non-ionic internal emulsifiers he could produce a water-dispersible glycidyl carbamate functional resin that could be formulated into ambient cured epoxy-amine thermoset coatings with excellent mechanical and chemical properties. Additionally, Harkal reported stable dispersions with particle sizes that ranged from 4-25 nm in volume without the use of cosolvents and surfactants. The development of water borne polyurethane dispersions has been widely employed across literature, thus it is natural that NIPU technology be applied to waterborne systems in order to broaden the scope of the cyclic carbonate amine applications. However, the number of articles investigating waterborne NIPUs using cyclic carbonates is limited.[22, 34, 35] A reasoning could be due to the fact that cyclic carbonates are prone to hydrolysis under alkaline conditions when in the presence of water.[36-39] Some literature investigating NIPU synthesis in water soluble systems reported low molecular weight, side reactions, and relatively slow reaction rates.[40-42] Still, utilizing the cyclic carbonate present in a dispersion where the pH is neutral with the utilization of non-ionic internal emulsifiers may offer an alternative way to utilize cyclic carbonate NIPU in waterborne systems. Hence, this work focuses on utilizing the ring-opening reaction of cyclic carbonates and amines for 5-membered and 6-membered rings in a water borne polyurethane dispersion.

4.3. Experimental

4.3.1. Materials

Triton X-165 (70%) was purchased from Dow chemical. Desmodur N 3600 was provided Covestro. Dibutyltin dilaurate (DBTDL), methoxy polyethylene glycol (m-PEG 750), chloroform-d, triazabicyclodecene (TBD), tris(2-aminoethyl)amine (TAEA) lithium trifluoromethanesulfonate (LiOTf), methyl ethyl ketone (MEK), and acetone, were purchased from Sigma-Aldrich, Milwaukee WI, USA. Glycerol carbonate (Jeffsol GC) was provided by Huntsman, Ringwood Il, USA.

4.3.2. Synthesis of 6-Membered Cyclic Carbonate

Synthesis of 6-memberec cyclic carbonate was carried out as a collaboration with the Sibi group at North Dakota State University. The general reaction is outlined in Scheme 4.1.

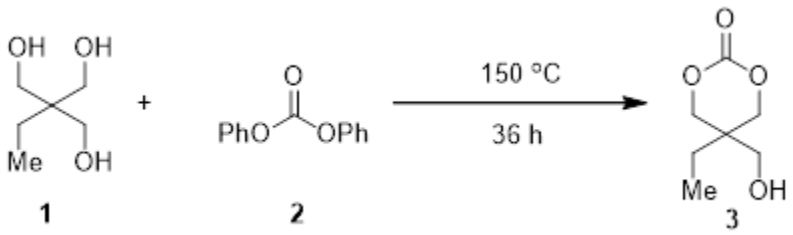

Scheme 4.1: Reaction scheme of 6-membered cyclic carbonates.

Trimethylol propane (**1**; 26.8 g, 200 mmol) and diphenyl carbonate (**2**; 42.8 g, 200 mmol) were mixed in a 250 mL round bottom flask. The reaction mixture was heated to 150 ℃ with vigorous stirring. Reaction completion was monitored utilizing thin layer chromatography. After, the reaction was completed (36 h) the product was allowed to cool to room temperate. The crude product was purified via column flash chromatography (ethyl acetate: hexane = 1:1 to 4:1) to obtain the desired 6-membered cyclic carbonate. The solvent of the product was removed via rotary evaporation and the final product yields a yellowish liquid.

4.3.3. Reaction Ratio Calculations

Reaction ratio calculations were based off the following literature.[43] Isocyanate equivalent weight was calculated using equation 4.1

$$\frac{4200}{NCO\ content\ (\%)} = E_s \tag{4.1}$$

With *Es* equaling isocyanate equivalent weight. The hydroxyl number of the mix was calculated using the equation 2.

$$OH_m = OH_j a + OH_k(1 - a) \tag{4.2}$$

With OH_m being the hydroxyl number of the mix, *a* being the fractional component of hydroxyl species 1, OH_j hydroxyl value of component 1, OH_k hydroxyl value of component 2. Weight equivalent of hydroxyl mix was calculated using equation 3.

$$Ep_m = \frac{1000*56.1}{OH_m} \tag{4.3}$$

With Ep_m being the equivalent of hydroxyl mix. Weight of isocyanate required to react with hydroxyl mix was calculated using equation 4.

$$W_s = \frac{E_s*W_p*R}{Ep_m} \tag{4.4}$$

With W_s being the weight of isocyanate (g), W_p being the weight for the hydroxyl species mixture, and R being the ratio of isocyanate to polyol. These equations were utilized to formulate different polyurethane synthesis with varying fractional components. For this study R was kept at 1 for all synthesis. These polyurethanes are illustrated in Tables 4.1 and 4.2.

Table 4.1: The amounts (wt/wt%) of reactive components used in the synthesis of waterborne polyurethane dispersions utilizing 5-membered cyclic carbonates.

Polyurethane	1	2	3
Jeffsol GC	37%	35%	32%
a	0.9	0.8	0.7
m-PEG 750	4%	9%	14%
Desmodur N 3600	59%	56%	54%

Table 4.2: Table illustrating the different amount (wt/wt%) of reactive components used in the synthesis of waterborne polyurethane dispersions utilizing 6-membered cyclic carbonates.

Polyurethane	4
6-membered cyclic carbonate	41%
a	0.8
m-PEG 750	10%
Desmodur N 3600	49%

Catalyst (dibutyltin dilaurate) loading for all synthesis consisted of 0.1% of total resin weight. All polyurethanes utilized enough solvent (MEK) to yield a product with 70% solids.

4.3.4. Synthesis of Polyurethane

A 500 ml four necked round bottom flask was equipped with a condenser, nitrogen inlet, a J-KEM thermocouple attached to a module apollo J-KEM temperature controller, and a mechanical stirrer. The round bottom flask was charged with isocyanate (Desmodur N 3600) and methoxy polyethylene glycol (m-PEG 750). The contents of the flask were heated to 60 °C with stirring to allow mixing for 30 min. After mixing time had elapsed, dibutyl tin dilaurate (DBTDL) and methyl ethyl ketone (MEK) were added to the flask and the temperature was raised to 80 °C. Jeffsol GC was added through an addition funnel dropwise over 2h. In the reactions utilizing the

6-membered cyclic carbonate, the cyclic carbonate was first dissolved in MEK and then addition proceeded through a dropwise addition over a time period of 2h. The stirring and heating of the reaction was maintained until the isocyanate peak (2271 cm^{-1}) had disappeared from an FTIR spectrum. The completed reaction product was then transferred to a single neck 500 mL round bottom flask and the MEK solvent was removed using a rotary evaporator.

4.3.5. Dispersing of Polyurethane Into Water

The synthesized final product was dissolved in acetone so that the total solids content of the polyurethane formulation was 70%. Mixing of the acetone and polyurethane was carried out in a Flacktek highspeed mixer at 3500 rpms for 5 minutes. Water was added to a 125 ml French square bottle. The amount of water used was calculated so that the theoretical percent solids of the PUD would equal 30% after the removal of acetone. Using an omni Macro Es homogenizer, the mixture was mixed for 10 min at 18,000 RPMs while adding the polyurethane dropwise into to the water over the course of the 10 min. The vessel was kept in an ice bucket to prevent the mixture from heating excessively. Formulations that contained surfactant used distilled water that contained 0.5% (w/w%) Triton X-165. After the dispersion was completed, the acetone was removed using a rotary evaporator at room temperature, and the dispersion again mixed using the homogenizer for 2 min at 18,000 RPMs.

4.3.6. Coating Formulations

The crosslinker (TAEA), catalyst (TBD) and co-catalyst (LiOTf) were mixed in water before addition to the crosslinker. The ratio of primary amine:carbonate was kept at 1:1 equivalents for all coatings formulations. The catalyst weight percent was 1% of the total polyurethane amount. The co-catalyst was added in equimolar amount to the catalyst. The waterborne polyurethane dispersions, crosslinker and catalyst were weighed out and added to a scintillation

vial. The formulations were hand mixed for 3 minutes. After hand mixing the formulations were mixed using a Flacktek highspeed mixer at 3500 rpm for 30 seconds to remove foam/bubbles present in the formulation. Coatings were made on QD-36 stainless steel panels using a 20 mil BYK drawdown bar. Two different sets of coatings contained different curing conditions. One set of coatings was left to cure ambiently for two weeks before being tested. The other set of coatings were force cured for 80 °C for 2h. Average coating thickness ranged from 75-90 micrometers.

4.3.7. Percent Solids

Percent solids of the dispersed formulations were done in weighed aluminum pans. The waterborne polyurethane dispersion was weighted, approximately 1g, in aluminum pans. The samples were heated at 120 °C for 1 h so that all the water would evaporate. The final weight of the pans after heating was recorded. Percent solids were then calculated from an average of three replicates using Equation 4.5.

$$\%Solids = \frac{FinalWeight - PanWeight}{InitialWeight} x100 \tag{4.5}$$

4.3.8. Dynamic Light Scattering

Particle size distribution was observed using dynamic light scattering techniques. The samples were diluted in distilled water and analyzed using a Particle Sizing Systems Nicomp 380. The mean diameter of the particles was recorded using intensity weighting.

4.3.9. Nuclear Magnetic Resonance

^{1}H and ^{13}C NMR spectroscopy was performed using a JEOL system, ECA Series 400 MHz NMR Spectrometer (JEOL, Peabody, MA, USA) and data was processed using Delta NMR software. The solvent used was $CDCl_3$.

4.3.10. FTIR

In process checks for the completion of the polyurethane synthesis was done utilizing Fourier transform infrared (FTIR) spectra on a Thermo Scientific Nicolet 87000 using a DTGS KBr detector with a nitrogen blanket. The absorption spectra of the samples was collected by transferring a sample from the reaction flask to a potassium bromide crystal optic disc (25mm x 4mm) using 32 scans at $4cm^{-1}$ resolution.

4.3.11. Stability Test

A sample of the polyurethane dispersion was placed in a 40 mL scintillation vial immediately after dispersion formation. The sample was kept at room temperature and observed over a period of time. The state of the dispersion was observed and recorded after 7 days and 14 days. The same procedure was used for the samples containing surfactant.

4.3.12. Hydrolysis Study

Polyurethane dispersions were placed in aluminum pans and heated to 80 °C for 2h to study the extent of hydrolysis on the polyurethane dispersion. Samples consisted of pans with just the polyurethane dispersion and the polyurethane dispersion with the co-catalyst system. TBD catalyst was present at 1% (wt/wt) based on the polyurethane amount and the co-catalyst was added in equimolar amount of the catalyst. ATR spectra were taken after the samples were taken out of the oven and were compared to a FTIR graph of the polyurethane resin.

4.3.13. ATR-FTIR

Coatings were characterized utilizing FTIR-ATR on a Thermo Scientific Nicolet 87000 using an Smart iTR attenuated total reflectance accessory (ATR). The coated samples were placed on top of the diamond with ZnSe lens where the absorption spectra was collected using 32 scans at 4 cm^{-1} resolution. The reflectance was then converted to absorbance using +Delta software.

4.3.14. Water Drop Test

The coatings absorption of water was tested by carrying out water drop tests. A drop of water was placed on the surface of the coating and was cover with a glass slide of approximately 2 x 2 cm (l,w) to prevent water evaporation. After 1 h of time had elapsed, the glass slide was removed from the coating and the absorption was evaluated visually for bubble formation, blisters, or film delamination. A number grade was assigned based on the appearance of the coatings from 5 to 0 with 5 demonstrating no defects, to 0 demonstrating complete delamination.

4.3.15. Static Contact Angle

Static contact angle of the coatings was measured utilizing a drop shape analyzer (DSA100 Krüss). Three measurements of a deionized water droplet of approximately 10 µL was placed on the surface of a coating and static contact angle was measure 10 seconds after the water droplet had come into contact with the surface of the coating. Presented data replicates the mean of those value.

4.3.16. Drying Time

Drying time of the coatings was observed following ASTM D1640/D1640M–14. The test conducted include, set to touch time, dry to touch time, and dry-hard time.

4.3.17. Coating Properties

Coating properties were tested in accordance to ASTM procedures. Hardness was determined using both pencil hardness following ASTM D 3363 and König pendulum hardness following ASTM D 4366 König. Coating thickness was determined for cured coatings using a BYK-Test 8500 coating thickness gauge. Crosshatch adhesion was determined to characterize coating adhesion to the substrate using a Gardco® crosshatch paint adhesion test kit following ASTM D 3359. Slow deformation using a conical mandrel bend measured flexibility following

ASTM D 522. Reverse impact was used to measure flexibility under rapid deformation using ASTM D 2794. MEK Double rubs were done following a modified version of ASTM D 5402. Modifications include utilizing 3 layers of methyl ethyl ketone-soaked cheese cloth wrapped and tied around a 26-ounce hammerhead. The coating was rubbed back and forth with the hammer from the top of the coating to the base of the coating. Failure was reached when the substrate was exposed in the middle of the coating. The cloth was re-soaked in methyl ethyl ketone every 50 rubs.

4.3.18. Thermal Gravimetric Analysis

A Q500 thermogravimetric analysis (TGA) system (TA Instruments) with a heating rate of 10°C/min from room temperature to 600°C under a continuous nitrogen flow was used to determine the thermal stability of the thermosets.

4.3.19. Differential Scanning Calorimetry

A DSC Q1000 (TA Instruments) with heating and cooling rates of 10°C/min at a heat/cool/heat cycle scanned from -50 °C to 150°C under nitrogen atmosphere was used to measure the glass transition temperatures (T_g) of the coatings. Glass transition for ambient cured studies were analyzed in the first cycle while the oven cured utilized the third cycle.

4.4. Results and Discussion

4.4.1. Synthesis of Hydrophilic Cyclic Carbonate Functional Polyurethanes

A series of different hydrophilic polyurethanes with cyclic carbonate functionality was synthesized and the general reaction scheme is illustrated in Scheme 4.2.

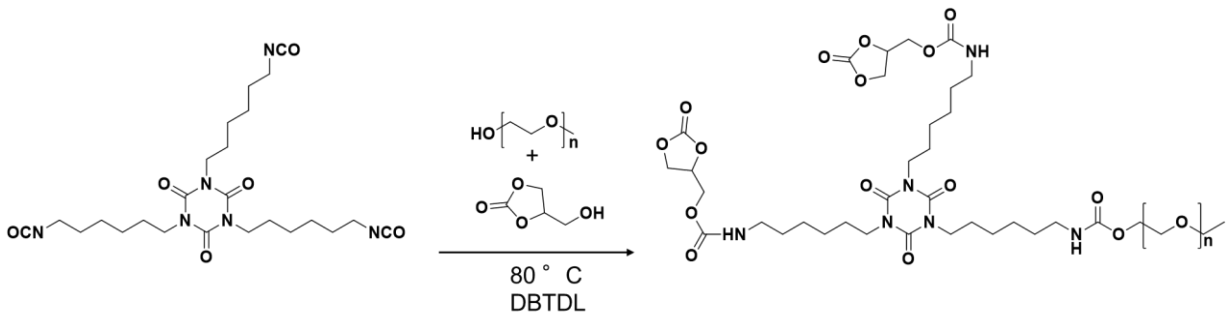

Scheme 4.2: Reaction scheme outlining the synthesis of an ideal carbamate functional polyurethane with hydrophilic m-PEG chains.

Confirmation of the polyurethane synthesis was done by evaluating NMR and FTIR spectra. The FTIR spectra shown in Figure 4.1 shows the difference between the incomplete and complete reaction of the polyurethane synthesis. The isocyanate peak can be observed at 2271 cm^{-1} in the incomplete reaction given an indication that the isocyanates in the Desmodur N 3600 have not reacted to completion. Hydroxyl peak disappearance is not as clear due to it overlapping with the NH peak at 3500-3300 from the formation of the urethane linkages. As the reaction time elapses, the disappearance of the isocyanate peak and the increase of peak 2271 cm^{-1} gives a clear indication that the urethane linkages are forming, and the reaction has reached completion.

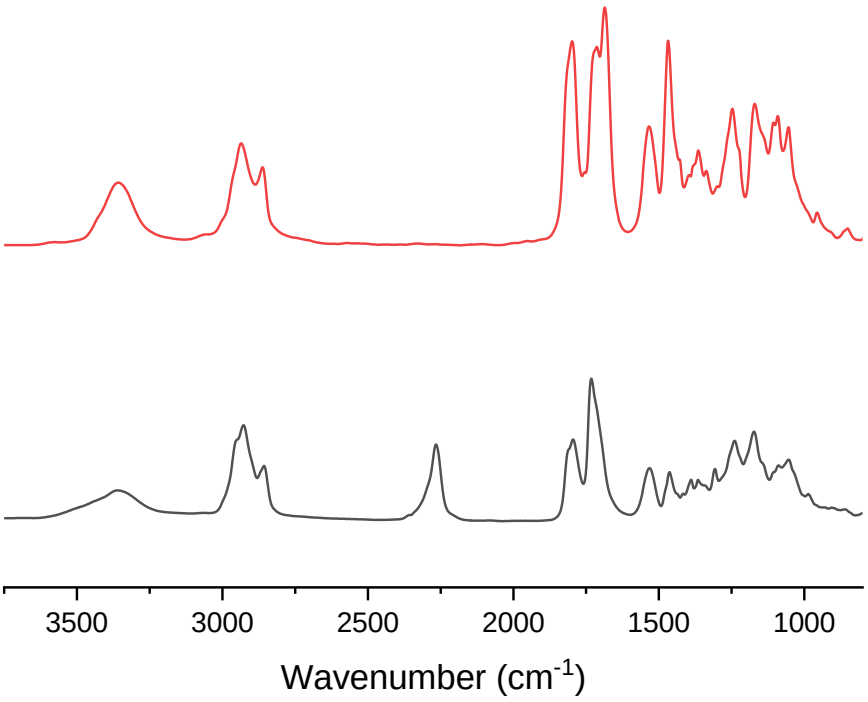

Figure 4.1: FTIR spectra of polyurethane undergoing synthesis. Spectrum at the bottom is the incomplete reaction, spectrum at the top is the completed reaction.

To reassure that the polyurethane resins had been successfully synthesized, NMR spectra was taken for the polyurethane resins and Desmodur N 3600. Figure 4.2 displays the proton NMR spectrum of Desmodur N 3600 compared against the proton NMR spectra of a polyurethane synthesized utilizing the 5 membered cyclic carbonates. Meanwhile, Figure 4.3 displays the carbon NMR spectrum of Desmodur N 3600.

The technical data sheet describes Desmodur N 3600 as an aliphatic polyisocyanate of HDI trimer. Knowing that, certain characteristics on the NMR spectra can be identified. In Figure 4.2, 3.29-3.32 ppm are the protons corresponding to the CH_2 closest to the isocyanate, 3.85-3.87 ppm are the CH_2 bonds that are furthest from the isocyanate in the aliphatic chain. 1.627 and 1.380 are the peaks corresponding to the other inner CH_2 peaks in the aliphatic chain.

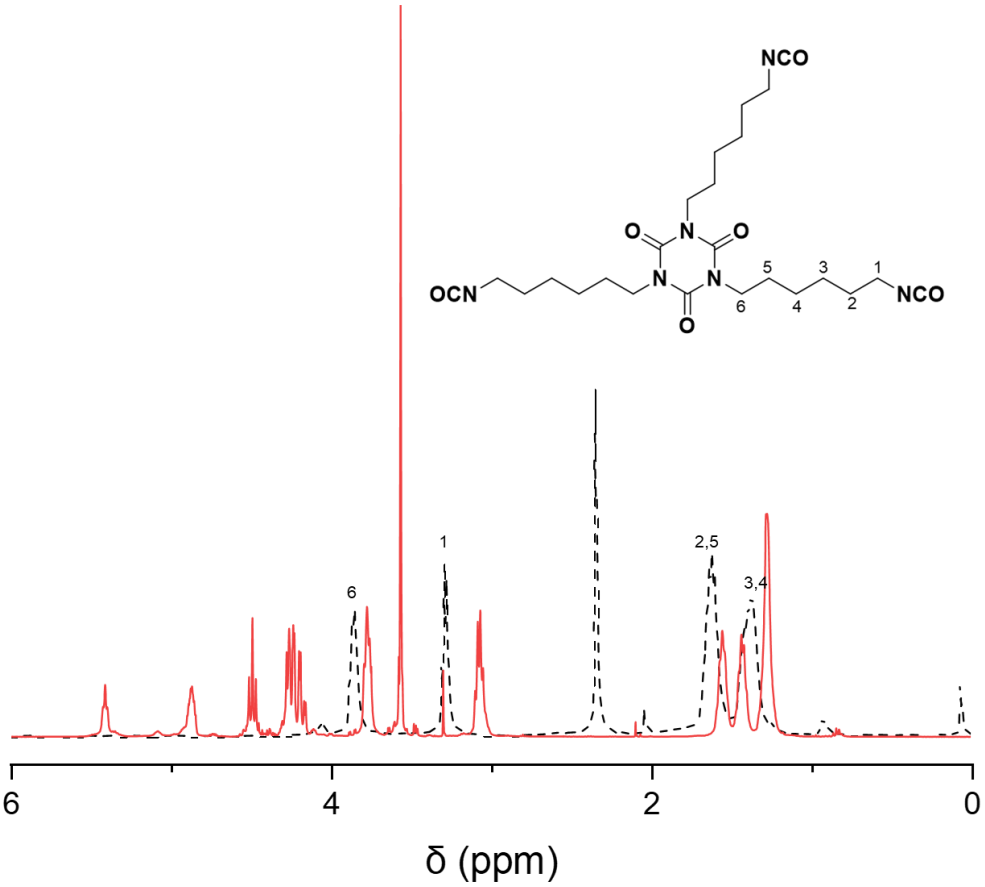

Figure 4.2: ^{1}H-NMR of polyurethane utilizing 5 membered cyclic carbonates (solid line) and Desmodur N 3600 (dashed line).

The shifts in the peaks corresponding to the isocyanate and the cyclic carbonate suggest that the reaction was successfully completed. The disappearance of a multiplet corresponding to the methylene group closest to the NCO in the isocyanate trimer at ~3.312, 3.296, 3.279 ppm suggest the isocyanate has reacted to yield urethane linkages. Additionally, the appearance of multiplet peaks at 4.87-4.86, 4.513-4.47, 4.278-4.190 ppm indicate that the cyclic carbonate is present in the polyurethane. Finally, the long alkyl chains on the m-PEG 750 are shown due to the peaks around 3.565 ppm with the CH_3 at the end of the chain appearing at 3.299 ppm.

For Figure 4.3, the peak at 149 ppm comes from the carbonyl carbons of the isocyanurate core. The peaks at approximately 129, 128, 125 ppm correspond to the carbons in the isocyanate functional groups of the compound. The peaks at 43, 31, 27, 26, 21, are from the aliphatic carbons contributing to the polyisocyanate that come from HDI.

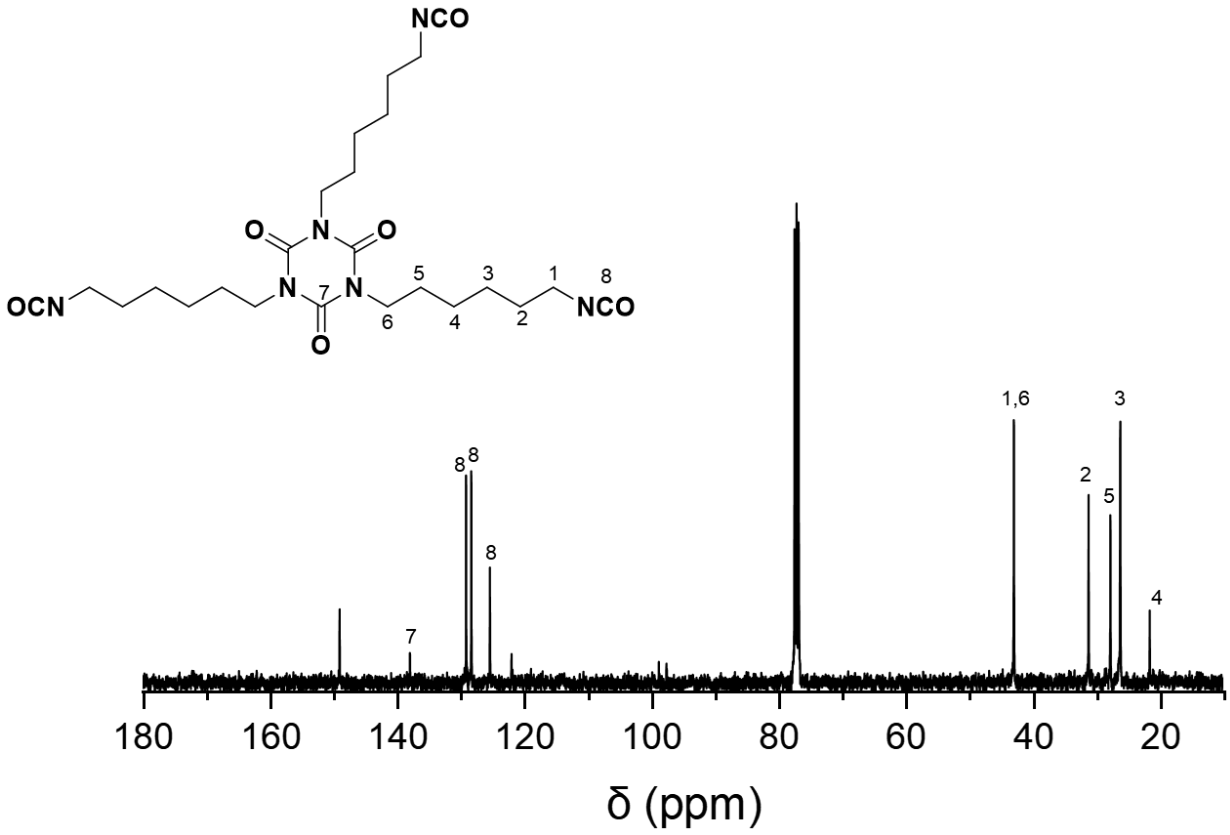

Figure 4.3: C-NMR spectra of Desmodur N 3600.

By observing Figure 4.4, it is clear that the carbon NMR for the polyurethane does not contain the presence of these peaks indicating that the isocyanates have fully reacted. The appearance of peaks 154.9 are from the carbonyl carbons from the cyclic carbonate being incorporated into the polyurethane. Other carbon peaks at, 43.5, 63.4, and 7.43 ppm are from the carbons in the cyclic isocyanurate core and the peak at 70.5 ppm is from the m-PEG chain.

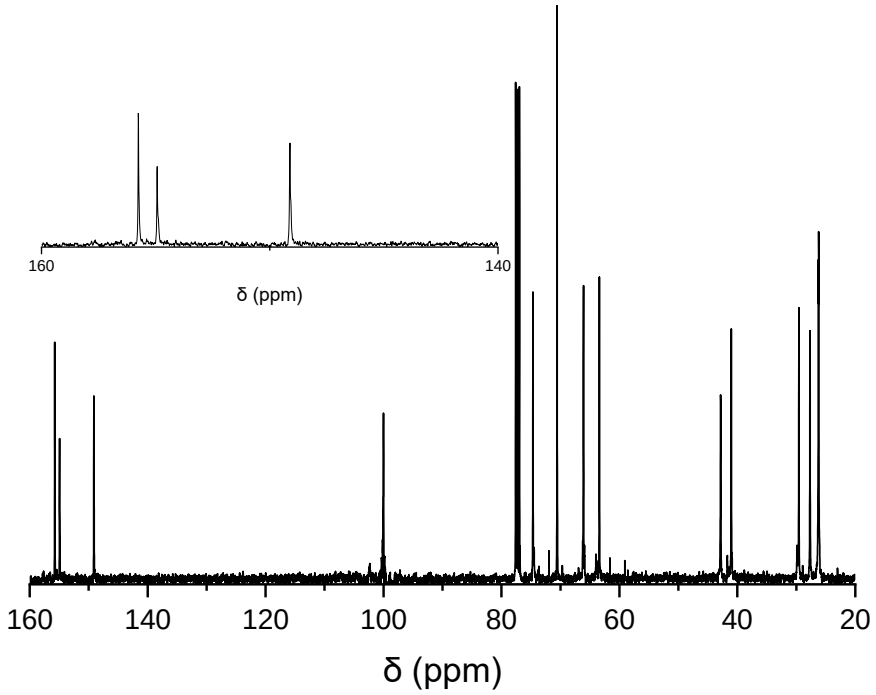

Figure 4.4: Carbon NMR of polyurethane utilizing 5-membered cyclic carbonates.

For the polyurethane synthesized using 6-membered cyclic carbonate the NMR spectra also show that the reagents were successfully reacted. The proton peaks appearing at 0.86 in Figure 4.5 are from the CH_3 at the end of the 6-membered cyclic carbonate. The peaks at 4.334-4.170 are the protons from the methylene peaks in the cyclic carbonate structure. The long alkyl chains on the m-PEG 750 are shown due to the peaks around 3.565 ppm with the CH_3 at the end of the chain appearing at 3.299 ppm.

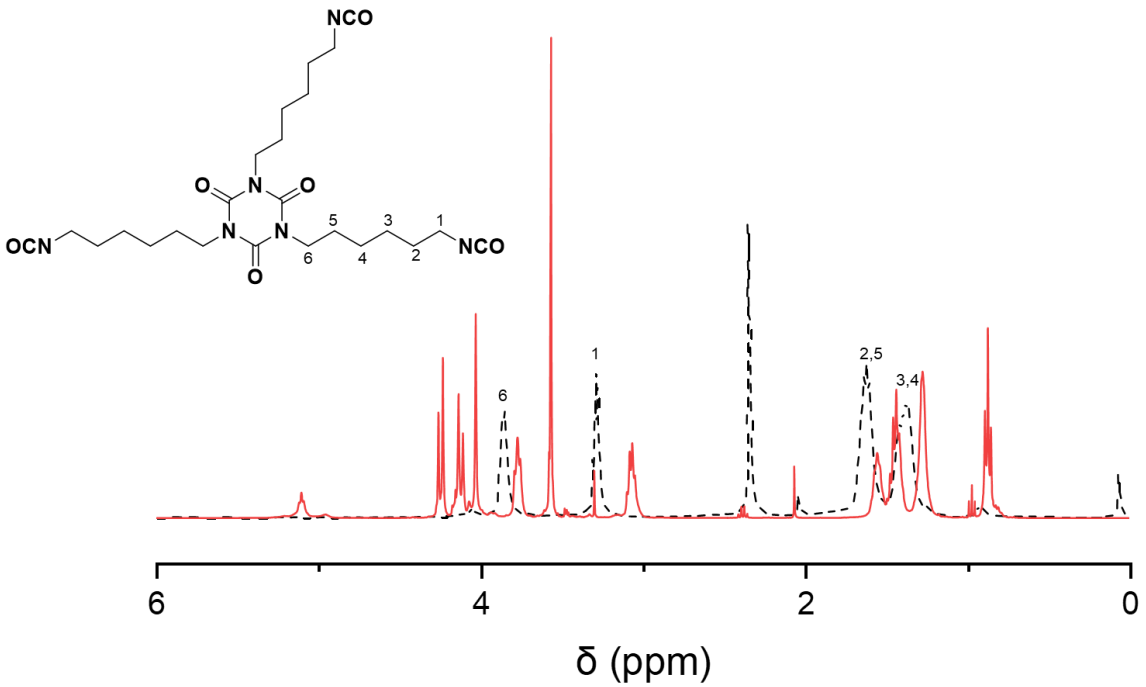

Figure 4.5: ^{1}H-NMR of polyurethane utilizing 6 membered cyclic carbonates (solids line) and Desmodur N 3600 (dashed line).

The peaks at 4.334-4.170 are the protons from the methylene peaks in the cyclic carbonate structure. The long alkyl chains on the m-PEG 750 are shown due to the peaks around 3.565 ppm with the CH_3 at the end of the chain appearing at 3.299 ppm.

The carbon NMR for the 6-membered cyclic carbonate, Figure 4.6, shows the carbonyl carbon from the cyclic carbonate to be at 148 ppm. The other carbons in the cyclic core correspond to 72.7 and 36.0 ppm. The remaining pendant carbons are shown in peaks 7.39, 22.92, and 60.97. Overall, we can conclude from the lack of isocyanate peaks in Figure 4.7 and shifts in peaks from both the carbon and the proton NMR in both polyurethane as well as the FTIR data, the reagents making up the polyurethane composition have reacted to completion.

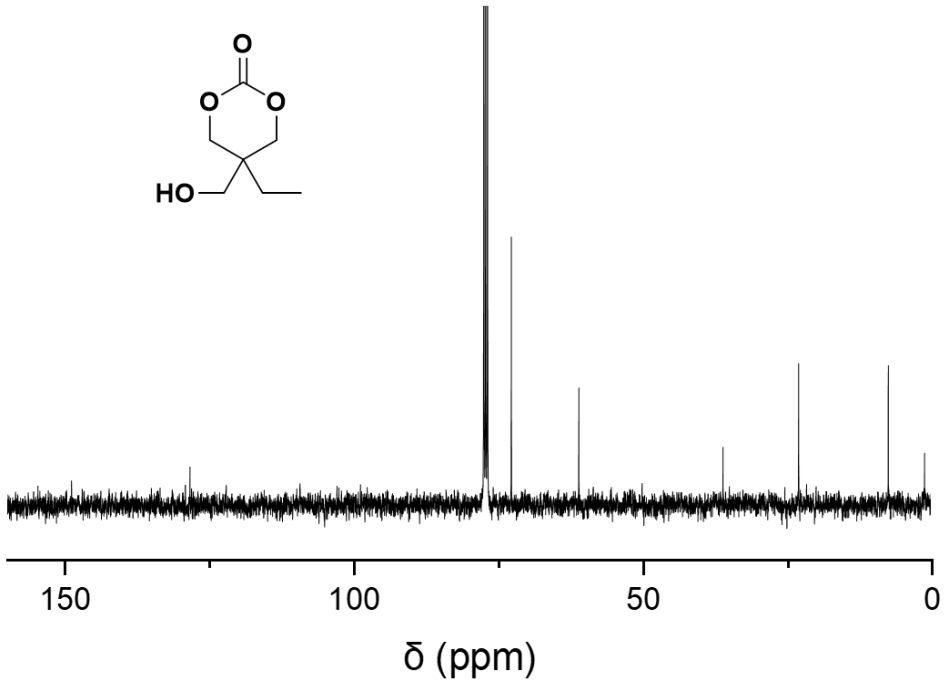

Figure 4.6: Carbon NMR spectra of the 6-membered cyclic carbonate.

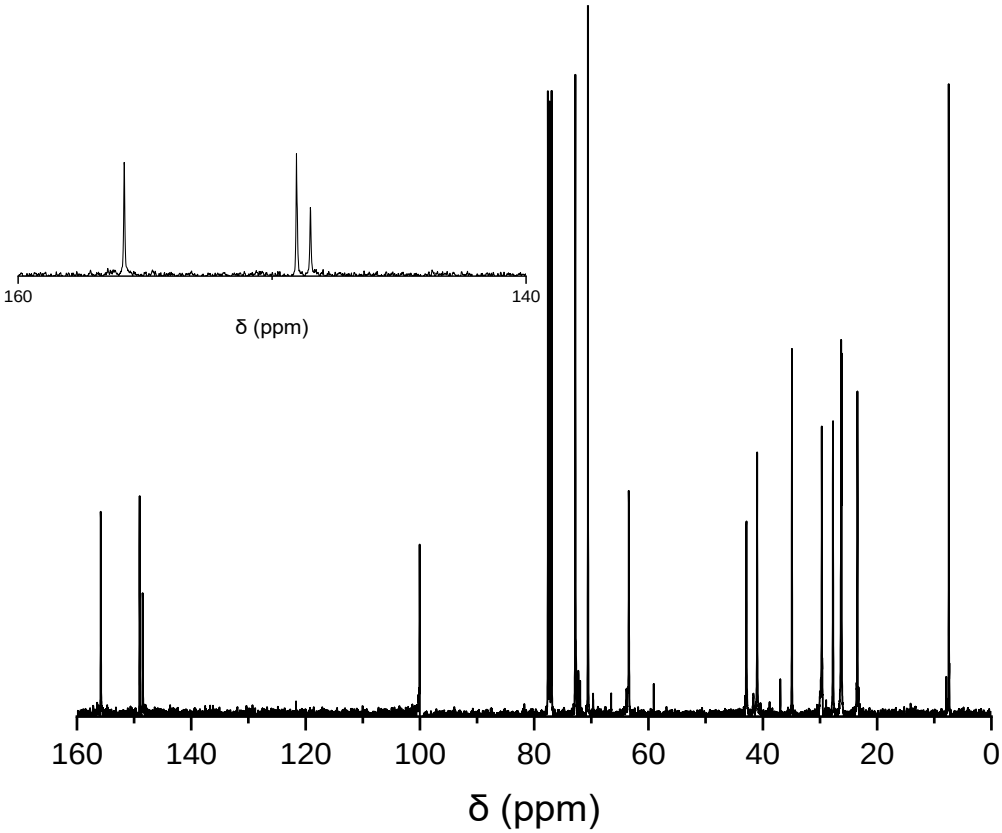

Figure 4.7: Carbon NMR of polyurethane utilizing 6-membered cyclic carbonates.

4.4.2. Aqueous Dispersions

The cyclic carbonate functional hydrophilic polyurethanes were then subjected to a solvent exchange process and then dispersed in water to create aqueous dispersions. After dispersion, the acetone was removed using vacuum distillation and the dispersions was transferred to two separate vials to be left undisturbed. The stability of the polyurethane dispersions in water was tested by visually observing the dispersions after a period time. In addition, particle size of the dispersions was examined, and the data was correlated with the visual tests. Figure 4.8 shows how the grades were assigned to each dispersion, with grade A being the best and grade D being the worst.

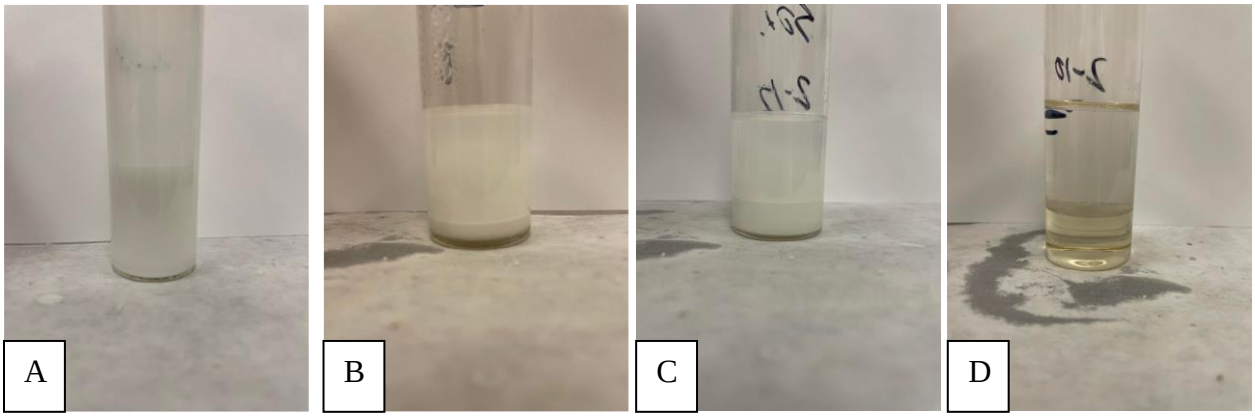

Figure 4.8: Photographs displaying the grades which were assigned to the dispersions. A consist of no visible separation, B consists of a gradient change that could be easily redispersed by shaking, C consist of a gradient change that could not easily be redispersed, D is two phase separation with no re-dispersibility characteristic.

The aqueous dispersion stabilization due to the m-PEG concentration are apparent and are shown in Table 4.3. The visual test showed that the dispersions which contained higher concentrations of m-PEG in the polyurethane synthesis yielded more stable dispersions. Addition of surfactant improved the stability only slightly with some formulations such as 1 and 2 on the lower end of m-PEG content just improving one letter grade meaning steric stabilization improved only slightly from the addition of a non-ionic surfactant. In addition, when examining the particle size data, a clear trend is established between the particle sizes and the stability of the dispersions.

The dispersions with lower particles sizes, higher m-PEG content, produced more stable dispersions. At sizes that are nearing 1 μm the effects of gravity in the particle dispersion become more significant and thus some sedimentation is present in the formulations.

Table 4.3: Stability of dispersion over a period of time and particle size data from given dispersions.

Formulation	Surfactant	Particle Size (nm)	Stability (7 days)*	Stability (14 days)*
4	No	860	B	C
3	No	727	A	B
2	No	768	B	C
1	No	1026	C	B
4	Yes	622	B	C
3	Yes	358	A	A
2	Yes	562	A	B
1	Yes	858	B	C

*details on the rating grade are detailed in Figure 4.8.

4.4.3. Extent of Hydrolysis

It has been reported that cyclic carbonate species can undergo hydrolysis when placed under alkaline conditions. Naturally, this too is a concern when utilizing cyclic carbonates to synthesize waterborne polyurethane dispersions given the fact that amines and base catalysts are being used in the crosslinking formulation. Figure 4.9 exhibits FTIR-ATR graphs of the 5 and 6 membered cyclic carbonate waterborne polyurethanes as a resin, a dispersed resin, and a dispersed resin with the co-catalyst system. The dispersions with the 5-membered cyclic carbonates do not appear to undergo under significant amounts of hydrolysis. A broadening of the hydroxyl peak and

a small appearance of an amide peak at 1650 cm^{-1} is present in the dispersions with the co-catalyst system present indicating that some hydrolysis did occur.

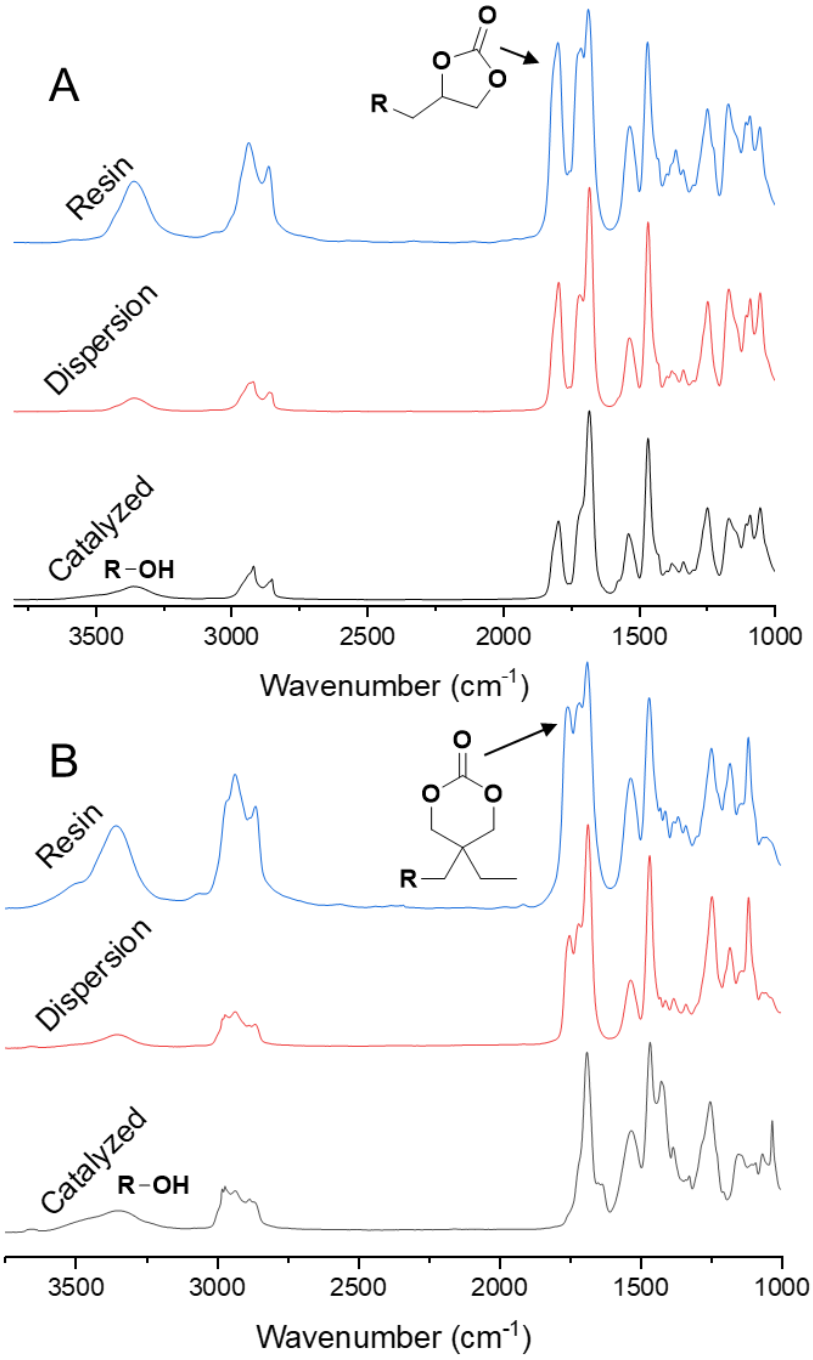

Figure 4.9: FTIR-ATR graphs of polyurethane resins, dispersion, and catalyzed dispersion after being subjected to heat. Bottom spectra (B) are the spectra for the 6-membered cyclic carbonates while the top spectra are the spectra (A) for the 5-membered cyclic carbonates.

The spectra of the polyurethanes utilizing the 6-membered cyclic carbonates hint that hydrolysis reactions are occurring. The polyurethane itself appears to undergo some of hydrolysis. Scheme 4.3 outlines the general reaction of hydrolysis of 5-membred cyclic carbonates.

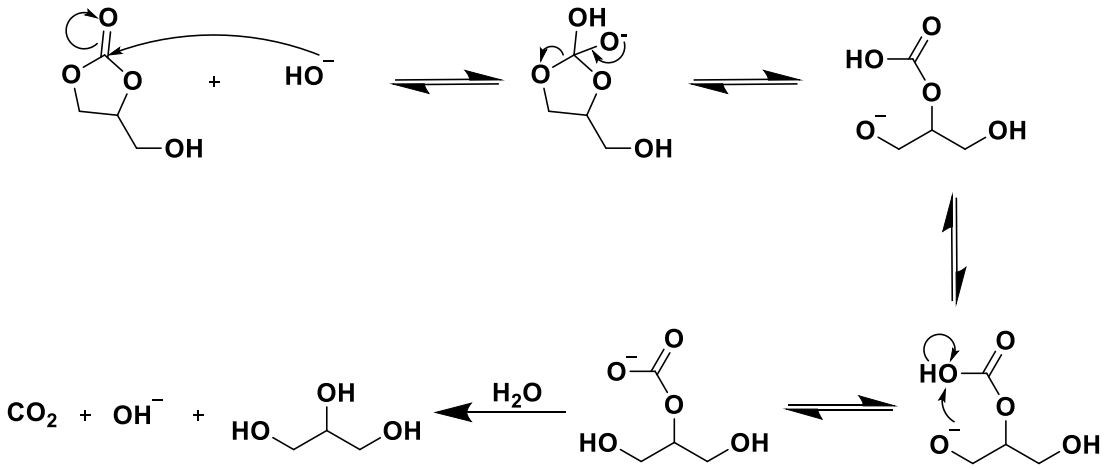

Scheme 4.3: General reaction scheme of cyclic carbonate undergoing hydrolysis.

A broadening of the hydroxyl peak [1] is present in the polyurethane dispersions when the co-catalyst system present indicating that some hydrolysis did occur. The appearance of peaks at 2850 – 2780 cm^{-1} is reminiscent of propylene glycol CH_2 stretching. This result indicates that opening of the cyclic carbonate ring is occurring. Furthermore, the catalyzed reaction shows a significant reduction of the carbonyl carbon peak at 1797 cm^{-1} along with an increase of the peaks at 2850 – 2780 cm^{-1} and a broadening of the hydroxyl region. A more detailed experimental methodology could be done in the future to investigate the hydrolysis of 6-membered cyclic carbonates.

4.4.4. Coating Curing

The coatings cured with TAEA with heating and under ambient conditions using catalyst (TBD) and co-catalyst (LiOTf) were compared against the uncured polyurethane FTIR Spectra. FTIR-ATR analysis provides additional insight by examining the differences in the uncured

polyurethane and the cured polyurethane coating spectra. The peak at 1797 cm^{-1} in Figure 4.10 for the uncured polyurethane corresponds to the cyclic carbonates present in the reaction.

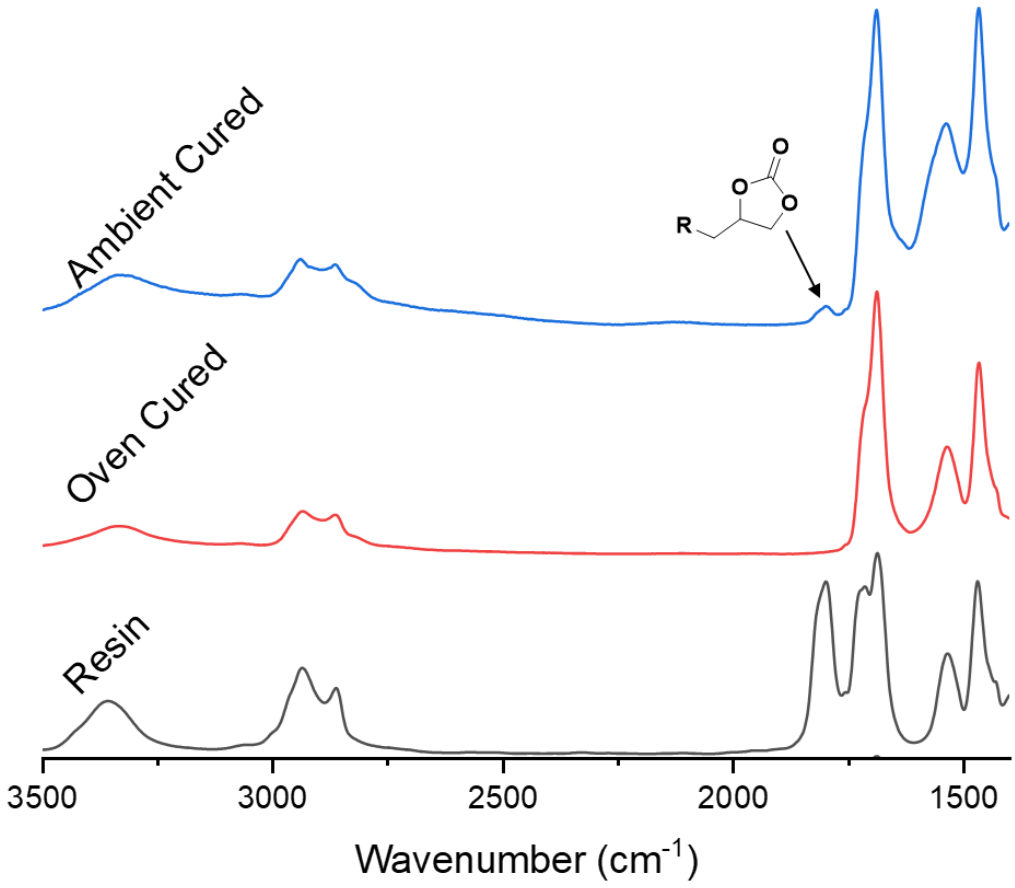

Figure 4.10: Comparison of FTIR-ATR spectra of polyurethanes utilizing 5-membered cyclic carbonates. The spectra are uncured polyurethane resin (bottom), oven cured polyurethane coating (middle) and 2 week ambient cured polyurethane coating (top).

As outlined in Scheme 4.4,[28] the curing reaction of cyclic carbonates and amines undergo a ring opening reaction which causes a shift in the IR peak of the cured spectra.

Scheme 4.4: Reaction of ring opening of 5 membered cyclic carbonates with amines.

Hence, a disappearance of peak 1797 cm^{-1} in the cured polyurethane is observed and an increase in peaks 1245 cm^{-1} and 1691 cm^{-1} is observed. Additionally, a broadening of the peak at

~3320-3500 cm^{-1} indicates an increase of amine and hydroxyl groups.[1] This result is due to the crosslinking reaction causing an increase in the number of hydroxyl functional groups and urethane linkages from the ring-opening reaction and thus it is observed in the IR. The ambient cured system contains a small peak in the 1797 cm^{-1}. This peak was observed in all samples including the dispersions utilizing 6-membered cyclic carbonates, Figure 4.11, indicating that the ambient cured systems are not completely cured.

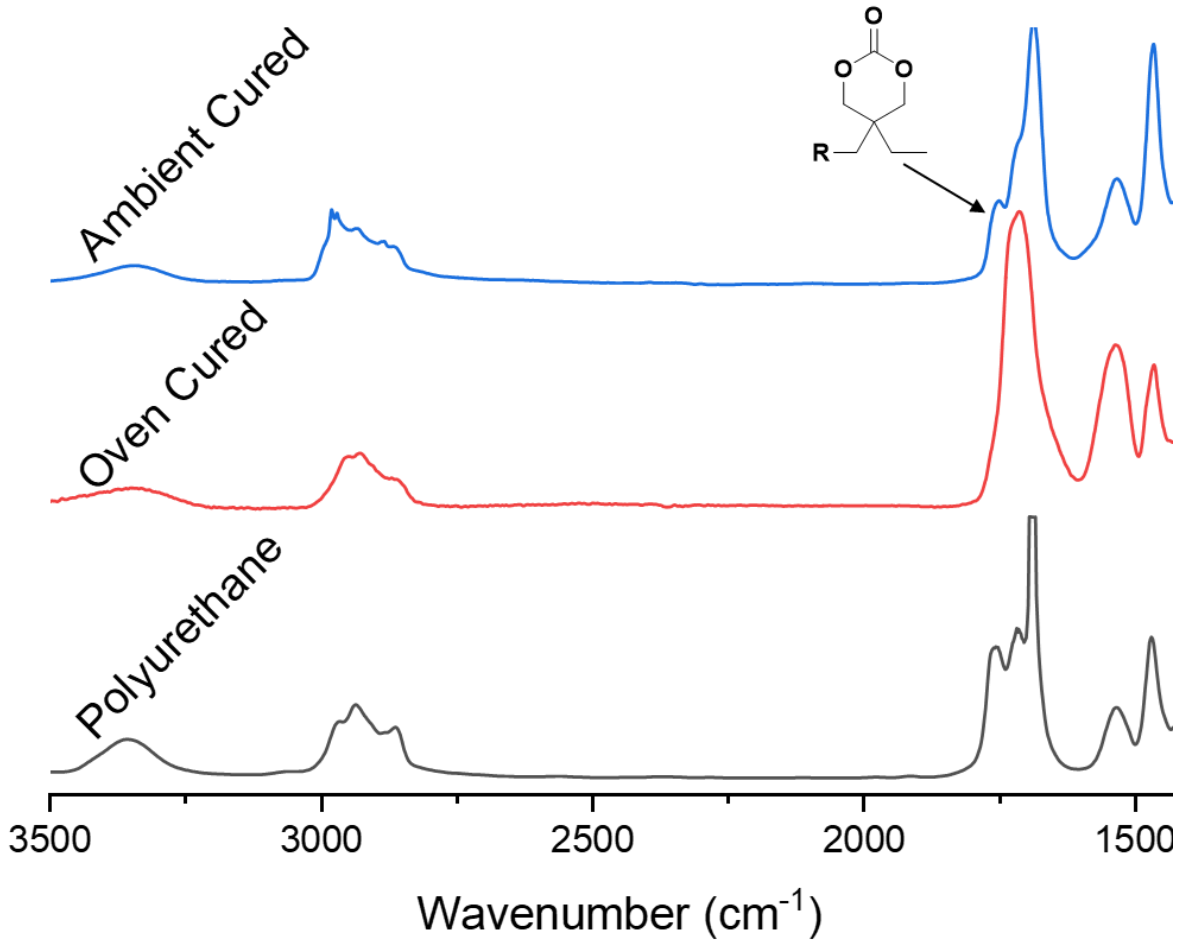

Figure 4.11: Comparison of FTIR-ATR spectra of polyurethanes utilizing 6-membered cyclic carbonates. The spectra are uncured polyurethane resin (bottom), oven cured polyurethane coating (middle) and ambient cured polyurethane coating (top).

4.4.5. Drying Time

This body of research works as a steppingstone for designing a non-isocyanate water borne polyurethane ambient curing system. Drying times of the coatings give a good indication of how long it would take for the coatings to reach a state where enough crosslinking had occurred to produce a surface that is tack free. Drying times for the formulations are summarized in Table 4.4. WBPUD containing 5-membered cyclic carbonates (formulation 1, 2, and 3) consisted of a set to touch time of 15 min, a "dry to touch" time of 1 h, and dry-hard time of 2h min. Meanwhile, formulation 4 consisting of a 6-membered cyclic carbonate consisted of a dry to touch time of 15 min, and "dry-hard" time of 30 min. No "set to touch" time was recorded for formulation 4 since it reaches a "dry to touch" state before it could be observed. An observation to note is that the drying times are limited by the rate of the water evaporating from the coating surface.

Table 4.4: Summarized drying time data for formulations.

Drying Test	Formulation 1, 2, and 3	Formulation 4
Set to Touch	15 min	N/A
Dry to touch	1h	15 min
Dry-hard	2h	30 min

Studies which have looked at the mechanism for this crosslinking reaction have found that in protic solvents, such as water, the reaction kinetics are limited by the deprotonation of the tetrahedral intermediate that forms.[44, 45] Given the observations made in the drying time data and the ATR analysis, this limitation may be why the coatings do not show signs of curing until the water begins to evaporates.

4.4.6. Coatings Properties

The coatings properties showed interesting results when comparing the different formulations. Table 4.5 summarizes the coatings properties for the formulations both ambient and oven cured. The oven cured coatings showed over all better coating properties than the ambient cured coatings due to the fact the ambient cured coatings showed signs that curing had not occurred to its fullest extent possible.

Table 4.5: Results of coating properties in ambient cured and oven cured coatings for 5-membered and 6-membered cyclic carbonates. Substrates are QD-36 cold rolled stainless steel.

Coatings Properties		Formulation			
	Curing	1	2	3	4
Pencil Hardness	Ambient	H	F	B	3H
	Oven	3H	2H	2H	3H
Adhesion	Ambient	5B	5B	5B	5B
	Oven	5B	5B	5B	5B
MEK Double Rubs	Ambient	263	162	157	292
	Oven	400+	400+	400+	400+
Reverse Impact (in·lb)	Ambient	<3.92	<3.92	<3.92	5.88
	Oven	7.84	7.84	15.36	<3.92
Mandrel Bend	Ambient	Pass	Pass	Pass	Fail (1.5cm)
	Oven	Pass	Pass	Pass	Pass
König Hardness (sec)	Ambient	83	80	43	132
	Oven	116	62	45	129
Thickness (µm	Ambient	63.4	68.4	63.5	62.9
	Oven	58.9	66.3	61.2	67.4

Additionally, coatings with higher m-PEG content contain less cyclic carbonates to undergo crosslinking. As a result, those coatings are expected to be softer and exhibit more ductile

characteristics which is exhibited by the pencil hardness and the König hardness. All coatings showed excellent adhesion to the metal substrate which is expected given the free hydroxyls present in the cured coatings. Solvent resistance of oven cured coatings outperformed the solvent resistance of the ambient cured coatings due to the higher degree of crosslinking in the oven cured coatings. The reverse impact of the coatings was all on the lower side implying that the coatings are lacking in flexibility. However, the good conical mandrel results can be explained due to the excellent adhesion to the substrate and slower deformation speeds when compared to the reverse impact test

Formulation 4 which utilizes 6-membered cyclic carbonate can be compared to its 5-memberd cyclic carbonate counterpart formulation 2. It is clear that the coatings produced by formulation 4 exhibit higher surface hardness than formulation 2. This result can be ascribed to the higher reactivity of the 6-membered cyclic carbonates. The higher reactivity would lower the amount of low molecular weight species present in the thermoset having a direct effect on the hardness of the coating.

4.4.7. Water Drop Test and Contact Angle

The surface of the coatings from the waterborne polyurethane dispersions was characterized utilizing static contact angle with deionized water. Because water absorption will occur due to the hydrophilic m-PEG chains, the static contact angle test provide insight on how hydrophobic/hydrophilic the surface of a coating is. Observing Table 4.6 the oven cured coatings containing higher m-PEG yielded overall lower contact angles than the coatings containing the lower m-PEG content. Formulations 1 and 2, containing m-PEG content of 4% and 9% respectively, expressed similar contact angles averaging at about 45°. However, the contact angle decreases to about 27° as the m-PEG content in the coating increases to 14%.

Table 4.6: Static water contact angle and water drop test data for waterborne polyurethane coatings.

Formulation	Curing	CA(M) [°]	CA(L) [°]	CA(R) [°]	WATER DROP TEST
4	Oven	66.68 (+-1.1)	66.41 (+-1.0)	66.96 (+-1.2)	3
	Ambient	19.79 (+-5.3)	20.98 (+-9.7)	18.59(+-0.9)	1
3	Oven	26.85 (+-4.29)	26.65 (+-4.59)	27.06 (+-3.99)	1
	Ambient	0.00	0.00	0.00	0
2	Oven	44.98 (+-5.60)	44.77 (+- 6.06)	45.20 (+-5.18)	2
	Ambient	0.00	0.00	0.00	0
1	Oven	44.74 (+-0.66)	44.64(+-0.69)	44.83 (+-0.70)	2
	Ambient	13.93 (+-0.80)	13.02 (+-1.59)	14.85 (+-1.44)	1

The water drop test agrees with the contact angle measurements in formulations 1 and 2 showed evidence for blistering and peeling while formulation 3 started to show signs of delamination. Ambient cured coatings show a similar trend but with lower contact angles and lower water drop test grades. Formulation 1 had very low water contact angle measurements at ambient curing condition while formulations 2 and 3 showed complete water droplet absorption, thus a contact angle could not be measured. The water drop test showed some delamination in formulation 1 and complete delamination for formulation 2 and 3 with the ambiently cured panels. Formulation 4 which utilized the 6-membered cyclic carbonate, and 10% m-PEG content showed the most hydrophobic characteristics with the oven cured samples containing contact angles of about 67° and the ambient cured samples of about 20°. The water drop test the oven cured samples were the most favorable from the group with a grade of 3 only showing slight blistering and the ambient at 1 showing some delamination. The higher the crosslinked network structure is, the more intermolecular forces of the coatings increase. The structure of the polymeric chains is more compacted and as a result, water cannot permeate through the coating and be absorbed as

efficiently. However, the presence of polar free hydroxyl groups present in the coatings will contribute to absorption of water on the surface of the coating due to its hydrophilic characteristics. Finally, the m-PEG chains contributions to hydrophilicity are apparent. This results are in line with what was shown by Harkal[33] given that the larger molecular weight m-PEG chains contain higher chain flexibility and longer chain length which increase its wetting characteristics.

4.4.8. Thermal Characteristics

Thermal gravimetric analysis was used to investigate the thermal decomposition of the coating samples. Little difference was observed between the thermal decomposition of ambient cured and oven cured systems and so the thermal decomposition values reported on table 6 are for the oven cured system.

Table 4.7: Thermal data for non-isocyanate waterborne polyurethane coatings.

Formulation	TGA(Td%5) (°C)	Oven Cured DSC (Tg) (°C)	Ambient Cured DSC (Tg) (°C)	Oven Cured DSC (Tg) (°C)
1	172.49	33.92	23.47	28.14
2	172.49	35.01	23.36	28.89
3	170.28	23.88	19.16	23.31
4	181.11	23.97	18.96	22.78

Generally, urethane linkages are known to contain some degree of bond reversibility. [46] As a result, low thermal stability of polyurethanes is expected. However, it's been reported in literature that the degradation of the urethane bonds occurs in three stages, but these can happen simultaneously.[47] From Figure 4.12 one can see that all three stages of degradation seem to be present in the non- isocyanate coating systems.

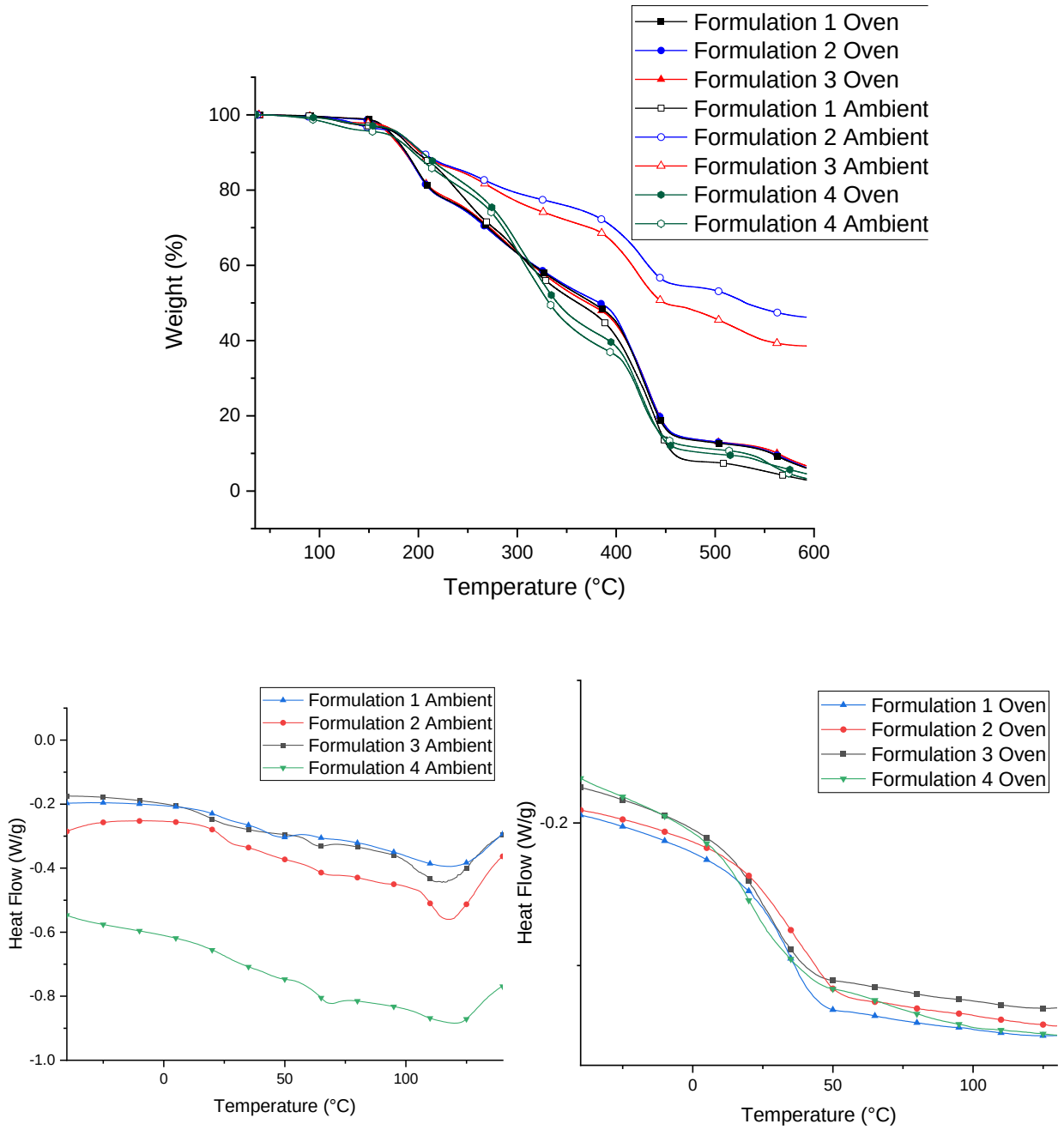

Figure 4.12: TGA curves (top) and DSC curves (bottom) for crosslinked waterborne NIPU.

For all systems thermal degradation (Td5%) begins, similarly to where other literature[48, 49] reports it, at around 170 °C to 180 °C depending on the coating system which is where the dissociation of isocyanate and alcohol take place.

The DSC measurement show clear differences between the ambient cured samples and the oven cured samples. The oven cured samples exhibit higher glass transition temperatures than the ambient cured samples. This data gives evidence for a higher crosslinking density in the oven cured samples restricting mobility of the polymer network. This effect is not as present in the ambient cured samples. Additionally, observing the cycle 1 DSC curves of the ambient cured samples in Figure 4.14 shows an exothermic peak around 120 °C, indicating that additional curing is taking place. The appearance of this endotherm led to a preliminary post curing study that was carried out by placing the ambiently cured panels in an oven for 10 min at 120°C and taking DSC measurements of the post cured samples. The post cured sample DSC graphs illustrated in Figure 4.13.

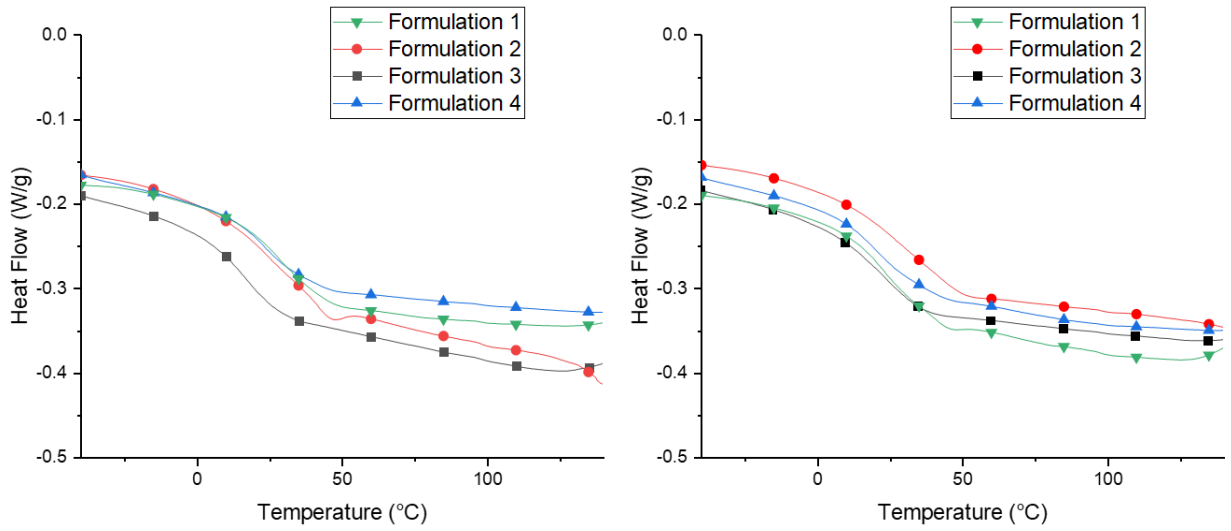

Figure 4.13: DSC curves of post cured ambiently cured samples. Graph on the left is 2nd heating cycle, while graph on the right is the 1st heating cycle.

The post cured samples showed disappearance of the exothermic peaks that were there previously. However, the glass transitions were not as high as the oven cured samples. To gain further insight, a study including post curing schedules for ambient cured coatings could be executed.

4.5. Conclusion

Non-isocyanate waterborne polyurethane dispersions were created utilizing 5 and 6-membered cyclic carbonates. Dispersions were successfully created, but particle sizes were too large for long term stability. Thermoset coatings characterized hinted that the systems are not reactive enough for ambient curing conditions in the presence of water. However, oven cured coatings do give decent coatings properties and utilization of a 6-membered cyclic carbonate yields products that are superior to 5-membered cyclic carbonates due to the higher reactivity. Some future work includes the use of 6-membered cyclic carbonates at different ratios as well as hydrolysis studies of 6-membered cyclic carbonates and utilization of different 6 membered cyclic carbonates.

4.6. References

1. Datta, J.; Kasprzyk, P., Thermoplastic polyurethanes derived from petrochemical or renewable resources: A comprehensive review. *Polymer Engineering and Science* **2018,** *58*, E14-E35.
2. Khatoon, H.; Iqbal, S.; Irfan, M.; Darda, A.; Rawat, N. K., A review on the production, properties and applications of non-isocyanate polyurethane: A greener perspective. *Progress in Organic Coatings* **2021,** *154*, 106124.
3. Bello, D.; Herrick Christina, A.; Smith Thomas, J.; Woskie Susan, R.; Streicher Robert, P.; Cullen Mark, R.; Liu, Y.; Redlich Carrie, A., Skin Exposure to Isocyanates: Reasons for Concern. *Environmental Health Perspectives* **2007,** *115* (3), 328-335.
4. Asemani, H. R.; Mannari, V., Synthesis and evaluation of non-isocyanate polyurethane polyols for heat-cured thermoset coatings. *Progress in Organic Coatings* **2019,** *131* (February), 247-258.
5. Bobade, S. K.; Paluvai, N. R.; Mohanty, S.; Nayak, S. K., Bio-Based Thermosetting Resins for Future Generation: A Review. *Polymer - Plastics Technology and Engineering* **2016,** *55* (17), 1863-1896.
6. Bullermann, J.; Friebel, S.; Salthammer, T.; Spohnholz, R., Novel polyurethane dispersions based on renewable raw materials - Stability studies by variations of DMPA content and degree of neutralisation. *Progress in Organic Coatings* **2013,** *76* (4), 609-615.
7. Cakić, S. M.; Špírková, M.; Ristić, I. S.; B-Simendić, J. K.; M-Cincović, M.; Poręba, R., The waterborne polyurethane dispersions based on polycarbonate diol: Effect of ionic content. *Materials Chemistry and Physics* **2013,** *138* (1), 277-285.

8. Carré, C.; Ecochard, Y.; Caillol, S.; Avérous, L., From the Synthesis of Biobased Cyclic Carbonate to Polyhydroxyurethanes: A Promising Route towards Renewable Non-Isocyanate Polyurethanes. *ChemSusChem* **2019,** *12* (15), 3410-3430.

9. Ghasemlou, M.; Daver, F.; Ivanova, E. P.; Adhikari, B., Polyurethanes from seed oil-based polyols: A review of synthesis, mechanical and thermal properties. *Industrial Crops and Products* **2019,** *142* (September).

10. Mucci, V. L.; Hormaiztegui, M. E. V.; Aranguren, M. I., Plant oil-based waterborne polyurethanes: A brief review. *Journal of Renewable Materials* **2020,** *8* (6), 579-601.

11. Samanta, S.; Selvakumar, S.; Bahr, J.; Wickramaratne, D. S.; Sibi, M.; Chisholm, B. J., Synthesis and Characterization of Polyurethane Networks Derived from Soybean-Oil-Based Cyclic Carbonates and Bioderivable Diamines. *ACS Sustainable Chemistry and Engineering* **2016,** *4* (12), 6551-6561.

12. Sawpan, M. A., Polyurethanes from vegetable oils and applications: a review. *Journal of Polymer Research* **2018,** *25* (8).

13. Surender, R.; Mahendran, A. R.; Wuzella, G.; Vijayakumar, C. T., Synthesis, characterization and degradation behavior of thermoplastic polyurethane from hydroxylated hemp seed oil. *Journal of Thermal Analysis and Calorimetry* **2016,** *123* (1), 525-533.

14. Burk, R. M.; Roof, M. B., A safe and efficient method for conversion of 1,2- and 1,3-diols to cyclic carbonates utilizing triphosgene. *Tetrahedron Letters* **1993,** *34* (3), 395-398.

15. Rehman, A.; Saleem, F.; Javed, F.; Ikhlaq, A.; Ahmad, S. W.; Harvey, A., Recent advances in the synthesis of cyclic carbonates via CO2 cycloaddition to epoxides. *Journal of Environmental Chemical Engineering* **2021,** *9* (2), 105113.

16. Pescarmona, P. P., Cyclic carbonates synthesised from CO2: Applications, challenges and recent research trends. *Current Opinion in Green and Sustainable Chemistry* **2021,** *29*, 100457.

17. Subramanian, S.; Song, Y.; Kim, D.; Yavuz, C. T., Redox and Nonredox CO₂ Utilization: Dry Reforming of Methane and Catalytic Cyclic Carbonate Formation. *ACS Energy Letters* **2020,** *5* (5), 1689-1700.

18. North, M.; Pasquale, R.; Young, C., Synthesis of cyclic carbonates from epoxides and CO2. *Green Chemistry* **2010,** *12* (9), 1514.

19. Singh Dhankhar, S.; Ugale, B.; Nagaraja, C. M., Co-Catalyst-Free Chemical Fixation of CO2 into Cyclic Carbonates by using Metal-Organic Frameworks as Efficient Heterogeneous Catalysts. *Chemistry – An Asian Journal* **2020,** *15* (16), 2403-2427.

20. Yadav, N.; Seidi, F.; Crespy, D.; D'Elia, V., Polymers Based on Cyclic Carbonates as Trait d'Union Between Polymer Chemistry and Sustainable CO2 Utilization. *ChemSusChem* **2019,** *12* (4), 724-754.

21. Suryawanshi, Y.; Sanap, P.; Wani, V., Advances in the synthesis of non-isocyanate polyurethanes. *Polymer Bulletin* **2019,** *76* (6), 3233-3246.

22. Webster, D. C.; Crain, A. L., Synthesis and applications of cyclic carbonate functional polymers in thermosetting coatings. *Progress in Organic Coatings* **2000,** *40* (1-4), 275-282.

23. Yu, A. Z.; Setien, R. A.; Sahouani, J. M.; Docken, J.; Webster, D. C., Catalyzed non-isocyanate polyurethane (NIPU) coatings from bio-based poly(cyclic carbonates). *Journal of Coatings Technology and Research* **2019,** *16* (1).

24. Morales-Cerrada, R.; Boutevin, B.; Caillol, S., Glycerol carbonate methacrylate: A cross-linking agent for hydroxyurethane-acrylate coatings. *Progress in Organic Coatings* **2021,** *151*, 106078.

25. Pathak, R.; Kathalewar, M.; Wazarkar, K.; Sabnis, A., Non-isocyanate polyurethane (NIPU) from tris-2-hydroxy ethyl isocyanurate modified fatty acid for coating applications. *Progress in Organic Coatings* **2015,** *89*, 160-169.

26. Wang, C.; Wu, Z.; Tang, L.; Qu, J., Synthesis and properties of cyclic carbonates and non-isocyanate polyurethanes under atmospheric pressure. *Progress in Organic Coatings* **2019,** *127*, 359-365.

27. Liu, G.; Wu, G.; Huo, S.; Jin, C.; Kong, Z., Synthesis and properties of non-isocyanate polyurethane coatings derived from cyclic carbonate-functionalized polysiloxanes. *Progress in Organic Coatings* **2017,** *112*, 169-175.

28. Capar, Ö.; Tabatabai, M.; Klee, J. E.; Worm, M.; Hartmann, L.; Ritter, H., Fast curing of polyhydroxyurethanes via ring opening polyaddition of low viscosity cyclic carbonates and amines. *Polymer Chemistry* **2020,** *11* (43), 6964-6970.

29. Lombardo, V. M.; Dhulst, E. A.; Leitsch, E. K.; Wilmot, N.; Heath, W. H.; Gies, A. P.; Miller, M. D.; Torkelson, J. M.; Scheidt, K. A., Cooperative Catalysis of Cyclic Carbonate Ring Opening: Application Towards Non-Isocyanate Polyurethane Materials. *European Journal of Organic Chemistry* **2015,** *2015* (13), 2791-2795.

30. Yuen, A.; Bossion, A.; Gómez-Bengoa, E.; Ruipérez, F.; Isik, M.; Hedrick, J. L.; Mecerreyes, D.; Yang, Y. Y.; Sardon, H., Room temperature synthesis of non-isocyanate polyurethanes (NIPUs) using highly reactive N-substituted 8-membered cyclic carbonates. *Polymer Chemistry* **2016,** *7* (11), 2105-2111.

31. Ghasemlou, M.; Daver, F.; Ivanova, E. P.; Adhikari, B., Bio-based routes to synthesize cyclic carbonates and polyamines precursors of non-isocyanate polyurethanes: A review. *European Polymer Journal* **2019,** *118*, 668-684.

32. Kathalewar, M. S.; Joshi, P. B.; Sabnis, A. S.; Malshe, V. C., Non-isocyanate polyurethanes: from chemistry to applications. *RSC Advances* **2013,** *3* (13), 4110.

33. Harkal, U. D.; Muehlberg, A. J.; Edwards, P. A.; Webster, D. C., Novel water-dispersible glycidyl carbamate (GC) resins and waterborne amine-cured coatings. *Journal of Coatings Technology and Research* **2011,** *8* (6), 735-747.

34. Bizet, B.; Grau, É.; Cramail, H.; Asua, J. M., Water-based non-isocyanate polyurethane-ureas (NIPUUs). *Polymer Chemistry* **2020,** *11* (23), 3786-3799.

35. Webster, D. C.; Crain, A. L., Synthesis of Cyclic Carbonate Functional Polymers. In *Functional Polymers*, American Chemical Society: 1998; Vol. 704, pp 303-320.

36. Sonnati, M. O.; Amigoni, S.; Taffin De Givenchy, E. P.; Darmanin, T.; Choulet, O.; Guittard, F., Glycerol carbonate as a versatile building block for tomorrow: synthesis, reactivity, properties and applications. *Green Chem.* **2013,** *15* (2), 283-306.

37. Yu, W.; Maynard, E.; Chiaradia, V.; Arno, M. C.; Dove, A. P., Aliphatic Polycarbonates from Cyclic Carbonate Monomers and Their Application as Biomaterials. *Chemical Reviews* **2021,** *121* (18), 10865-10907.

38. Sarel, S.; Levin, I.; Pohoryles, L. A., 614. Organic carbonates. Part V. The mechanism of hydrolysis of cyclic carbonates: tracer studies. *Journal of the Chemical Society (Resumed)* **1960**, 3079.

39. Rollin, P.; Soares, L. K.; Barcellos, A. M.; Araujo, D. R.; Lenardão, E. J.; Jacob, R. G.; Perin, G., Five-Membered Cyclic Carbonates: Versatility for Applications in Organic Synthesis, Pharmaceutical, and Materials Sciences. *Applied Sciences* **2021,** *11* (11).

40. Rix, E.; Grau, E.; Chollet, G.; Cramail, H., Synthesis of fatty acid-based non-isocyanate polyurethanes, NIPUs, in bulk and mini-emulsion. *European Polymer Journal* **2016,** *84*, 863-872.

41. Ochiai, B.; Satoh, Y.; Endo, T., Nucleophilic polyaddition in water based on chemo-selective reaction of cyclic carbonate with amine. *Green Chemistry* **2005,** *7* (11), 765.

42. Sardon, H.; Engler, A. C.; Chan, J. M. W.; Coady, D. J.; O'Brien, J. M.; Mecerreyes, D.; Yang, Y. Y.; Hedrick, J. L., Homogeneous isocyanate- and catalyst-free synthesis of polyurethanes in aqueous media. *Green Chemistry* **2013,** *15* (5), 1121.

43. Monument, C., Terms and Formulas Used in Urethane Polymer Preparations. **2010**.

44. Cornille, A.; Blain, M.; Auvergne, R.; Andrioletti, B.; Boutevin, B.; Caillol, S., A study of cyclic carbonate aminolysis at room temperature: effect of cyclic carbonate structures and solvents on polyhydroxyurethane synthesis. *Polymer Chemistry* **2017,** *8* (3), 592-604.

45. Lambeth, R. H.; Henderson, T. J., Organocatalytic synthesis of (poly)hydroxyurethanes from cyclic carbonates and amines. *Polymer* **2013,** *54* (21), 5568-5573.

46. Polyurethane, N.-i.; Delebecq, E.; Pascault, J.-p.; Boutevin, B.; Lyon, U. D., On the Versatility of Urethane / Urea Bonds : Reversibility , Blocked. **2013**.

47. Carré, C.; Bonnet, L.; Avérous, L., Original biobased nonisocyanate polyurethanes: solvent- and catalyst-free synthesis, thermal properties and rheological behaviour. *RSC Adv.* **2014,** *4* (96), 54018-54025.

48. Mumtaz, F.; Zuber, M.; Zia, K. M.; Jamil, T.; Hussain, R., Synthesis and properties of aqueous polyurethane dispersions: Influence of molecular weight of polyethylene glycol. *Korean Journal of Chemical Engineering* **2013,** *30* (12), 2259-2263.

49. Yu, F.; Cao, L.; Meng, Z.; Lin, N.; Liu, X. Y., Crosslinked waterborne polyurethane with high waterproof performance. *Polymer Chemistry* **2016,** *7* (23), 3913-3922.

CHAPTER 5. FEASIBILITY OF THE CARBAMATE ALDEHYDE CROSSLINKING REACTION IN WATER BORNE POLYURETHANE DISPERSIONS

5.1. Abstract

The feasibility of the carbamate-aldehyde curing reaction was explored in both waterborne and solvent borne systems to understand the reaction's potential in thermoset coatings. The polyurethanes were synthesized by reacting isocyanate trimers with hydroxymethylfurfural to create aldehyde functional polyurethanes or hydroxyl propyl carbamate to create primary carbamate functional polyurethanes. The successful synthesis was confirmed by FTIR and NMR spectroscopy. The influence of the use of different dispersion methods to produce waterborne polyurethane dispersions on dispersion stability and coating appearance through was evaluated. Particle size and stability of dispersions were evaluated. Stable dispersions were then used to create thermoset coatings. The coatings made from the waterborne systems were then evaluated in comparison to coatings made from the same components in the absence of water. Water contact angle, water drop test, coating properties, and thermal properties of the coatings were evaluated. It was indicated that the coatings made from solvent borne formulations were more crosslinked than coatings made from the waterborne formulation. Further exploration of the carbamate-aldehyde curing reaction is required to fully understand the influence of water in the crosslinking reaction.

5.2. Introduction

Polyurethanes are highly versatile polymers that are used in a variety of different applications such as adhesives, foams for upholstery and automobile coatings.[1] Their widespread utility can be attributed to the urethane linkages in the polymeric backbone which give thermosets

produced from polyurethanes desirable characteristics such as high elasticity, mechanical resistance and chemical resistance.

Polyurethanes are commonly synthesized by reacting isocyanate resins and hydroxyl functional species (Scheme 5.1). This reaction produces the urethane linkages that act as the building block of polyurethanes. This method of synthesizing polyurethanes has attracted a significant amount of attention manly due to the health concerns surrounding the topic of exposure to isocyanate functional reagents. [2, 3] As a result, there is a great deal of literature exploring alternative paths, such as non-isocyanate polyurethanes (NIPU), to synthesizing polyurethanes with the goal of minimizing the use of isocyanates.[4-14]

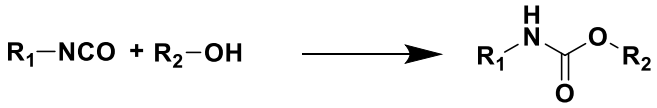

Scheme 5.1: General reaction scheme between isocyanate and hydroxyl to yield a urethane linkage.

A method used to create polyurethanes with low VOC content is to disperse the polymers in water and create what is known as a waterborne-polyurethane dispersion (WBPUD).[15-28] These waterborne polyurethane dispersions may utilize internal emulsifiers that are incorporated into the polymeric backbone. These internal emulsifiers may come from ionic or non-ionic species and change the interactions between polyurethane particles in a water medium to provide a mechanism of stability. Non-ionic WBPUD contribute to steric stabilization of particles which are more resistant to changes in pH making non-ionic WBPUD more viable in crosslinking systems that utilize acidic reagents such as the carbamate-aldehyde reaction.[29]

The carbamate-aldehyde reaction is a potential pathway for creating non-isocyanate polyurethane coatings. However, literature exploring this reaction is lacking and so far this curing

reaction has not been explored in a waterborne system. The tentative reaction scheme was taken from literature[30] and is displayed in Scheme 5.2.

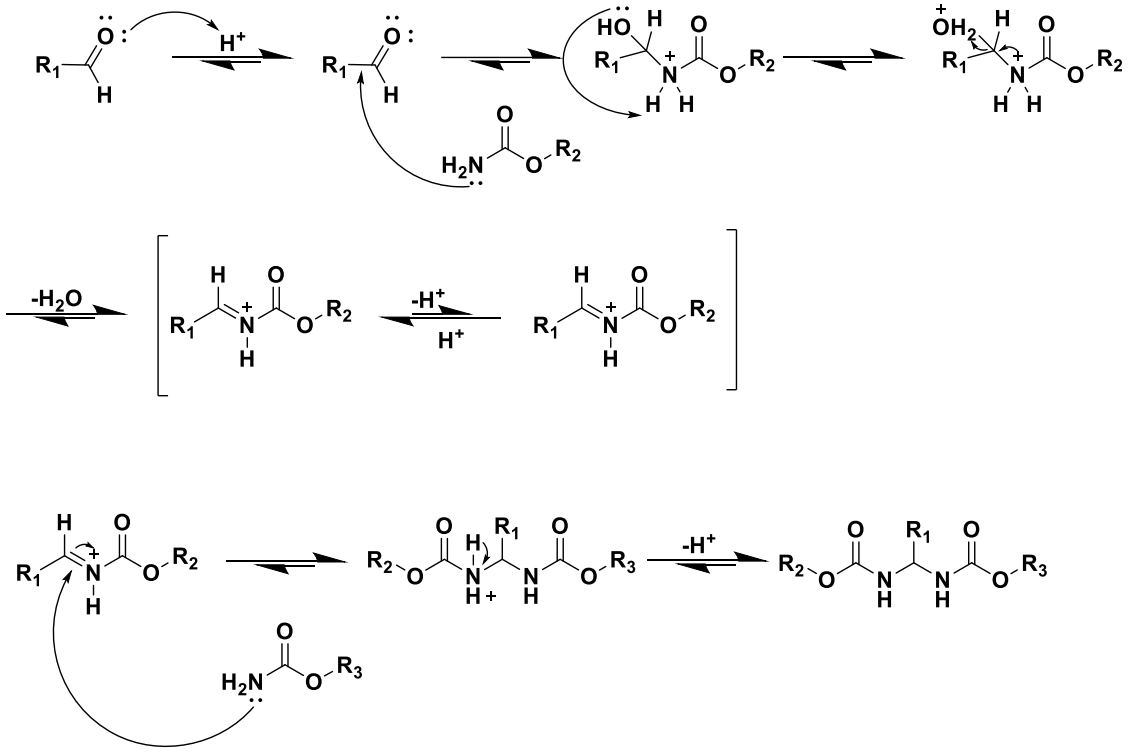

Scheme 5.2: Tentative mechanism for the crosslinking reaction of carbamates and aldehyde. Proposed in literature.[30]

The reaction starts by the activation of the aldehyde carbonyl via the acidic proton generated by an acid catalyst. Then nucleophilic attack of the carbonyl carbon by the carbamate takes place. Then, a structural rearrangement occurs to yield a hemiaminal structure. Water is released from the molecule to from an Iminium intermediate which is self-stabilized via resonance in the form of an imine structure. The iminium intermediate undergoes a nucleophilic attack by an additional carbamate species and an acidic proton is released to form a diurethane structure. This reaction has already been utilized in solvent borne systems and was shown to be effective in producing bio-based NIPU coatings, but no attempts as of yet have been made to incorporate it in waterborne systems. [13]

This body of work attempts to incorporate this crosslinking chemistry in non-isocyanate WBPUD exploring the use of hydroxyl propyl carbamate and hydroxymethylfurfural to create thermoset coatings.

5.3. Experimental

5.3.1. Materials

Desmodur N 3600 was provided Covestro. Propylene carbonate (PC), ammonia 7N in methanol, dibutyltin dilaurate (DBTDL), methoxy polyethylene glycol (m-PEG 750), chloroform-d, p-toluene sulfonic acid (PTSA), and acetone, were purchased from Sigma-Aldrich, Milwaukee WI, USA. Hydroxyl propyl carbamate (HPC) was synthesized utilizing procedures below. Hydroxymethylfurfural (HMF) was purchased from Matrix scientific Mount Prospect, IL,USA and was purified by column chromatography.

5.3.2. Reaction Ratio Calculations

Reaction ratio calculations were based off the following literature. Isocyanate equivalent weight was calculated using equation 5.1

$$\frac{4200}{NCO\ content\ (\%)} = E_s \tag{5.1}$$

With *Es* equaling isocyanate equivalent weight. The hydroxyl number of the mix was calculated using the equation 5.2.

$$OH_m = OH_j a + OH_k(1 - a) \tag{5.2}$$

With OH_m being the hydroxyl number of the mix, $\boldsymbol{a}$ being the fractional component of hydroxyl species 1, OH_j hydroxyl value of component 1, OH_k hydroxyl value of component 2. In this study component 1 is considered either HMF or HPC while component 2 is m-PEG 750. Weight equivalent of hydroxyl mix was calculated using equation 5.3.

$$Ep_m = \frac{1000*56.1}{OH_m} \quad (5.3)$$

With Ep_m being the equivalent of hydroxyl mix. Weight of isocyanate required to react with hydroxyl mix was calculated using equation 5.4.

$$W_s = \frac{E_s*W_p*R}{Ep_m} \quad (5.4)$$

With W_s being the weight of isocyanate (g), W_p being the weight for the hydroxyl species mixture (g), and R being the ratio of isocyanate to polyol. These equations were utilized to formulate different polyurethane synthesis with varying fractional components. These polyurethanes are illustrated in Table 5.1.

Table 5.1: Table illustrating the different amount (wt/wt%) of reactive components used in the synthesis of waterborne polyurethane dispersions with either primary carbamate or aldehyde functionality. The α value for the synthesis are as follows: 1 = 0.9, 2 = 0.8, 3 = 0.7, and 1a = 0.6.

Polyurethane	1	2	3	1a
Hydroxyl propyl carbamate	37.4	35.1	32.6	0
Hydroxymethylfurfural	0	0	0	30.5
m-PEG 750	4.2	8.8	14	20.3
Desmodur N 3600	58.3	56	53.4	49.1

Catalyst (dibutyltin dilaurate) loading for all synthesis consisted of 0.1% of total resin weight. All polyurethanes utilized enough solvent (acetone) to yield a product with 70% solids.

5.3.3. Synthesis of 2-Hydroxypropyl Carbamate

A two neck 500 mL round bottom flask is equipped with a magnetic stirrer, a water-cooled condenser, and a nitrogen inlet. The flask is charged with propylene carbonate (351.8 g) and 7N ammonia solution in methanol (391.12 g). The mixture is heated using an oil bath to 50 °C for 2 hours. Afterwards, the temperature of the mixture is then increased to 67 °C for 1 hr. The flask is then connected to a rotary evaporator and the excess methanol is removed from the reaction flask. An FTIR check is done to monitor the conversion of propylene carbonate to 2-hydroxypropyl

carbamate. If unreacted propylene carbonate remains, additional ammonia solution (150 g) is added to the mixture at 67 °C. Excess methanol is once again removed from the mixture using a rotary evaporator. The final product is collected in the form of a viscous light-yellow liquid.

5.3.4. Synthesis of Polyurethane

A 500 mL four necked round bottom flask was equipped with a condenser, nitrogen inlet, a J-KEM thermocouple attached to a module apollo J-KEM temperature controller, an addition funnel, and an Arrow 1750 overhead mechanical stirrer. The round bottom flask was charged with polyisocyanate (Desmodur N 3600) and methoxy polyethylene glycol (m-PEG 750). The contents of the flask were heated to 40 °C with stirring to allow mixing for 30 min. After mixing time had elapsed, dibutyl tin dilaurate (DBTDL) was added to the flask. HPC dissolved in acetone was added through the addition funnel dropwise and the reaction temperature was maintained at 60 °C. The addition was done over a time period of 2 h. The reaction was maintained at 60 °C with stirring until the isocyanate peak (2271 cm^{-1}) had disappeared from the FTIR spectra. The completed reaction product was then transferred to a single neck 500 mL round bottom flask and the acetone solvent was removed using a rotary evaporator.

5.3.5. Dispersion and Crosslinking Formulation

Dispersion method 1 consisted of dissolving primary carbamate functional polyurethane in acetone so that the total percent solids of the polyurethane formulation was 70%. Mixing of the acetone and polyurethane was carried out in a Flacktek highspeed mixer at 3500 rpms for 5 minutes. Meanwhile, enough water was added to a separate 200 mL container to theoretically yield a 30% wt. dispersion. The polyurethane solution was added dropwise to the 200 mL container over the course of 15 min while mixing with an Arrow type 316 stainless steel propeller stirrer at stirring speed 5. The acetone was removed utilizing a rotary evaporator. The waterborne polyurethae

dispersion was transferred another 200 mL container and was subjected to continuous stirring with an Arrow type 316 over head stirrer with stirring speed set at 5. PTSA was added to the waterborne polyurethane dispersion at 5% wt. of total primary carbamate functionality followed by HMF at 2:1 carbamate to aldehyde equivalent ratio. The contents of the 200 mL container were transferred to a Flacktek Inc MAX 100 CUP and were mixed in Flacktek highspeed mixer at 3500 rpms for 30 seconds to remove bubbles that had formed in the dispersion.

Dispersion method 2 consisted of heating the HPC functional polyurethane in an oven at 100°C so that the viscosity of the overall polyurethane is lowered to a workable range. Meanwhile, enough water was added to a separate 200 mL container to theoretically yield a 30% wt. dispersion. The heated polyurethane was added dropwise to the 200 mL container over the course of 15 min while mixing with an Arrow type 316 overhead stirrer equipped with a stainless-steel propeller stirrer at stirring speed 5. The waterborne polyurethane dispersion was transferred another 200 mL container and was subjected to continuous stirring with an Arrow type 316 over head stirrer with stirring speed set at 5. PTSA was added to the waterborne polyurethane dispersion at 5% wt. of total primary carbamate functionality followed by HMF at 2:1 carbamate to aldehyde equivalent ratio. The contents of the 200 mL container were transferred to a Flacktek Inc MAX 100 CUP and were mixed in Flacktek highspeed mixer at 3500 rpms for 30 seconds to remove bubbles that had formed in the dispersion.

Dispersion method 3 consisted of heating the HPC functional polyurethane in an oven at 100°C so that the viscosity of the overall polyurethane is lowered to a workable range. Meanwhile, enough water was added to a separate 200 mL container to theoretically yield a 30% wt. dispersion. HMF was added to the 200 mL container at a 2:1 carbamate to aldehyde equivalent ratio and dissolved with the water in the 200 mL container using an Arrow type 316 over head stirrer with

stirring speed set to 2. The heated polyurethane was added dropwise to the 200 mL container over the course of 15 min while mixing with an Arrow type 316 overhead stirrer equipped with a stainless-steel propeller stirrer at stirring speed 5. PTSA was then added to the waterborne polyurethane dispersion at 5% wt. of total primary carbamate functionality. Stirring continued for one minute. The contents of the 200 mL container were transferred to a Flacktek Inc MAX 100 CUP and were mixed in Flacktek highspeed mixer at 3500 rpms for 30 seconds to remove bubbles that had formed in the dispersion.

Dispersing method 4 consisted of heating the primary carbamate functional polyurethane in an oven at 100°C so that the viscosity of the overall polyurethane is lowered to a workable range. Meanwhile, enough water was added to a separate 200 mL container to theoretically yield a 30% wt. dispersion. Both aldehyde functional and primary carbamate functional polyurethanes were added in small increments to the 200 mL container over the course of 15 min while mixing with an Arrow type 316 overhead stirrer equipped with a stainless-steel propeller stirrer at stirring speed 5. PTSA was then added to the waterborne polyurethane dispersion at 5% wt. of total primary carbamate functionality. Stirring continued for one minute. The contents of the 200 mL container were transferred to a Flacktek Inc MAX 100 CUP and were mixed in Flacktek highspeed mixer at 3500 rpms for 30 seconds to remove bubbles that had formed in the dispersion.

5.3.6. Solvent Borne Formulations

In a 40 mL scintillation vial, HMF, ethanol (1.5 equiv ethanol/aldehyde), pTSA (5% of the total carbamate functional polyurethane mass) were dissolved until the solution underwent a color change of yellow to dark blue (1 min). Using a Flacktek high speed mixer at 3500 rpms for 5 min, primary carbamate functional polyurethane was mixed with ethyl acetate to yield a solution of 30% solids. The primary carbamate functional polyurethane solution, crosslinker and catalyst

solution were mixed together using a Flacktek highspeed mixer at 3500 rpms for 2 min to yield a formulation.

5.3.7. Coating Curing

Coatings were made on R-36-I steel panels using a 20 mil BYK drawdown bar. The curing conditions for the coatings were 80 °C for 1h and 120 for 2h.

5.3.8. Percent Solids

Percent solids of the dispersed formulations were done in weighed, approximately 1 g, aluminum pans. The waterborne polyurethane dispersion was weighed in aluminum pans. The samples were heated at 120 °C for 1 h so that all the water would evaporate. The final weight of the pans after heating was recorded. Percent solids were then calculated from an average of three replicates using Equation 5.5.

$$\%Solids = \frac{FinalWeight - PanWeight}{InitialWeight} x100 \tag{5.5}$$

5.3.9. Dynamic Light Scattering

Particle size distribution was observed using dynamic light scattering techniques. The samples were diluted in distilled water and were analyzed using a Particle Sizing Systems Nicomp 380. The mean diameter of the particles was recorded using intensity weighting.

5.3.10. Nuclear Magnetic Resonance

^{13}C NMR spectroscopy was performed using a JEOL system, ECA Series 400 MHz NMR Spectrometer (JEOL, Peabody, MA, USA) and data was processed using Delta NMR software. The solvent used was CDCl3

5.3.11. FTIR

In-process FTIR checks were done on polyurethane synthesis to check for completion utilizing a Thermo Scientific Nicolet 87000 with a DTGS KBr detector with a nitrogen blanket. The absorption spectra of the samples were collected by transferring a sample from the reaction flask to a potassium bromide crystal optic disc (25mm x 4mm) using 32 scans at 4 cm^{-1} resolution.

5.3.12. Stability Test

A sample of the polyurethane dispersion was placed in a 40 mL scintillation vial immediately after formation of dispersion. The sample was kept at room temperature and observed over a period of time. Result of the state of the dispersion was observed and recorded after 7 days and 14 days.

5.3.13. FTIR-ATR

Coatings were characterized utilizing FTIR-ATR on a Thermo Scientific Nicolet 87000 using a Smart iTR attenuated total reflectance accessory (ATR). The coated samples were placed on top of the diamond with ZnSe lens where the absorption spectra were collected using 32 scans at 4 cm^{-1} resolution. The reflectance was then converted to absorbance using delta software.

5.3.14. Water Drop Test

The coatings absorption of water was tested by carrying out water drop tests. A drop of water was placed on the surface of the coating and was covered with a glass slide of approximately 2 x 2 cm (l,w) to prevent water evaporation. After 1 h of time had elapsed, the glass slide was removed from the coating and the absorption was evaluated visually for bubble formation, blisters, or film delamination. A number grade was assigned based on the appearance of the coatings from 0 to 5 with 0 demonstrating no defects, to 5 demonstrating complete delamination.

5.3.15. Static Contact Angle

Static contact angle of the coatings was measured utilizing a drop shape analyzer (DSA100 Krüss). Three measurements of a deionized water droplet of approximately 10 µL was placed on the surface of a coating and static contact angle was measure 10 seconds after the water droplet had come into contact with the surface of the coating. Presented data replicates the mean of those values.

5.3.16. Coating's Properties

Coating's properties were tested in accordance to ASTM procedures. Hardness was determined using both pencil hardness following ASTM D 3363 and König pendulum hardness following ASTM D 4366 König, Coating thickness was determined for cured coatings using a BYKO-Test 8500 coating thickness gauge. Crosshatch adhesion was determined to characterize coating adhesion to the substrate using a Gardco® crosshatch paint adhesion test kit following ASTM D 3359. Slow deformation using a conical mandrel bend measured flexibility following ASTM D 522. Reverse impact was used to measure flexibility under rapid deformation using ASTM D 2794. MEK Double rubs were done following a modified version of ASTM D 5402. Modifications include utilizing six layers of methyl ethyl ketone-soaked cheese cloth wrapped and tied around a 26-ounce hammerhead. The coating was rubbed back and forth with the hammer from the top of the coating to the base of the coating. Failure was reached when the substrate was exposed in the middle of the coating. The cloth was re-soaked in methyl ethyl ketone every 50 rubs.

5.3.17. Thermal Gravimetric Analysis

A Q500 thermogravimetric analysis (TGA) system (TA Instruments) with a heating rate of 10°C/min from room temperature to 600°C under a continuous nitrogen flow was used to determine the thermal stability of the thermosets.

5.3.18. Dynamic Scanning Calorimetry

A DSC Q1000 (TA Instruments) with heating and cooling rates of 10°C/min at a heat/cool/heat cycle scanned from -50°C to 150°C under nitrogen atmosphere was used to measure the glass transition temperatures (Tg) of the coatings.

5.4. Results and Discussion

To synthesize carbamate functional polyurethanes HPC needs to be synthesized. The hydroxyl functionality of HPC allows for the incorporation of the carbamate functional species in a polyurethane. IR was taken to confirm the synthesis of HPC. Figure 5.1 displays the FTIR spectra of PC and HPC. The most notable difference is the wide broadening of the peaks corresponding to the NH_2 of the primary carbamates generated in the HPC around 3600-3100 cm^{-1} region. This evidence is supported by the appearance of a peak at 1608 cm^{-1} which corresponds to the primary amines in the carbamate functionality. The other notable difference is the peak corresponding to the carbonyl in the propylene carbonate has shifted from 1790 cm^{-1} to 1701 cm^{-1} indicating that the cyclic ring of the PC has opened, and the presence of the carbamate functionality has caused a shift in the absorption band. Overall, it can be deduced that HPC was successfully synthesized from PC.

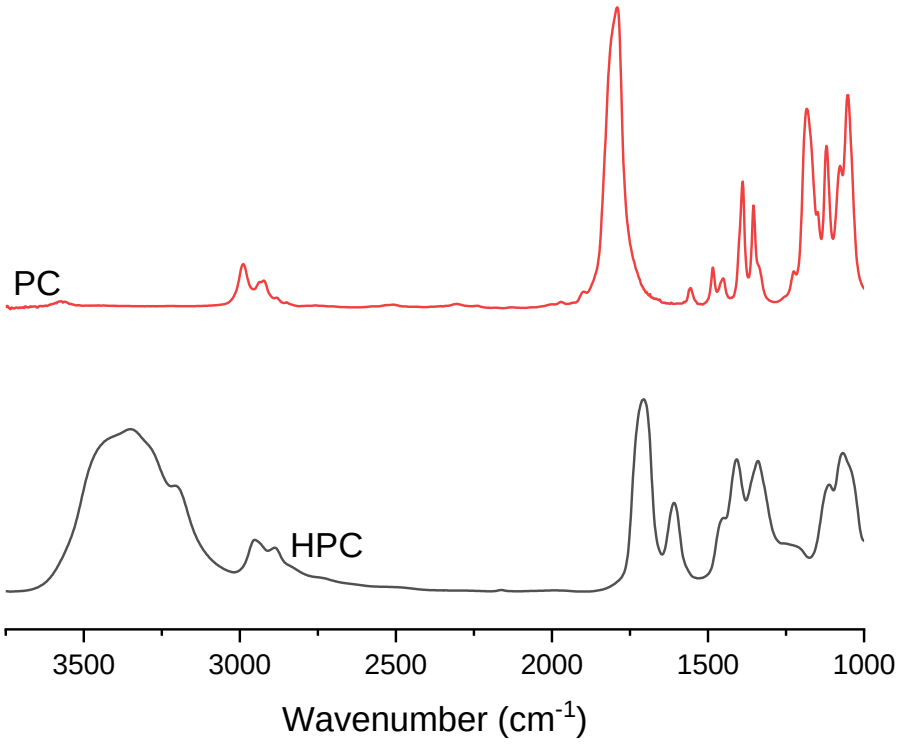

Figure 5.1: FTIR spectra of PC and HPC. Spectrum on top corresponds to PC. Spectrum on bottom corresponds to HPC.

The synthesis of the polyurethane resins was then carried out to produce carbamate functional polyurethanes and aldehyde functional polyurethane. Figure 5.2 shows the incomplete and complete reaction for the synthesis of an aldehyde polyurethane. The isocyanate peak can be observed at 2271 cm^{-1} and it disappears in the completed reaction indicating that the isocyanates have fully reacted. The narrowing of the peak in the hydroxyl region at around 3500-3300 cm^{-1} are from the reduction of hydroxyl functional species and increase in urethane linkages as the reaction occurs.

Figure 5.3 corresponding to the synthesis of carbamate functional polyurethane also displays the disappearance of the isocyanate peak at 2271 cm^{-1}. The multiple peaks at the hydroxyl region in 3500-3300 indicates the incorporation of primary carbamates from the HPC into the

polyurethane resin. Overall, the polyurethane FTIR indicate that the polyurethanes were synthesized successfully.

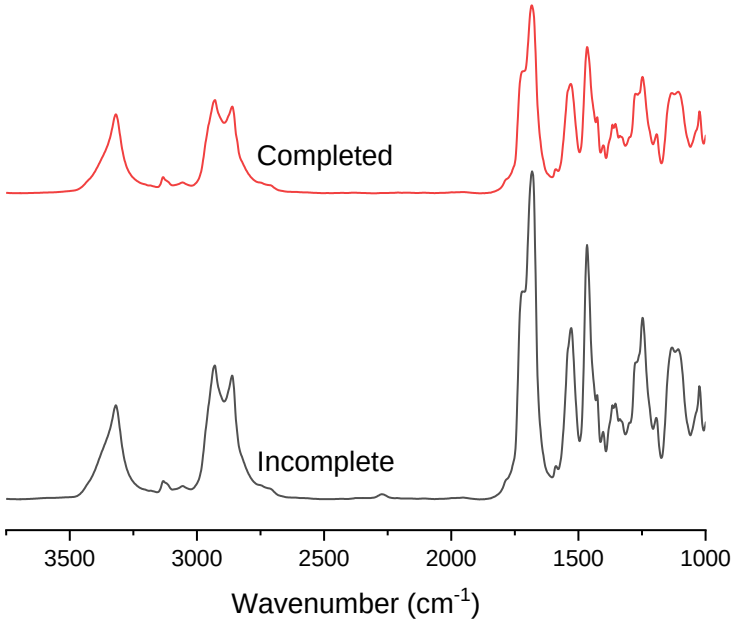

Figure 5.2: FTIR of aldehyde functional polyurethane. Incomplete reaction is the bottom spectrum while the completed reaction is the top spectrum.

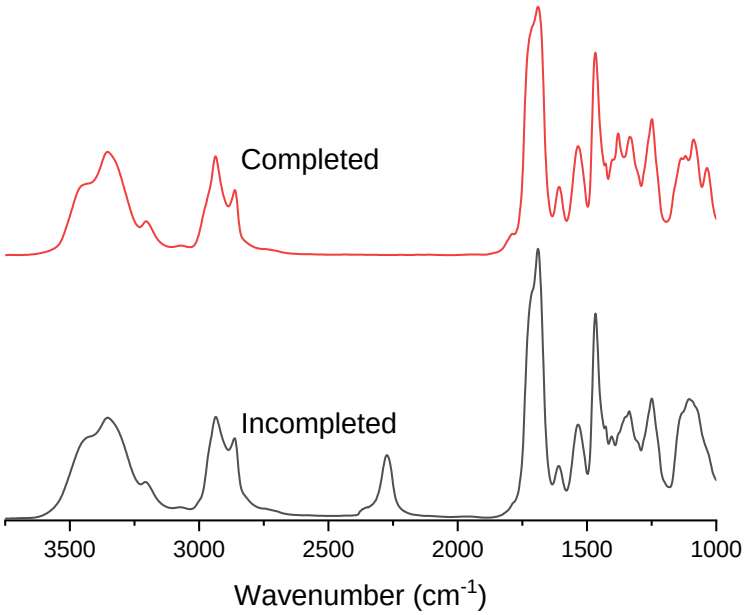

Figure 5.3: FTIR spectra of Carbamate functional polyurethanes. Incomplete reaction is the bottom spectrum wile the completed reaction is the top spectrum.

5.4.1. NMR

To reassure that the polyurethane resins had been successfully synthesized, carbon NMR spectra was taken for the polyurethane resins and Desmodur N 3600. Figure 5.4 displays the carbon NMR spectrum of Desmodur N 3600.

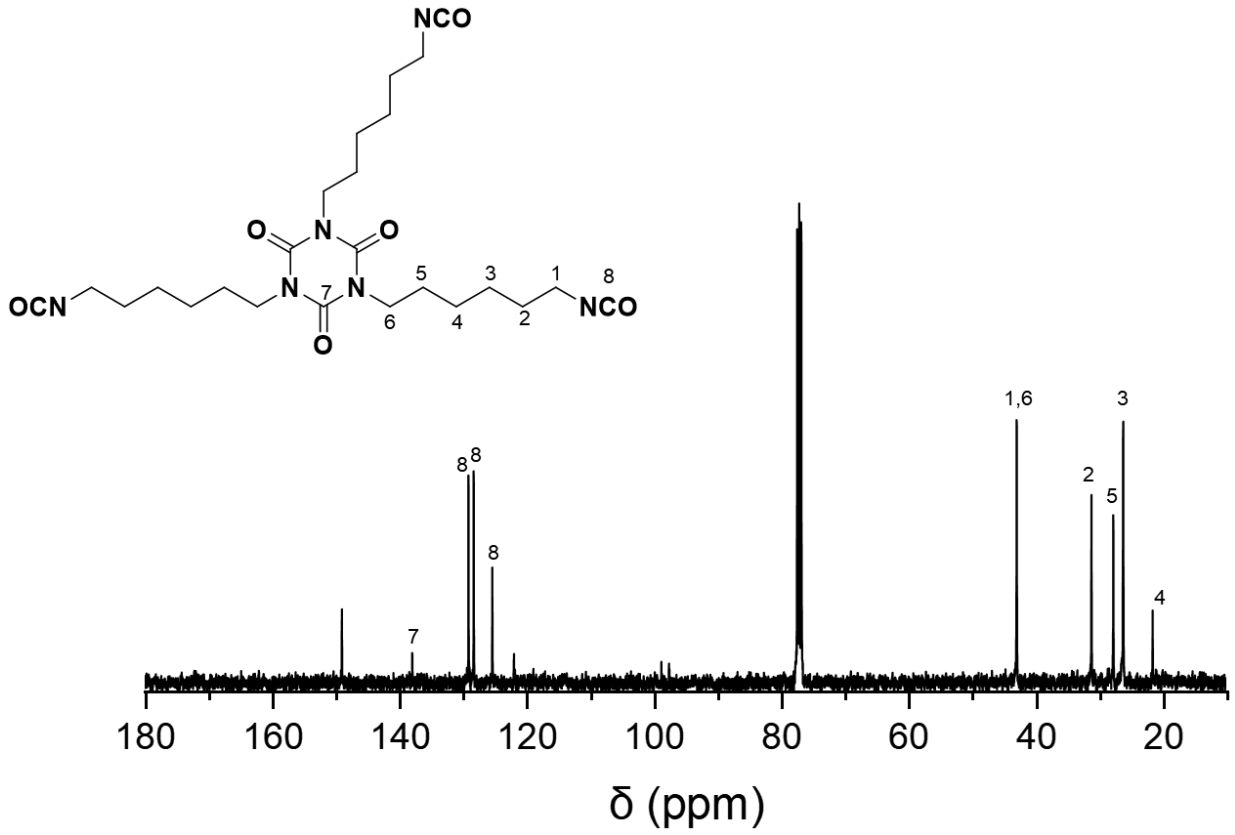

Figure 5.4: ^{13}C-NMR spectrum of Desmodur N 3600.

The technical data sheet describes Desmodur N 3600 as an aliphatic polyisocyanate of HDI trimer. Knowing that, certain characteristics on the ^{13}C-NMR spectrum can be identified. The peak at 149 comes from the carbonyl carbons of the isocyanurate core. The peaks at approximately 129, 128, 125 ppm correspond to the carbons in the unreacted isocyanate functional groups of the compound. The peaks at 43, 31, 27, 26, 21, are from the aliphatic carbons contributing to the polyisocyanate that come from HDI.

Examining Figure 5.5 and Figure 5.6 of the polyurethane C-NMR one can deduce that complete reaction of the isocyanates has occurred in both carbamate and aldehyde functional polyurethanes, since the peaks corresponding to the isocyanate functional groups have disappeared, but there are some differences in the spectra due to the functionality.

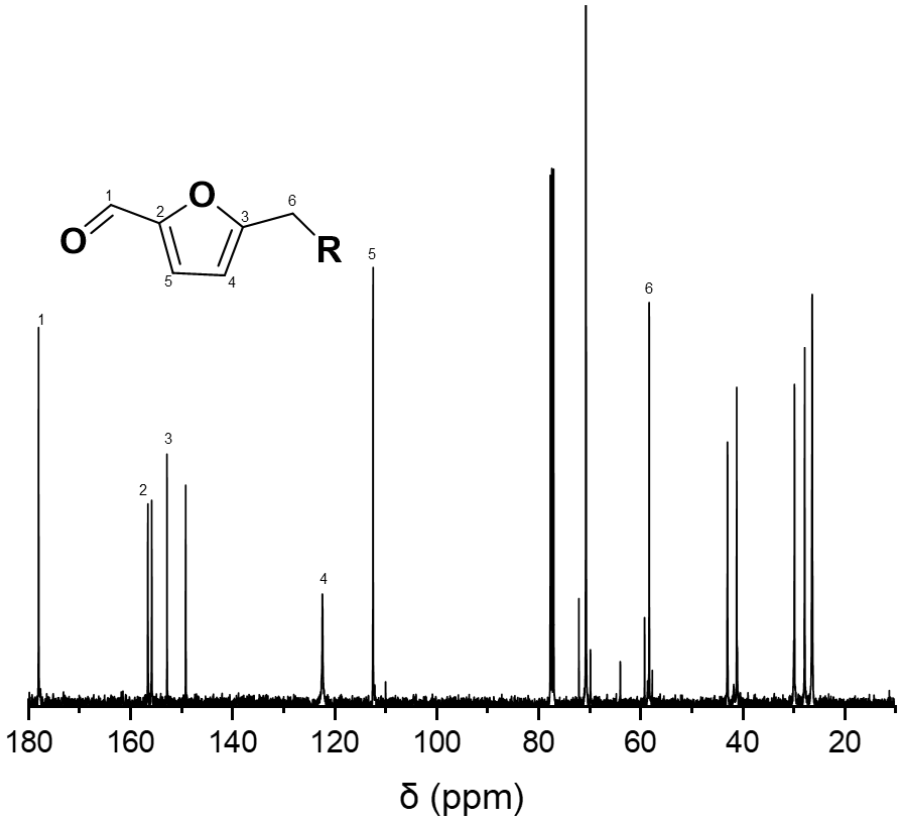

Figure 5.5: ^{13}C-NMR spectrum of aldehyde functional polyurethane resin.

In Figure 5.5 the spectrum displays the presence of the aldehyde component at 178 ppm. The other peaks that appear are due to the cyclic furan ring from HMF and can be seen at 157,152, 123, 110, and 57 ppm indicating an aldehyde functional polyurethane was successfully synthesized.

For Figure 5.6 the carbamate functionality is present from the appearance of multiple peaks at 159-157 ppm. The appearance of multiple peaks is due to the several isomers or side products that have been known to form in primary carbamate structures.[31]

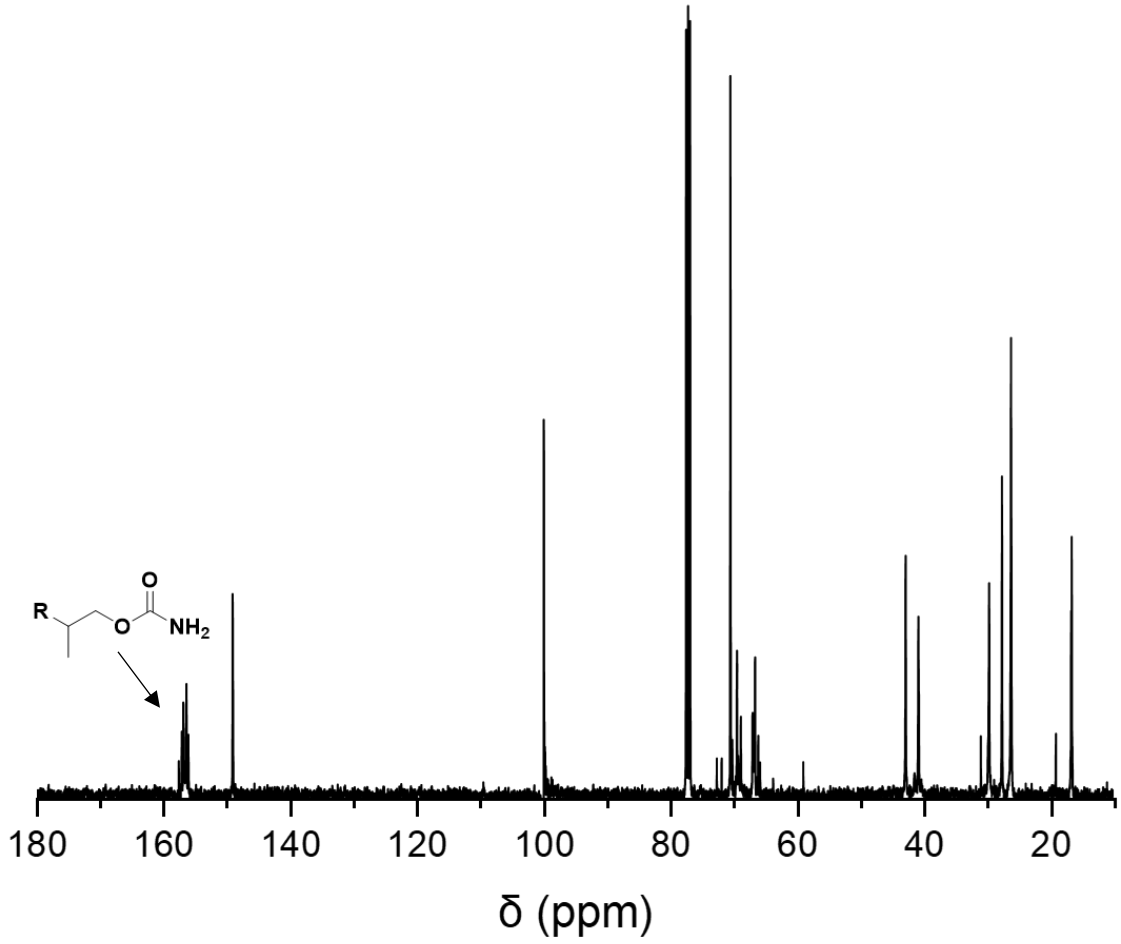

Figure 5.6: ^{13}C-NMR spectrum of carbamate functional resin.

Overall, the data gathered from both the FTIR and ^{13}C-NMR spectra indicate that the polyurethane resins had been successfully synthesized and could be utilized to produce a waterborne polyurethane dispersion.

5.4.2. Dispersion Methods

The dispersion methods for the polyurethanes were explored to identify how changes in dispersion methodology would affect stability and coating appearance Table 5.2 summarizes the results as well as providing a naming convection for the rest of the data presented in this body of research.

Table 5.2: Naming conventions for the dispersions and reagents used.

Dispersion	Dispersion Method	Polyurethane	Crosslinker	Assigned Label	Successful Dispersion
Yes	1	1	HMF	P1D1-H	No
Yes	1	2	HMF	P2D1-H	No
Yes	1	3	HMF	P3D1-H	No
Yes	2	1	HMF	P1D2-H	No
Yes	2	2	HMF	P2D2-H	Yes
Yes	2	3	HMF	P3D2-H	Yes
Yes	3	1	HMF	P1D3-H	No
Yes	3	2	HMF	P2D3-H	Yes
Yes	3	3	HMF	P3D3-H	Yes
Yes	4	1	1a	P1D4-AP	No
Yes	4	2	1a	P2D4-AP	Yes
Yes	4	3	1a	P3D4-AP	Yes
No	Solvent	2	HMF	P2S-H	N/A
No	Solvent	3	HMF	P3S-H	N/A

Dispersion method 1 could not be utilized with any polyurethane to yield a stable polyurethane dispersion. Coagulation was immediately observed when removal of the acetone took place which could be due to the acetone acting as a co-solvent dissolving the polymer and removing the acetone causes the polyurethane to precipitate from the solution. Polyurethane 1 could not be dispersed in any of the dispersion method due to two reasons. One is not containing enough hydrophilic m-PEG chains to disperse the particles in the water phase. Additionally, the viscosity of the polyurethane 1 is much higher due to the additional hydrogen bonding of the primary carbamate groups that the shear force applied to the polyurethane droplets is not enough to disperse it before it cools to room temperature and solidifies in the water. However, the polyurethanes with higher m-PEG content, 2 and 3, were dispersible in water. The lower viscosities are due to the reduction of primary carbamates and increase of hydrophilic m-PEG content allow for the resins to be dispersed. While a successful dispersion for dispersion method 2 was produced,

phase separation was observed to occur quite rapidly and the stability of it was too short for it to be evaluated. Dispersion method 3 and 4 produced stable dispersions and thus those were used for further examination against the solvent borne systems.

5.4.3. Particle Size and Stability

The polyurethane dispersion stability in water was tested by visual examination of the dispersions after a period time. Additionally, particle size of the dispersions was examined, and the data was correlated with the visual tests. The effects of the steric interactions of the m-PEG concentration in the polyurethane dispersion are apparent and are shown in Table 5.3.

Table 5.3: Stability of dispersion over time and particle size data from given dispersions.

Formulation	Particle Size (nm)	Stability (7 days)	Stability (14 days)
P2D3-H	1077	B	C
P3D3-H	623	A	B
P2D4-AP	701	A	B
P3D4-AP	578	A	B

* for details on the rating grade refer to previous chapter using Figure 4.8.

The is clear that the dispersions which contained higher concentrations of m-PEG in the polyurethane structure yielded more stable dispersions. In addition, when examining the particle size data, a clear trend is established between the particle sizes and the stability of the dispersions. The formulations with lower m-PEG content yielded dispersions with higher particle sizes due to the lower amount of hydrophilic content within the particles. Formulations P2D4-AP and P3D4-AP yielded lower average particle size when compared to P2D3-H, and P3D3-H. This trend is due to the overall higher amount of m-PEG content in the overall dispersion since the formulations dispersed utilizing method 4 contain two different of polyurethane species that are synthesized with m-PEG. The effects of steric stabilization from the hydrophilic m-PEG chains will have

greater contribution as the concentration is increased. Dispersion containing higher m-PEG content contained lower particle sizes and as a result more stable dispersions were produced given that the effects of gravity are more pronounced in large particles of 1μm in size.

5.4.4. Coating Appearance

The effect of the dispersion methodology seems to influence the appearance of the final cured coatings. That being stated, it is important to discuss why the appearances and how they may later affect coatings properties. Reference pictures of the coatings are given in Figure 5.7.

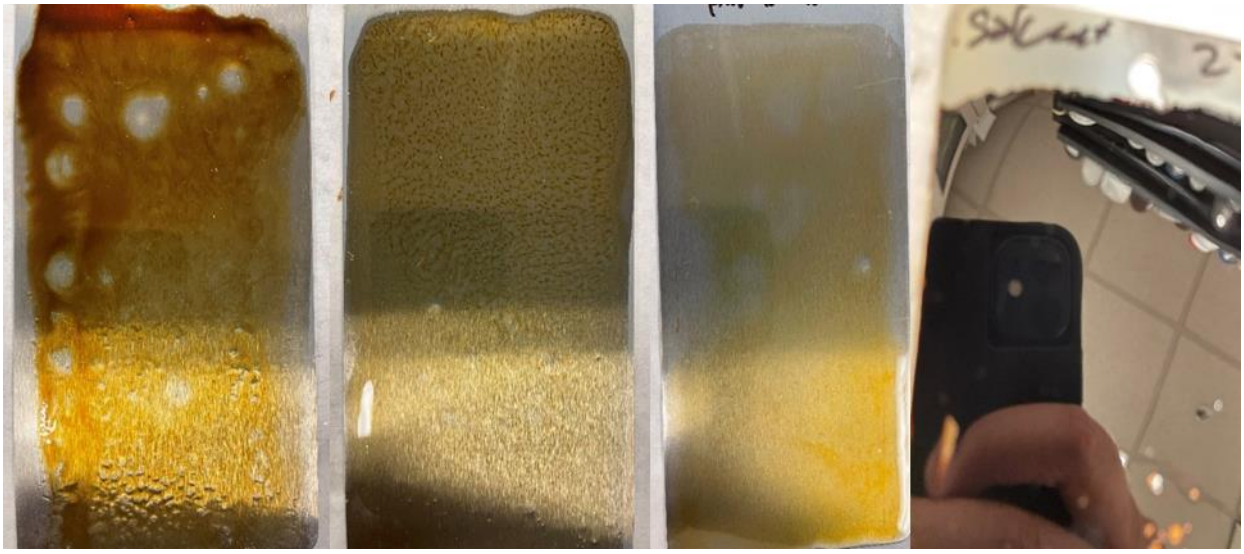

Figure 5.7: Photographs of coatings produced utilizing different dispersal methods. Naming from left to right the photographs corresponds to P2D2-H, P2D3-H, P2D4-AP, and P2S-H.

P2D2-H showed signs of phase separation as well as a large generation of "fisheyes" most likely due to the phase separation causing changes in surface tension of the coating while curing occurred given that dispersion method 2 did not yield stable dispersions and phase separation may be enhanced by the presence of heat in the oven curing conditions. Coatings preprepared utilizing dispersion method 3 produced coatings with minimal defects, but slight dark brown markings scattered about the surface of the coating. The minimization of defects comes from dissolving the HMF crosslinker first in water and allow for more equal dispersion of the crosslinking along the

waterborne polyurethane dispersion. The dark brown marking could be explained by the precipitation of the unreacted HMF crosslinker as the water evaporates from the coating's formulation. Dispersion method 4 utilized the use of aldehyde functional polyurethane to improve compatibility between the polyurethane resin and the crosslinker as the reagents are dispersed in water. The coatings formulated utilizing dispersion method 4 were the most uniform with little defects. The intense yellowing that was present in the other methods was not as apparent.

Coatings made utilizing solvent produced coatings with very interesting appearance. The cured coatings had little to no defects and had a very smooth and glossy appearance. An observation to note is that the coatings had a dark-purple color appearance that was not present in any of the other coatings made from the different dispersion method. Given these findings, the only dispersions and coatings suitable for further characterization were, P2D3-H, P3D3-H, P2D4-AP, P3D4-AP, P2S-H, and P3S-H.

5.4.5. FTIR-ATR

FTIR-ATR of the coatings made using dispersion method 3 and 4 as well as the solvent borne coatings are displayed in Figure 5.8. No obvious difference between the three different samples can be observed. At first glance, the narrowing of the peak corresponding to the carbonyl region of 1710-1690 cm^{-1} in the primary carbamate functionality would allude to the idea that crosslinking is occurring and thus the narrow peaks are a result of the urethane linkages forming. However, the intermediate iminium and imine formed in the crosslinking reaction, Scheme 5.2, are also present in the carbonyl region of 1690-1640 cm^{-1} meaning that even though the carbamate peak is reduced in the spectra, it does not mean crosslinking has occurred.

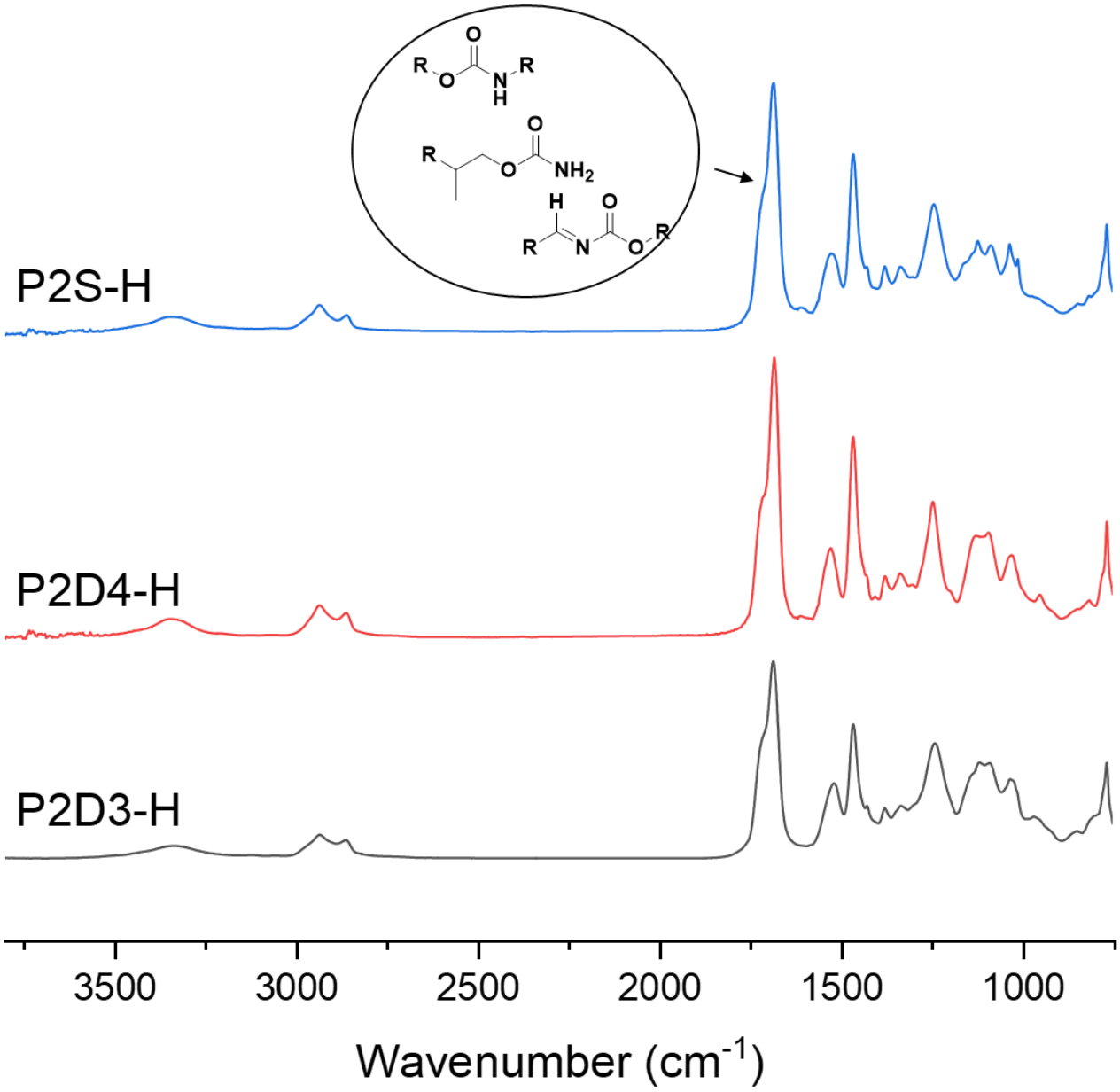

Figure 5.8: FTIR ATR of cured coatings for P2D3-H, P2D4-H, P2S-H.

5.4.6. Water Drop Test and Contact Angle

The water drop test was done to observe the absorption of water onto the surface of the coating to gain some insight on the water resistance of the coatings. The static water contact angle was done to correlate hydrophobic/hydrophilic properties of the coatings with the water drop test. The data is exhibited on Table 5.4. Data shows relatively lower static water contact angles when

using dispersion methods 3 and 4 and a significant increase in static water contact angle when utilizing the solvent borne formulation. The changes within the same dispersion method but different carbamate functional polyurethanes can be explained by the amount of m-PEG content in the polyurethane. The long chain length and chain flexibility of m-PEG 750 affects the water absorption characteristics on the surface of the coating. As a result, it is expected that the coatings utilizing higher amount of m-PEG will yield coatings with lower contact angles and exhibit more wetting characteristics. Additionally, degree of crosslinking affects the water drop test and static contact angle measurements of the coatings. A higher degree of crosslinking will cause a higher amount of contribution from intermolecular forces of the coatings causing the structure of the polymeric chains to be more compacted producing a network where water cannot permeate through the crosslinked structure as efficiently. The results overall indicate that the structure of the solvent borne system contains a higher degree of crosslinking when compared to the waterborne system and thus the solvent borne system have a higher contact angle and perform better in the water drop test.

Table 5.4: Static contact angle and water drop test measurements for formulated coatings.

Formulation	CA(m) [°]	CA(l) [°]	CA(r) [°]	*Water Drop Test
P2D3-H	62.8 (+-2.8)	58.8 (+8.7)	63.5 (+-1.6)	1
P3D3-H	57.5 (+-6.9)	57.2 (+-7.0)	57.8 (+-6.9)	1
P2D4-AP	63.3 (+-0.9)	62.9 (+-0.4)	63.8 (+-1.4)	3
P3D4-AP	62.6 (+-2.6)	62.7 (+-2.4)	62.5 (+-2.8)	3
P2S-H	76.7 (+-2.7)	77.0 (+-3.1)	76.3 (+-2.4)	5
P3S-H	71.6 (+-1.1)	71.3 (+-0.9)	71.8 (+-1.3)	5

*(l) and (r) being the left and right sided contact angles respectively. (m) is the mean of the left and right sided contact angles. Test rating are 0 to 5 with 0 demonstrating no defects, to 5 demonstrating complete delamination.

5.4.7. Coatings Properties

The coatings properties testing various aspects of the performance of the coatings is summarized in Table 5.5 to compare the different dispersion methods and the different carbamate functional polyurethanes. P2D3-H which contained a lower amount of m-PEG produced harder and more crosslinked coatings that P3D3-H due to the higher amount of carbamates present in the formulations that had lower m-PEG content. For the same reason, the adhesion to substrate was lower in P2D3-H than P3D3-H. Similarly, the solvent resistance of P2D3-H is higher than that of P3D3-H.

A general improvement was seen in coatings utilizing the dispersible aldehyde polyurethane as opposed to the dissolved HMF crosslinker. P2D4-AP and P3D4-AP produced coatings that were the softest and most ductile form the set when observing pencil hardness, König hardness, and mandrel bend. The flexibility of the coatings can be attributed to the much higher m-PEG content that is present in the formulations that use the aldehyde functional polyurethane. However, the higher solvent resistance could indicate that the interaction between the aldehyde and carbamate is more prevalent when the aldehyde functional species is dispersed in the polymer phase as opposed to being dissolved in water like in P2D3-H than P3D3-H.

Table 5.5: Coatings properties.

Coatings Properties	P2D3-H	P3D3-H	P2D4-AP	P3D4-AP	P2S-H	P3S-H
Pencil Hardness	H	HB	2B	2B	3H	2H
Adhesion	2B	4B	4B	4B	1B	1B
MEK Double Rubs	120	90	220	270	400+	400+
Reverse Impact (in·lb)	3.92	3.92	156.8	168.56	3.92	3.92
Mandrel Bend	Fail	Fail (8cm)	Pass	Pass	Fail	Fail
König Hardness (sec)	112	53	47	41	155	112
Thickness (µm)	63.7	58.4	68.5	68.7	55.7	62.8

Solvent borne coatings exhibited properties of a highly crosslinked system with the hardness exceed the other coating sets and the solvent resistance passing 400 MEK double rubs. This result hints that the coatings are curing relatively quickly in the solvent borne formulations and thus a high amount of internal stress in the coating/substrate interface would be high. Therefore, the adhesion of those coatings to the substrate was very low and complete delamination was observed in the mandrel bend test. Similar adhesion issues were observed by Silbert[13] on a solvent borne carbamate aldehyde crosslinking system. Overall, these results indicate that the waterborne formulations may be affected by the presence of water and further testing must be take place in order to further understand the crosslinking chemistry.

5.4.8. Thermal Characteristics

Thermal properties of the coating systems were determined and are displayed in Table 5.6 and Figure 5.9. The Thermal decomposition of all samples were within a range of 200-220 °C.

These values are not far from values reported in literature since urethane linkages are known to contain some degree of bond reversibility..

Table 5.6: Thermal decomposition and glass transition values of coatings samples.

Formulation	TGA (Td%5) (°C)	Oven Cured DSC (Tg) (°C)
P2D3-H	202.21	22.74
P3D3-H	203.82	18.04
P2D4-AP	197.34	16.50
P3D4-AP	216.36	11.87
P2S-H	212.31	48.14
P3S-H	210.69	34.45

The glass transitions of samples varied widely depending on the dispersion method used to formulate the coatings. The glass transitions of P2D3-H and P3D3-H were higher than the glass transitions of P2D4-AP and P3D4-AP due to the lower amount of m-PEG content in the coatings using HMF as a crosslinker due to the limited chain mobility of the crosslinked systems. Since m-PEG does not participate in the crosslinking reaction, the crosslinking density would be lower and thus the degrees of freedom in the molecular chains is increased in the crosslinked network when m-PEG content is higher.

Additionally, the solvent borne systems P2S-H, and P3S-H had a much higher glass transition temperature than the waterborne samples. These results suggest that the crosslinking density of the solvent borne systems is higher than that of the waterborne systems. Higher crosslinking density limits the molecular motion of polymeric chains and thus the glass transition temperature is at a higher temperature. The crosslinking reaction of the aldehyde and primary carbamate may be hindered by the presence of water and thus the solvent borne systems yield a more crosslinked coating. This theory is further backed by a study lead by Gerard where a similar conclusion was reached.[30] The thermal analysis in conjunction with the coatings properties

indicate that the crosslinking reaction is more prevalent in solvent borne systems that waterborne systems.

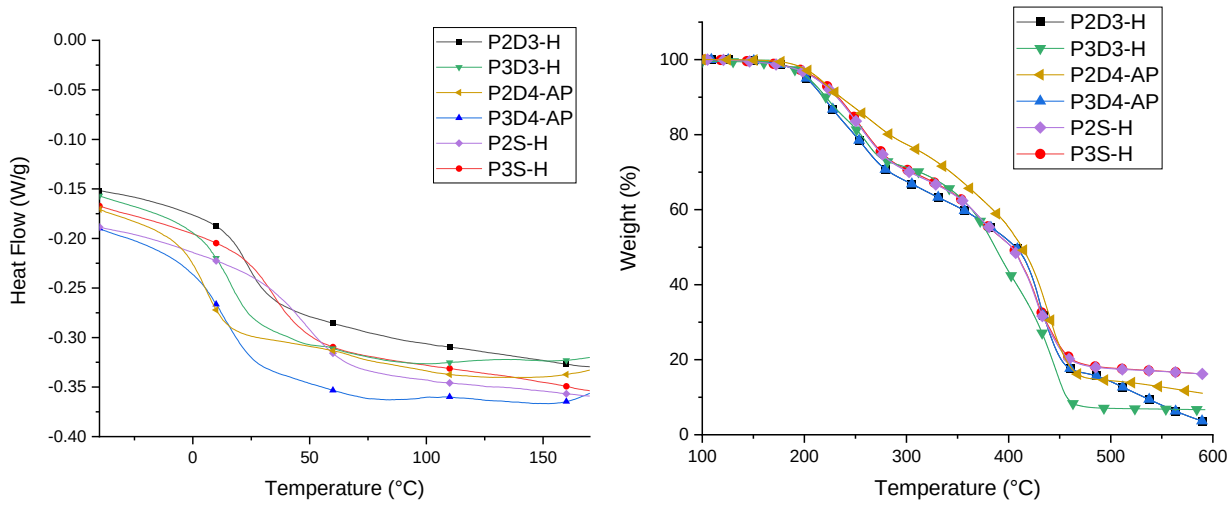

Figure 5.9: DSC (left) and TGA (right) graphs of cured P2D3-H, P3D3-H, P2D4-AP, P3D4-AP, P2S-H, and P3S-H.

5.5. Conclusion

This body of work illustrates the deep complexity that comes when designing a WBPUD. It is clear from the results that the method of dispersion has a significant influence on the overall coatings properties when utilizing a WBPUD. Furthermore, the use of the carbamate-aldehyde crosslinking chemistry in solvent borne systems displays some desirable properties. However, the use the reaction in waterborne systems remains in question due to the possibility of water interfering with the crosslinking kinetics. Additional work needs to be carried out to fully understand the carbamate-aldehyde reaction and utilize it to its full potential.

5.6. References

1. Datta, J.; Kasprzyk, P., Thermoplastic polyurethanes derived from petrochemical or renewable resources: A comprehensive review. *Polymer Engineering and Science* **2018,** *58*, E14-E35.
2. Khatoon, H.; Iqbal, S.; Irfan, M.; Darda, A.; Rawat, N. K., A review on the production, properties and applications of non-isocyanate polyurethane: A greener perspective. *Progress in Organic Coatings* **2021,** *154*, 106124.
3. Bello, D.; Herrick Christina, A.; Smith Thomas, J.; Woskie Susan, R.; Streicher Robert, P.; Cullen Mark, R.; Liu, Y.; Redlich Carrie, A., Skin Exposure to Isocyanates: Reasons for Concern. *Environmental Health Perspectives* **2007,** *115* (3), 328-335.
4. Asemani, H. R.; Mannari, V., Synthesis and evaluation of non-isocyanate polyurethane polyols for heat-cured thermoset coatings. *Progress in Organic Coatings* **2019,** *131* (February), 247-258.
5. Błażek, K.; Datta, J., Renewable natural resources as green alternative substrates to obtain bio-based non-isocyanate polyurethanes-review. *Critical Reviews in Environmental Science and Technology* **2019,** *49* (3), 173-211.
6. Cornille, A.; Auvergne, R.; Figovsky, O.; Boutevin, B.; Caillol, S., A perspective approach to sustainable routes for non-isocyanate polyurethanes. *European Polymer Journal* **2017,** *87*, 535-552.
7. Ghasemlou, M.; Daver, F.; Ivanova, E. P.; Adhikari, B., Bio-based routes to synthesize cyclic carbonates and polyamines precursors of non-isocyanate polyurethanes: A review. *European Polymer Journal* **2019,** *118*, 668-684.

8. Gomez-Lopez, A.; Elizalde, F.; Calvo, I.; Sardon, H., Trends in non-isocyanate polyurethane (NIPU) development. *Chemical Communications* **2021,** *57* (92), 12254-12265.

9. Kathalewar, M. S.; Joshi, P. B.; Sabnis, A. S.; Malshe, V. C., Non-isocyanate polyurethanes: from chemistry to applications. *RSC Advances* **2013,** *3* (13), 4110.

10. Lombardo, V. M.; Dhulst, E. A.; Leitsch, E. K.; Wilmot, N.; Heath, W. H.; Gies, A. P.; Miller, M. D.; Torkelson, J. M.; Scheidt, K. A., Cooperative Catalysis of Cyclic Carbonate Ring Opening: Application Towards Non-Isocyanate Polyurethane Materials. *European Journal of Organic Chemistry* **2015,** *2015* (13), 2791-2795.

11. Pathak, R.; Kathalewar, M.; Wazarkar, K.; Sabnis, A., Non-isocyanate polyurethane (NIPU) from tris-2-hydroxy ethyl isocyanurate modified fatty acid for coating applications. *Progress in Organic Coatings* **2015,** *89*, 160-169.

12. Rix, E.; Grau, E.; Chollet, G.; Cramail, H., Synthesis of fatty acid-based non-isocyanate polyurethanes, NIPUs, in bulk and mini-emulsion. *European Polymer Journal* **2016,** *84*, 863-872.

13. Silbert, S. D.; Serum, E. M.; Lascala, J.; Sibi, M. P.; Webster, D. C., Biobased, Nonisocyanate, 2K Polyurethane Coatings Produced from Polycarbamate and Dialdehyde Cross-linking. *ACS Sustainable Chemistry and Engineering* **2019,** *7* (24), 19621-19630.

14. Yu, A. Z.; Setien, R. A.; Sahouani, J. M.; Docken, J.; Webster, D. C., Catalyzed non-isocyanate polyurethane (NIPU) coatings from bio-based poly(cyclic carbonates). *Journal of Coatings Technology and Research* **2019,** *16* (1), 41-57.

15. Cakić, S. M.; Špírková, M.; Ristić, I. S.; B-Simendić, J. K.; M-Cincović, M.; Poręba, R., The waterborne polyurethane dispersions based on polycarbonate diol: Effect of ionic content. *Materials Chemistry and Physics* **2013,** *138* (1), 277-285.

16. Chattopadhyay, D. K.; Raju, K. V. S. N., Structural engineering of polyurethane coatings for high performance applications. *Progress in Polymer Science (Oxford)* **2007,** *32* (3), 352-418.

17. Etxaniz, I.; Llorente, O.; Aizpurua, J.; Martín, L.; González, A.; Irusta, L., Dispersion Characteristics and Curing Behaviour of Waterborne UV Crosslinkable Polyurethanes Based on Renewable Dimer Fatty Acid Polyesters. *Journal of Polymers and the Environment* **2019,** *27* (1), 189-197.

18. Fuensanta, M.; Jofre-Reche, J. A.; Rodríguez-Llansola, F.; Costa, V.; Iglesias, J. I.; Martín-Martínez, J. M., Structural characterization of polyurethane ureas and waterborne polyurethane urea dispersions made with mixtures of polyester polyol and polycarbonate diol. *Progress in Organic Coatings* **2017,** *112* (April), 141-152.

19. García-Pacios, V.; Jofre-Reche, J. A.; Costa, V.; Colera, M.; Martín-Martínez, J. M., Coatings prepared from waterborne polyurethane dispersions obtained with polycarbonates of 1,6-hexanediol of different molecular weights. *Progress in Organic Coatings* **2013,** *76* (10), 1484-1493.

20. Harkal, U. D.; Muehlberg, A. J.; Edwards, P. A.; Webster, D. C., Novel water-dispersible glycidyl carbamate (GC) resins and waterborne amine-cured coatings. *Journal of Coatings Technology and Research* **2011,** *8* (6), 735-747.

21. Honarkar, H., Waterborne polyurethanes: A review. *Journal of Dispersion Science and Technology* **2018,** *39* (4), 507-516.

22. Hwang, H. D.; Park, C. H.; Moon, J. I.; Kim, H. J.; Masubuchi, T., UV-curing behavior and physical properties of waterborne UV-curable polycarbonate-based polyurethane dispersion. *Progress in Organic Coatings* **2011,** *72* (4), 663-675.

23. Kwak, Y. S.; Park, S. W.; Kim, H. D., Preparation and properties of waterborne polyurethane-urea anionomers - Influences of the type of neutralizing agent and chain extender. *Colloid and Polymer Science* **2003,** *281* (10), 957-963.

24. Liang, H.; Wang, S.; He, H.; Wang, M.; Liu, L.; Lu, J.; Zhang, Y.; Zhang, C., Aqueous anionic polyurethane dispersions from castor oil. *Industrial Crops and Products* **2018,** *122* (June), 182-189.

25. Patel, R.; Kapatel, P., Waterborne polyurethanes: A three step synthetic approach towards environmental friendly flame retardant coatings. *Progress in Organic Coatings* **2018,** *125* (August), 186-194.

26. Wang, L.; Shen, Y.; Lai, X.; Li, Z.; Liu, M., Synthesis and properties of crosslinked Waterborne polyurethane. *Journal of Polymer Research* **2011,** *18* (3), 469-476.

27. Xu, H.; Qiu, F.; Wang, Y.; Wu, W.; Yang, D.; Guo, Q., UV-curable waterborne polyurethane-acrylate: Preparation, characterization and properties. *Progress in Organic Coatings* **2012,** *73* (1), 47-53.

28. Xu, J.; Jiang, Y.; Zhang, T.; Dai, Y.; Yang, D.; Qiu, F.; Yu, Z.; Yang, P., Synthesis of UV-curing waterborne polyurethane-acrylate coating and its photopolymerization kinetics using FT-IR and photo-DSC methods. *Progress in Organic Coatings* **2018,** *122* (May), 10-18.

29. Florence, A. T.; Rogers, J. A., Emulsion stabilization by non-ionic surfactants: experiment and theory. *Journal of Pharmacy and Pharmacology* **2011,** *23* (3), 153-169.

30. Gérard, D.; Méchin, F.; Saint-Loup, R.; Fleury, E.; Pascault, J.-P., Study of the carbamate/aldehyde reaction, a new pathway towards NIPU materials. *Progress in Organic Coatings* **2022,** *165*, 106728.

31. Ghosh, A. K.; Brindisi, M., Organic Carbamates in Drug Design and Medicinal Chemistry. *Journal of Medicinal Chemistry* **2015,** *58* (7), 2895-2940.

CHAPTER 6. FUTURE DIRECTIONS

6.1. Oxone Epoxidation

The use of Oxone to epoxidized species can be further improved upon. The drawbacks summarized in the body of work come from the high amounts of solvents that are used and the long reaction time that is limited by the Oxone solution addition rate to the reaction vessel. There are two very clear pathways to remedy these issues that would improve the viability of the synthesis method.

The biphasic system that the Oxone method of epoxidation undergoes forces the reaction to be limited to the transfer of dimethyldioxirane intermediates to the oil phase where the unsaturated oils are located. By utilizing a phase transfer catalyst, the migration of the dimethyldioxirane intermediates to the oils phase could be sped up. [1-3] As a result, the rate of addition of the Oxone solution could be increased and thus the overall reaction time would be decreased. However, careful selection of phase transfer catalyst must be considered. If not, utilization of a phase transfer catalyst that can facilitate the transfer of unwanted side products will negatively affect the overall conversion rate and facilitate the generation of side products.

Given that the synthesis follows a biphasic system, other ways to improve the reaction time is by utilizing different reaction set ups to encourage the interaction between dimethyldioxirane and the unsaturated sites of the fatty acids. One example is shown in literature[4] where an dimethyldioxirane intermediates where generated utilizing Oxone and acetone in a separate reaction vessel. The generated dimethyldioxirane could then be directly distilled into the reaction flask that contains the unsaturated component. Other methods could include implementation of high shear methods such as homogenizers and study the effects of shear force in the epoxidation

of soybean oil species. By applying higher shear force the migration of dimethyl dioxirane intermediates from the water phase to the oil phase is facilitated by the high shear application.

6.2. Cationic Photopolymerization

The use of epoxidized sucrose soyate and epoxidized soybean oil in cationic homopolymerization revealed that epoxidized sucrose soyate when used with petroleum-based epoxy resins could be used to increase the biobased content of UV curable formulations. Incorporations of other oils like hempseed oil which contain a much high degree of unsaturation when compared to soybean oil would yield some interesting properties. Our study in Chapter 2 as well as other studies have indicated that epoxidized hempseed oil will yield a highly crosslinked species due the high number of epoxy functional groups in the molecule.[5, 6] Simultaneously, the long aliphatic carbon chains will contribute flexibility and mechanical strength the cured coating which may mitigate some of the negative effects that are seen in highly crosslinked epoxies. Other follow up studies would be the kinetics of soybean oil and sucrose soyate. Doing kinetic studies for the cationic photopolymerization of epoxidized sucrose soyate and epoxidized soybean oil will provide insight to what calculating conversions based of off theoretical heat of enthalpy. This data would also provide a means to more accurately implement a post UV thermal curing cycle to improve conversion of the crosslinked systems.

6.3. Waterborne-Polyurethane Dispersions Utilizing 5 and 6 Membered Cyclic Carbonates

Creating dispersion which contain smaller particle sizes would improve the over stability of the waterborne polyurethane dispersion and could potentially lead to increasing the overall solids content of the dispersions. Stability could be achieved by implementing the use of surfactants that have a direct effect of the stability of the dispersion. Other means to achieve

dispersion stability include using anionic or cationic internal emulsifiers to further improve the dispersion characteristics of the compounds.

Another project that is vital to understanding the feasibility of these systems is having a direct measurement of the degree of hydrolysis that is occurring in the 5-membered cyclic carbonates and 6-membered cyclic carbonates. Webster[7, 8] studied the effects of aminolysis on cyclic carbonate functional polymers utilizing IR instrumentation and heated cell chambers to detect the disappearance of the corresponding carbonyl group and compare it against the appearance of the final product. Different solvents and different amines where tested and the susceptibility of cyclic carbonates to react in the presence of amines greatly varies with amine reactivity. Carrying out similar studies with the TBD-LiOTf co catalysts system in the presence of water for both 5-membered cyclic rings and 6-membered cyclic rings should offer valuable insight on the feasibility of this chemistry in water. Additionally, other 6-membered cyclic carbonates with varying pendant chains could be observed to investigate the influence of said pendant chains on coatings properties.

6.4. Carbamate Functional Polyurethanes

The use of the carbamate-aldehyde reaction still requires further insight. The presence of water to the crosslinking system influences the overall reaction kinetics which hinders the use of it in waterborne polyurethane dispersions. Having a further understanding of the reaction kinetics would allow for better utilization of the carbamate-aldehyde system in crosslinking chemistries.

The solvent-borne coatings utilizing the carbamate-aldehyde crosslinking chemistry showed promising results. The crosslinking could be further enhanced by implementing the primary carbamates within the polyurethane backbone by the ring opening of glycerol carbonate with ammonia which would yield a diol with carbamate functionality that could be easily reacted

onto a polymer backbone allowing for more versatility when designing non-isocyanate polyurethanes for highly crosslinked thermoset coating applications.

6.5. References

1. De Kruijff, G. H. M.; Goschler, T.; Derwich, L.; Beiser, N.; Türk, O. M.; Waldvogel, S. R., Biobased Epoxy Resin by Electrochemical Modification of Tall Oil Fatty Acids. *ACS Sustainable Chemistry and Engineering* **2019,** *7* (12), 10855-10864.
2. Alavi Nikje, M. M.; Rafiee, A.; Haghshenas, M., Epoxidation of polybutadiene using in situ generated dimethyl dioxirane (DMD) in the presence of tetra-n-butyl ammonium bromide. *Designed Monomers and Polymers* **2006,** *9* (3), 293-303.
3. Li, W.; Fuchs, P. L., A new protocol for in situ dioxirane reactions: Stoichiometric in oxone and catalytic in fluorinated acetophenones. *Organic Letters* **2003,** *5* (16), 2853-2856.
4. Mikula, H.; Svatunek, D.; Lumpi, D.; Glöcklhofer, F.; Hametner, C.; Fröhlich, J., Practical and efficient large-scale preparation of dimethyldioxirane. *Organic Process Research and Development* **2013,** *17* (2), 313-316.
5. Anusic, A.; Resch-Fauster, K.; Mahendran, A. R.; Wuzella, G., Anhydride Cured Bio-Based Epoxy Resin: Effect of Moisture on Thermal and Mechanical Properties. *Macromolecular Materials and Engineering* **2019,** *304* (7), 1900031.
6. Di Mauro, C.; Malburet, S.; Genua, A.; Graillot, A.; Mija, A., Sustainable Series of New Epoxidized Vegetable Oil-Based Thermosets with Chemical Recycling Properties. *Biomacromolecules* **2020,** *21* (9), 3923-3935.
7. Webster, D. C.; Crain, A. L., Synthesis and applications of cyclic carbonate functional polymers in thermosetting coatings. *Progress in Organic Coatings* **2000,** *40* (1-4), 275-282.

8. Webster, D. C.; Crain, A. L., Synthesis of Cyclic Carbonate Functional Polymers. *ACS Symposium Series* **1998,** *704*, 303-320.